



รายงานวิจัยฉบับสมบูรณ์

โครงการ
การทำแห้งผลิตภัณฑ์อาหารโดยใช้ไอน้ำร้อนยวดยิ่งที่สภาวะ
ความดันต่ำ (ระยะที่ 2)

โดย

รศ.ดร. สักกมน เทพหัสติน ณ อรุณา

มิถุนายน พ.ศ. 2551

รายงานวิจัยฉบับสมบูรณ์

โครงการ

การทำแห้งผลิตภัณฑ์อาหารโดยใช้ไอน้ำร้อนยวดยิ่งที่สภาวะ ความดันต่ำ (ระยะที่ 2)

รศ.ดร. สักกมณ เทพหัสดิน ณ อยุธยา

ภาควิชาวิศวกรรมอาหาร คณะวิศวกรรมศาสตร์

มหาวิทยาลัยเทคโนโลยีพระจอมเกล้าธนบุรี

สนับสนุนโดยสำนักงานคณะกรรมการอุดมศึกษาและสำนักงานกองทุนสนับสนุนการวิจัย

(ความเห็นในรายงานนี้เป็นของผู้วิจัย สกอ. และ สกว. ไม่จำเป็นต้องเห็นด้วยเสมอไป)

Acknowledgements

The investigator expresses his sincere appreciation to the Commission on Higher Education (CHE) and the Thailand Research Fund (TRF) for supporting this study financially through the grant no. RMU4880001. Additional support from the International Foundation for Science (IFS), Sweden is also appreciated.

บทคัดย่อ

รหัสโครงการ: RMU4880001

ชื่อโครงการ: การทำแห้งผลิตภัณฑ์อาหารโดยใช้ไอน้ำร้อนยวดยิ่งที่สภาวะความดันต่ำ (ระยะที่ 2)

ชื่อนักวิจัย: รศ.ดร. สักกมน เทพหัตถิน ณ อุทยาน

E-mail Address: sakamon.dev@kmutt.ac.th

ระยะเวลาโครงการ: 3 ปี (1 มิถุนายน พ.ศ. 2548 – 31 พฤษภาคม พ.ศ. 2551)

โครงการวิจัยนี้เป็นโครงการต่อเนื่องจากโครงการวิจัยเรื่อง การทำแห้งผลิตภัณฑ์อาหารโดยใช้ไอน้ำร้อนยวดยิ่งที่สภาวะความดันต่ำ (TRG 4580099) โดยโครงการแบ่งออกเป็น 5 ส่วนย่อย แต่ละส่วนย่อยมุ่งศึกษาประเด็นต่างๆ ที่เกี่ยวกับการทำแห้งอาหารโดยใช้ไอน้ำร้อนยวดยิ่งที่สภาวะความดันต่ำ (LPSSD)

ส่วนแรกของโครงการวิจัยเป็นการมุ่งศึกษา LPSSD ในระดับพื้นฐาน โดยมีการพัฒนาแบบจำลองทางคณิตศาสตร์ ซึ่งสามารถใช้ทำนายการเปลี่ยนแปลงความชื้นและอุณหภูมิของอาหาร (หรือวัสดุชีวภาพ) ใดๆ ระหว่าง LPSSD นอกจากนี้ยังได้เสนอแนะการใช้การวิเคราะห์แฟรคทัล เพื่อเป็นเครื่องมือในการหาความสัมพันธ์ระหว่างข้อมูลการเปลี่ยนแปลงเชิงโครงสร้างและเชิงกายภาพ ซึ่งความสัมพันธ์ในลักษณะนี้จะนำไปสู่การพัฒนาตัวชี้วัดการเปลี่ยนแปลงเชิงกายภาพ/โครงสร้างของอาหารในระหว่างการอบแห้งได้ต่อไป

ในส่วนที่สองของโครงการวิจัย ได้ทำการทดลองเพื่อศึกษาผลของ LPSSD และกระบวนการอบแห้งแบบอื่นๆ ที่มีต่อคุณค่าทางโภชนาการของอาหารต่างชนิด ซึ่งรวมถึงการศึกษาจลนพลศาสตร์การเกิดไอโซเมอร์ไรเซชันและการเสื่อมสลายของเบต้าแคโรทีนในแครอท การศึกษาการเสื่อมสลายของกรดแอสคอร์บิกในมะขามป้อม และการศึกษาผลของวิธีการทำแห้งและอุณหภูมิที่ใช้ในการชงชาที่มีต่อปริมาณวิตามินซีในน้ำชามะขามป้อม ส่วนถัดมาของโครงการวิจัยเป็นการศึกษาการใช้ LPSSD และการเตรียมการก่อนการทำแห้งที่เหมาะสมในการผลิตขนมขบเคี้ยวสุขภาพ ซึ่งก็คือ มันฝรั่งแผ่นแบบไร้ไขมัน ซึ่งผลการศึกษาในส่วนนี้แสดงให้เห็นว่า LPSSD มีศักยภาพที่จะมาแทนที่กระบวนการทอดในการผลิตมันฝรั่งแผ่นได้

ส่วนที่สี่ของงานวิจัยเป็นการศึกษาวิธีการต่างๆ ซึ่งอาจนำมาใช้ในการเพิ่มประสิทธิภาพของ LPSSD โดยพิจารณาทั้งในแง่ของจลนพลศาสตร์การอบแห้งและคุณภาพของผลิตภัณฑ์ ในงานวิจัยส่วนนี้ได้มีการทดสอบการใช้การแผ่รังสีอินฟราเรดไกล เพื่อเป็นแหล่งพลังงานเสริมในการเร่งกระบวนการทำแห้งและช่วยเพิ่มการระเหยของความชื้นภายในผลิตภัณฑ์อันจะส่งผลให้เกิดโครงสร้างที่มีลักษณะเป็นรูพรุนมากขึ้น นอกจากนี้ยังได้ศึกษาการทำแห้งแบบเป็นช่วง ซึ่งพบว่าสามารถลดการใช้พลังงานในการอบแห้งลงได้ดี สำหรับส่วนสุดท้ายของงานวิจัยเป็นการประยุกต์ใช้ LPSSD ในการผลิตฟิล์มบริโอคได้สำหรับประยุกต์ใช้ในการพัฒนาบรรจุภัณฑ์แบบใหม่ จากผลการวิจัยพบว่า ฟิล์มบริโอคได้ซึ่งเตรียมโดย LPSSD มีสมบัติเชิงกลดีกว่าฟิล์มที่ได้จากการทำแห้งแบบอื่นๆ อย่างมีนัยสำคัญ

คำหลัก: การจำลองทางคณิตศาสตร์ การทำแห้ง การทำแห้งแบบเป็นช่วง การแผ่รังสีอินฟราเรดไกล การวิเคราะห์แฟรคทัล ขนมขบเคี้ยวสุขภาพ คุณค่าทางโภชนาการ ความสัมพันธ์ระหว่างโครงสร้าง-คุณภาพ วัสดุชีวภาพ สมบัติทางกายภาพ

Abstract

Project Code: RMU4880001

Project Title: Low-pressure Superheated Steam Drying of Food Products (Stage 2)

Investigator: Associate Professor Dr. Sakamon Devahastin

E-mail Address: sakamon.dev@kmutt.ac.th

Project Period: 3 years (June 1, 2005-May 31, 2008)

The present research project is a continuation of the project entitled “Low-pressure Superheated Steam Drying of Food Products” (TRG4580099). The project could be divided into 5 parts (groups), each focusing on different aspects of low-pressure superheated steam drying (LPSSD) of foods products.

The first part of the project focused on the fundamental study of LPSSD of food products. This included the development of a mathematical model, which allows prediction of evolutions of moisture and temperature of a food product (or, in fact, any biomaterial) undergoing LPSSD. The use of fractal analysis was also proposed as a means to correlate structural and various physical changes data, thus allowing one to obtain a more universal indicator of physical/structural changes of foods and biomaterials during drying.

In the second part of the study, experiments were performed to study the effects of LPSSD and other drying techniques on nutritive quality of foods. This included the study of β -carotene isomerization and degradation in carrot, ascorbic acid degradation in Indian gooseberry and the study of the effects of drying methods and tea preparation temperature on the vitamin C content in Indian gooseberry tea. The following part of the study involved the use of LPSSD and appropriate pretreatments to produce health snack viz. fat-free potato chip. The results illustrated feasibility of LPSSD as an alternative to deep-fat frying to produce potato chip.

The fourth part investigated various means to enhance LPSSD, both from the drying kinetics and product quality points of view. The use of far-infrared radiation (FIR) as an additional heat source to augment drying and to induce more vigorous vaporization of moisture within a food product, thus creating more porous structure within a dried product, was attempted and found to be successful. The use of intermittent drying was also investigated and was found helpful in conserving the energy for LPSSD. Finally, the use of LPSSD to produce edible films for active packaging applications was investigated. It was found that LPSSD could produce edible films with superior mechanical properties to films produced by other conventional drying methods.

Keywords: Biomaterials; Drying; Far-infrared radiation; Fractal analysis; Health snack; Intermittent drying; Mathematical modeling; Nutritive quality; Physical properties; Structure-quality relationships.

1. Introduction

The present research project is a continuation of the project entitled “Low-pressure Superheated Steam Drying of Food Products” (TRG4580099). The project continued to investigate detailed effects of various drying parameters and strategies on the drying kinetics as well as physical and chemical (nutritive) qualities of selected food products deemed important for both domestic and international markets. The project could be casually divided into 5 parts (groups), each focusing on different aspects of low-pressure superheated steam drying (LPSSD) of food products.

The first part of the project focused on the fundamental study of LPSSD of food products. This included the development of a three-dimensional liquid-diffusion based mathematical model, which allows prediction of evolutions of moisture and temperature of a food product (or, in fact, any biomaterial) undergoing LPSSD (Suvarnakuta et al., 2007). The model was validated with the available experimental data and it was found that the simulated and observed moisture and temperature evolutions agreed well with each other. The effect of product shrinkage on the model predictability was also investigated. It was noted that the model, which took into account the product shrinkage performed better than the one assuming no product shrinkage.

The use of combined fractal and image analysis was also proposed as a means to correlate structural and various physical changes data, thus allowing one to obtain a more universal indicator (in terms of the dimensionless change of fractal dimension of a microstructural image of a drying product) of physical/structural changes of foods and biomaterials during drying (Kerdpi boon et al., 2006; Kerdpi boon and Devahastin, 2007; Kerdpi boon et al., 2007). In addition, a means to monitor non-uniform product deformation was proposed and tested. It was found that the use of the so-called Heywood shape factor was effective in describing non-uniform product deformation (Panyawong and Devahastin, 2007). This indicator was also found to correlate well with the drying kinetics data, allowing indication of different changes during different periods of drying.

In the second part of the study, experiments were performed to study the effects of LPSSD and other drying techniques on nutritive quality of foods. This included the study of β -carotene isomerization (Hiranvarachat et al., 2008) and degradation (Suvarnakuta et al., 2005) in carrot, ascorbic acid degradation in Indian gooseberry (Methakhup et al., 2005) and the study of the effects of drying methods and tea preparation temperature on the vitamin C content in Indian gooseberry tea

(Kongsoontornkijkul et al., 2006). In almost all cases, LPSSD performed better than other competing technologies, i.e., hot air drying and vacuum drying, in preserving the nutritive quality of the products. This is due to the oxygen-free environment of LPSSD, which prevented oxidative degradation of active compounds during drying.

The following part of the study involved the use of LPSSD and appropriate physical or chemical pretreatment methods to produce health snack viz. fat-free potato chip (Leeratanarak et al., 2006; Pimpaporn et al., 2007; Kingcam et al., 2008). By blanching (to achieve starch gelatinization) and freezing (to achieve starch retrogradation) potato slices prior to LPSSD, it was possible to obtain potato chips that had only slightly inferior quality to commercially available fried chips. The results illustrated feasibility of LPSSD as an alternative to deep-fat frying to produce potato chip. Further work is underway to improve the quality of LPSSD chip.

The fourth part investigated various means to enhance LPSSD, both from the drying kinetics and product quality points of view. The use of far-infrared radiation (FIR) as an additional heat source to augment drying was attempted and found to be successful (Nimmol et al., 2007a). In addition to being able to speed up drying the use of FIR also induced more vigorous vaporization of moisture within a food product, thus creating more porous structure within the dried product. This helped improve the texture of the dried product (banana chips) significantly, especially in terms of the hardness and crispness (Nimmol et al., 2007b), which are two important parameters affecting the consumer preference of a snack product. The enhanced product porosity was also evident from the X-ray microtomographic results; both the average total porosity and the pore size distribution moved towards the directions of higher and larger sizes, respectively (Léonard et al., 2008).

The use of intermittent drying, i.e., supplying either energy or vacuum only intermittently instead of doing so continuously, was also investigated and was found helpful in conserving the energy for LPSSD. The quality of a heat- and oxygen-sensitive product viz. banana slice was found to be insignificantly different or, in some cases, even better than that obtained via the continuous drying process (Thomkapanish et al., 2007).

Finally, the use of LPSSD to produce edible films for active packaging applications was investigated. It was found that LPSSD could produce edible films with superior mechanical properties to films produced by other conventional drying methods (Mayachiew and Devahastin, 2008a). The effects of different drying methods on the

retention and release behavior of active compounds, i.e., galangal and Indian gooseberry extracts, which have been shown to have high antimicrobial and antioxidant activities, respectively (Mayachiew and Devahastin, 2008b), will also be investigated.

2. Materials and Methods

Please refer to appropriate papers in the Appendix for detailed Materials and Methods used in the project.

3. Results and Discussion

Please refer to appropriate papers in the Appendix for detailed Results and Discussion of the various studies mentioned earlier.

4. Conclusion

Please refer to appropriate papers in the Appendix for detailed Conclusion of the various studies mentioned earlier.

5. References

- Hiranvarachat, B., Suvarnakuta, P., Devahastin, S., 2008, "Isomerization Kinetics and Antioxidant Activities of β -Carotene in Carrots Undergoing Different Drying Techniques and Conditions," *Food Chemistry*, 107(4), pp. 1538-1546.
- Kerdpi boon, S., Kerr, W.L., Devahastin, S., 2006, "Neural Network Prediction of Physical Property Changes of Dried Carrot as a Function of Fractal Dimension and Moisture Content," *Food Research International*, 39(10), pp. 1110-1118.
- Kerdpi boon, S., Devahastin, S., 2007, "Fractal Characterization of Some Physical Properties of a Food Product under Various Drying Conditions," *Drying Technology*, 25(1), pp. 135-146.
- Kerdpi boon, S., Devahastin, S., Kerr, W.L., 2007, "Comparative Fractal Characterization of Physical Changes of Different Food Products during Drying," *Journal of Food Engineering*, 83(4), pp. 570-580.
- Kingcam, R., Devahastin, S., Chiewchan, N., 2008, "Effect of Starch Retrogradation on Texture of Potato Chips Produced by Low-Pressure Superheated Steam Drying," *Journal of Food Engineering*, 89(1), pp. 72-79.

- Kongsoontornkijkul, P., Ekwongsupasarn, P., Chiewchan, N., Devahastin, S., 2006, "Effects of Drying Methods and Tea Preparation Temperature on the Amount of Vitamin C in Indian Gooseberry Tea," *Drying Technology*, 24(11), pp. 1509-1513.
- Leeratanarak, N., Devahastin, S., Chiewchan, N., 2006, "Drying Kinetics and Quality of Potato Chips Undergoing Different Drying Techniques," *Journal of Food Engineering*, 77(3), pp. 635-643.
- Léonard, A., Blacher, S., Nimmol, C., Devahastin, S., 2008, "Effect of Far Infrared Radiation Assisted Drying on Microstructure of Banana Slices: An Illustrative Use of X-Ray Microtomography in Microstructural Evaluation of a Food Product," *Journal of Food Engineering*, 85(1), pp. 154-162.
- Mayachiew, P., Devahastin, S., 2008a, "Comparative Evaluation of Physical Properties of Edible Chitosan Films Prepared by Different Drying Methods," *Drying Technology*, 26(2), pp. 176-185.
- Mayachiew, P., Devahastin, S., 2008b, "Antimicrobial and Antioxidant Activities of Indian Gooseberry and Galangal Extracts," *LWT – Food Science and Technology*, 41(7), pp. 1153-1159.
- Methakhup, S., Chiewchan, N., Devahastin, S., 2005, "Effects of Drying Methods and Conditions on Drying Kinetics and Quality of Indian Gooseberry Flake," *LWT – Food Science and Technology*, 38(6), pp. 579-587.
- Nimmol, C., Devahastin, S., Swasdisevi, T., Soponronnarit, S., 2007a, "Drying and Heat Transfer Behavior of a Food Product Undergoing Combined Low-Pressure Superheated Steam and Far-Infrared Radiation Drying," *Applied Thermal Engineering*, 27(14&15), pp. 2483-2494.
- Nimmol, C., Devahastin, S., Swasdisevi, T., Soponronnarit, S., 2007b, "Drying of Banana Slices Using Combined Low-Pressure Superheated Steam and Far-Infrared Radiation," *Journal of Food Engineering*, 81(3), pp. 624-633.
- Panyawong, S., Devahastin, S., 2007, "Determination of Deformation of a Food Product Undergoing Different Drying Methods and Conditions via Evolution of a Shape Factor," *Journal of Food Engineering*, 78(1), pp. 151-161.
- Pimpaporn, P., Devahastin, S., Chiewchan, N., 2007, "Effects of Combined Pretreatments on Drying Kinetics and Quality of Potato Chips Undergoing Low-Pressure Superheated Steam Drying," *Journal of Food Engineering*, 81(2), pp. 318-329.

- Suvarnakuta, P., Devahastin, S., Mujumdar, A.S., 2007, "A Mathematical Model for Low-Pressure Superheated Steam Drying of a Biomaterial," *Chemical Engineering and Processing*, 46(7), pp. 675-683.
- Suvarnakuta, P., Devahastin, S., Mujumdar, A.S., 2005, "Drying Kinetics and β -Carotene Degradation in Carrot Undergoing Different Drying Processes," *Journal of Food Science*, 70(8), pp. S520-S526.
- Thomkapanish, O., Suvarnakuta, P., Devahastin, S., 2007, "Study of Intermittent Low-Pressure Superheated Steam and Vacuum Drying of a Heat-Sensitive Material," *Drying Technology*, 25(1), pp. 205-223.

Outputs of the Project

I. Refereed papers in international journals (18 papers)

Group I Fundamental study of LPSSD for food products

1. Suvarnakuta, P., Devahastin, S., Mujumdar, A.S., 2007, "A Mathematical Model for Low-Pressure Superheated Steam Drying of a Biomaterial," *Chemical Engineering and Processing*, 46(7), pp. 675-683 (IF = 1.129).
2. Kerdpi boon, S., Devahastin, S., 2007, "Fractal Characterization of Some Physical Properties of a Food Product under Various Drying Conditions," *Drying Technology*, 25(1), pp. 135-146 (IF = 1.100).
3. Kerdpi boon, S., Devahastin, S., Kerr, W.L., 2007, "Comparative Fractal Characterization of Physical Changes of Different Food Products during Drying," *Journal of Food Engineering*, 83(4), pp. 570-580 (IF = 1.696).
4. Panyawong, S., Devahastin, S., 2007, "Determination of Deformation of a Food Product Undergoing Different Drying Methods and Conditions via Evolution of a Shape Factor," *Journal of Food Engineering*, 78(1), pp. 151-161 (IF = 1.696).
5. Kerdpi boon, S., Kerr, W.L., Devahastin, S., 2006, "Neural Network Prediction of Physical Property Changes of Dried Carrot as a Function of Fractal Dimension and Moisture Content," *Food Research International*, 39(10), pp. 1110-1118 (IF = 1.652).

Group II Study of the effects of drying methods on quality of food products

1. Hiranvarachai, B., Suvarnakuta, P., Devahastin, S., 2008, "Isomerization Kinetics and Antioxidant Activities of β -Carotene in Carrots Undergoing Different Drying Techniques and Conditions," *Food Chemistry*, 107(4), pp. 1538-1546 (IF = 2.433).
2. Kongsoontornkijkul, P., Ekwongsupasarn, P., Chiewchan, N., Devahastin, S., 2006, "Effects of Drying Methods and Tea Preparation Temperature on the Amount of Vitamin C in Indian Gooseberry Tea," *Drying Technology*, 24(11), pp. 1509-1513 (IF = 1.100).
3. Suvarnakuta, P., Devahastin, S., Mujumdar, A.S., 2005, "Drying Kinetics and β -Carotene Degradation in Carrot Undergoing Different Drying Processes," *Journal of Food Science*, 70(8), pp. S520-S526 (IF = 1.004).
4. Methakhup, S., Chiewchan, N., Devahastin, S., 2005, "Effects of Drying Methods and Conditions on Drying Kinetics and Quality of Indian Gooseberry Flake," *LWT – Food Science and Technology*, 38(6), pp. 579-587 (IF = 1.299).

Group III Use of LPSSD and related technologies to produce health snacks

1. Kingcam, R., Devahastin, S., Chiewchan, N., 2008, "Effect of Starch Retrogradation on Texture of Potato Chips Produced by Low-Pressure Superheated Steam Drying," *Journal of Food Engineering*, 89(1), pp. 72-79 (IF = 1.696).
2. Pimpaporn, P. Devahastin, S., Chiewchan, N., 2007, "Effects of Combined Pretreatments on Drying Kinetics and Quality of Potato Chips Undergoing Low-Pressure Superheated Steam Drying," *Journal of Food Engineering*, 81(2), pp. 318-329 (IF = 1.696).
3. Leeratanarak, N., Devahastin, S., Chiewchan, N., 2006, "Drying Kinetics and Quality of Potato Chips Undergoing Different Drying Techniques," *Journal of Food Engineering*, 77(3), pp. 635-643 (IF = 1.696).

Group IV Enhancement of LPSSD

1. Nimmol, C., Devahastin, S., Swasdisevi, T., Soponronnarit, S., 2007, "Drying and Heat Transfer Behavior of a Food Product Undergoing Combined Low-Pressure Superheated Steam and Far-Infrared Radiation Drying," *Applied Thermal Engineering*, 27(14&15), pp. 2483-2494 (IF = 0.814).
2. Nimmol, C., Devahastin, S., Swasdisevi, T., Soponronnarit, S., 2007, "Drying of Banana Slices Using Combined Low-Pressure Superheated Steam and Far-Infrared Radiation," *Journal of Food Engineering*, 81(3), pp. 624-633 (IF = 1.696).
3. Thomkapanich, O., Suvarnakuta, P., Devahastin, S., 2007, "Study of Intermittent Low-Pressure Superheated Steam and Vacuum Drying of a Heat-Sensitive Material," *Drying Technology*, 25(1), pp. 205-223 (IF = 1.100).
4. Léonard, A., Blacher, S., Nimmol, C., Devahastin, S., 2008, "Effect of Far Infrared Radiation Assisted Drying on Microstructure of Banana Slices: An Illustrative Use of X-Ray Microtomography in Microstructural Evaluation of a Food Product," *Journal of Food Engineering*, 85(1), pp. 154-162 (IF = 1.696).

Group V Production of advanced material using LPSSD

1. Mayachiew, P., Devahastin, S., 2008, "Comparative Evaluation of Physical Properties of Edible Chitosan Films Prepared by Different Drying Methods," *Drying Technology*, 26(2), pp. 176-185 (IF = 1.100).
2. Mayachiew, P., Devahastin, S., 2008, "Antimicrobial and Antioxidant Activities of Indian Gooseberry and Galangal Extracts," *LWT – Food Science and Technology*, 41(7), pp. 1153-1159 (IF = 1.299).

II. Papers presented at international conferences (6 papers)

1. Jinorose, M., Devahastin, S., 2007, "Describing Deformation during Drying Using Indicators Calculated from External and Microstructural Changes of a Food Product," *Proceedings of the 5th Asia-Pacific Drying Conference*, Hong Kong, pp. 158-165.
2. Léonard, A., Blacher, S., Devahastin, S., 2007, "Characterization of Dried Banana Porous Structure by X-Ray Microtomography Coupled with Image Analysis," *Proceedings of the 5th Asia-Pacific Drying Conference*, Hong Kong, pp. 197-202.
3. Mayachiew, P., Devahastin, S., 2007, "Characterization of Edible Chitosan Films Prepared by Different Drying Methods," *Proceedings of the 5th Asia-Pacific Drying Conference*, Hong Kong, pp. 1011-1018.
4. Hiranvarachat, B., Suvarnakuta, P., Chiewchan, N., Devahastin, S., 2007, "Determination of Isomerization Kinetics of β -Carotene in Carrots Undergoing Different Drying Techniques and Conditions," *Proceedings of the 5th Asia-Pacific Drying Conference*, Hong Kong, pp. 1019-1024.
5. Kerdpi boon, S., Devahastin, S., 2006, "Use of Fractal Analysis to Monitor Physical Property Changes of Biomaterials under Various Drying Conditions," *Proceedings of the 15th International Drying Symposium*, Budapest, Hungary, pp. 547-553.
6. Mujumdar, A.S., Devahastin, S., 2005, "Recent Advances in Drying Technologies for Roots," *2nd International Symposium on Sweet Potato and Cassava*, Kuala Lumpur, Malaysia (invited).

II. Book chapters (2 chapters)

1. Jinorose, M., Devahastin, S., Blacher, S., Léonard, A., "Application of Image Analysis in Food Drying," in C. Ratti (Ed.) *Advances in Food Dehydration*, CRC Press, Boca Raton. (*In press*, to appear in 2008).
2. Devahastin, S., Suvarnakuta, P., "Low-Pressure Superheated Steam Drying of Food Products," in X.D. Chen and A.S. Mujumdar (Eds.) *Drying Technologies for Food Processing*, Wiley-Blackwell, Oxford. (*In press*, to appear in 2008).

Contents

Acknowledgements	i
Abstract	ii
บทคัดย่อ	iii
Contents	iv
1. Introduction	1
2. Materials and Methods	3
3. Results and Discussion	3
4. Conclusion	3
5. References	3
Outputs of the Project	6
Appendix	9
I. Refereed papers in international journals	
<u>Group I</u> Fundamental study of LPSSD of food products	
<u>Group II</u> Study of the effects of drying methods on quality of food products	
<u>Group III</u> Use of LPSSD and related technologies to produce health snacks	
<u>Group IV</u> Enhancement of LPSSD	
<u>Group V</u> Production of advanced material using LPSSD	
II. Papers presented at international conferences	
III. Book chapters	

Antimicrobial and antioxidant activities of Indian gooseberry and galangal extracts

Pornpimon Mayachiew, Sakamon Devahastin*

Department of Food Engineering, King Mongkut's University of Technology Thonburi, 126 Pracha u-tid Road, Bangkok 10140, Thailand

Received 19 June 2007; received in revised form 26 July 2007; accepted 26 July 2007

Abstract

The antimicrobial and antioxidant activities of Indian gooseberry (*Phyllanthus emblica* Linn.) and galangal (*Alpinia galanga*) extracts were investigated. Two different methods (disc diffusion and agar dilution methods) were employed to evaluate the antimicrobial activities of plant extracts against *Staphylococcus aureus*. The minimum inhibitory concentration (MIC) values of Indian gooseberry and galangal extracts were found to be 13.97 and 0.78 mg/ml and the minimum biocidal concentration (MBC) values were 13.97 and 2.34 mg/ml, respectively. The antioxidant activities of Indian gooseberry and galangal extracts, which were evaluated by the β -carotene bleaching method, were 86.4% and 70.3%, respectively. The total phenolic contents of Indian gooseberry and galangal extracts, as determined by the Folin–Ciocalteu method, were 290.4 ± 0.7 and 40.9 ± 0.2 mg/g plant extract (in GAE), respectively. The GC–MS analysis showed that the main compounds of galangal extract are 1,8-cineole (20.95%), β -bisabolene (13.16%), β -caryophyllene (17.95%) and β -selinene (10.56%). On the other hand, the use of high-performance liquid chromatography (HPLC) with UV detection indicated many compounds within the Indian gooseberry extract.

© 2007 Swiss Society of Food Science and Technology. Published by Elsevier Ltd. All rights reserved.

Keywords: GC–MS; Minimum inhibitory concentration; Natural antioxidants; *Staphylococcus aureus*; Total phenolic contents; UV–HPLC

1. Introduction

Herbs and spices are known for their antimicrobial and antioxidative properties. Due to an increasing demand for natural food additives, herbs and spices have emerged as popular ingredients and have a tendency of replacing synthetic antimicrobial and antioxidant agents. Generally, essential oils of spices possess strong antibacterial properties against foodborne pathogens and contain high concentrations of phenolic compounds (Burt, 2004; Delaquis, Stanich, Girard, & Mazza, 2002; Nevas, Korhonen, Lindström, Turkki, & Korkeala, 2004). These compounds exhibit a wide range of biological effects, including antioxidant properties.

Indian gooseberry (*Phyllanthus emblica* Linn.) or “Ma-khaam Pom” in Thai or “Amla” in Hindi is one of the most often used herbs and is widely available in most tropical and

subtropical countries. Its fruit is reputed to probably have the highest content of vitamin C compared with any other naturally occurring substances in nature. Active extracts of *P. emblica* have been shown to possess several pharmacological properties, e.g., analgesic, anti-inflammatory, antioxidant and chemoprotective activities (Khan et al., 2002).

Galangal (*Alpinia galanga*) or “Kha” in Thai has traditionally been used as spice in Thai foods. This spice is, like other spices, rich in phenolic compounds such as flavonoids and phenolic acids. In Thailand, galangal is used for medical purposes such as carminative, stomachic, antispasmodic, antiphlogistic and antibacterial drugs. Galangal is also readily available and inexpensive in Thailand. Among the predominant bacteria involved in food-borne diseases, *Staphylococcus aureus* is one of the leading causes of gastroenteritis resulting from the consumption of contaminated foods. Staphylococcal food poisoning is due to the absorption of staphylococcal enterotoxins in foods. *S. aureus* is an important pathogen due to a combination of toxin-mediated virulence,

*Corresponding author. Tel.: +66 2 470 9246; fax: +66 2 470 9240.

E-mail address: sakamon.dev@kmutt.ac.th (S. Devahastin).

invasiveness and antibiotic resistance (Jablonski & Bohach, 2001).

Since food processors and consumers have expressed a desire to reduce the use of synthetic chemicals in food preservation, common culinary herbs and spices that exhibit antimicrobial and antioxidant activities could be a source of natural alternatives. Although herbs and spices in Thailand, including Indian gooseberry and galangal, contain potent antimicrobials and antioxidants, they have not been sufficiently tested for their activities. The aims of the present investigation were therefore to assess the antimicrobial and antioxidant activities of Indian gooseberry and galangal, which are common plants of Thailand. From our preliminary study, it was found that Indian gooseberry and galangal juices exhibited very low antimicrobial and antioxidant activities, hence only the ethanolic extracts of these plants were investigated in the present study. The antimicrobial activities of the extracts were determined by the disc diffusion and agar dilution methods, while the antioxidant activities were determined by the β -carotene bleaching method. The chemical composition of the galangal extract and of its fractions was studied using gas chromatography–mass spectrometry (GC–MS). The composition of the Indian gooseberry extract was determined by the UV-high performance liquid chromatography (HPLC).

2. Materials and methods

2.1. Chemicals

Ascorbic acid was purchased from Riedel-de-Haën (Seelze, Germany). Linoleic acid, β -carotene and gallic acid were obtained from Fluka (Buchs, Switzerland). Folin–Ciocalteu reagent, orthophosphoric acid, sodium carbonate and absolute ethyl alcohol were purchased from Carlo Erba (Vigevano, Italy) while polyoxyethylene (20) sorbitan monolaurate (Tween 20) was obtained from BDH (Dorset, England). Methanol and acetonitrile were of HPLC grade and were purchased from Lab-Scan Analytical Sciences (Bangkok, Thailand). For antimicrobial tests Tryptic Soy Agar (TSA), Tryptic Soy Broth (TSB), Mueller Hinton agar (MHA) and buffer peptone water were purchased from Difco (Detroit, USA).

2.2. Materials

Indian gooseberry fruits (*P. emblica* Linn.) and galangal (*A. galanga*) rhizomes were purchased from a local market. The Indian gooseberry fruits were first washed thoroughly to remove impurities. After washing the fruits were cut into small pieces and dried overnight in a tray dryer at 40 °C. They were then ground with a blender (Waring, model HGB2WT, Torrington, CT) to make a powder. For preparation of galangal, the fresh rhizomes were cleaned, washed with water, cut into small pieces and dried in a tray

dryer at 40 °C, after which they were ground in a blender to make a powder.

2.3. Extraction procedures

To prepare Indian gooseberry extract, the dried Indian gooseberry powder (10 g dry basis) was extracted with 50 ml of 95% ethanol (Ahmad, Mehmood, & Mohammad, 1998). The extract was filtered through a filter paper (Ø110 mm, Cat. no. 1001 110, Schleicher and Schuell GmbH, Dassel, Germany); the filtrate was collected and concentrated in a rotary evaporator (Resona Technics, Labo Rota 300, Gossau, Switzerland) at 40 °C for 10 min and kept at 4 °C until its use.

The dried galangal powder (10 g dry matter) was extracted with 100 ml of 95% ethanol (Oonmetta-aree, Suzuki, Gasaluck, & Eumkeb, 2006) and left at room temperature overnight. The extract was filtered through a filter paper (Ø110 mm, Cat. no. 1001 110, Schleicher and Schuell GmbH, Dassel, Germany); the filtrate was collected and concentrated by the rotary evaporator at 40 °C for 15 min and kept at 4 °C until its use.

2.4. Antimicrobial activity evaluation

2.4.1. Microbial culture

S. aureus (ATCC 25923) was obtained from the Department of Medical Sciences, Ministry of Public Health, Thailand. The microorganism was maintained in TSA at 5 °C. Stock culture of *S. aureus* was grown in TSB at 37 °C for 18 h at 160 rpm (cell in early stationary phase). The maximum level of the microorganism was 10^{10} CFU/ml; the concentration was subsequently adjusted to 10^8 CFU/ml using buffer peptone water.

2.4.2. Disc diffusion method

The agar diffusion method was employed for screening of the antimicrobial activities of the extracts. Briefly, a suspension of the tested microorganism (0.1 ml of 10^8 CFU/ml) was spread on the MHA. Filter paper discs (6 mm in diameter) were soaked with 15 μ l of the extracts and placed on the inoculated plates (Vardar-Ünlü et al., 2003). After being kept at 4 °C for 2 h, the plates were incubated at 37 °C for 24 h. The diameters of the inhibition zones were then measured in millimeters. All experiments were performed in duplicate.

2.4.3. Agar dilution method

A series of two-fold dilutions of each extract, ranging from 20 to 0.1 ml/l, were prepared in MHA with 5 ml/l Tween 20. Plates were dried at 37 °C for 30 min prior to inoculation with 1–2 μ l spots containing approximately 10^4 CFU of microorganism (Hammer, Carson, & Riley, 1999). MHA, with 5 ml/l Tween 20 but with no extracts, was used as a positive growth control. Inoculated plates were incubated at 37 °C. The minimum inhibitory concentration (MIC) was determined as the lowest concentration

of each extract that completely inhibited growth of microorganism up to 24 h, whereas the minimum bactericidal concentration (MBC) was the lowest concentration at which no growth was observed after incubation up to 5 days. All experiments were performed in duplicate.

2.5. Antioxidant activity evaluation

2.5.1. β -Carotene bleaching method

The antioxidant activity of each extract was examined by the β -carotene bleaching method following a modification of the procedures described by Juntachote and Berghofer (2005). Two milligrams of β -carotene was dissolved in 20 ml of chloroform. A 3 ml aliquot of the solution was put into a 50 ml beaker; 40 mg of linoleic acid and 400 mg of Tween 20 were then added. Chloroform was removed by purging with nitrogen. One hundred milliliters of oxygenated distilled water, which was prepared by aerating air bubble into distilled water for 1 h, was added into the β -carotene emulsion and mixed well by using a vortex mixer (Scientific Industries, model G-560, Bohemia, NY). Three milliliters of aliquot of the oxygenated β -carotene emulsion and 0.12 ml of each ethanolic plant extract were placed in test tubes and mixed thoroughly. The tubes were immediately placed in a water bath and incubated at 50 °C. Oxidation of β -carotene emulsion was monitored spectrophotometrically by measuring the absorbance at 470 nm via a Shimadzu UV-2101 spectrophotometer (Shimadzu Scientific Instruments, model UV-2101 PC, Kyoto, Japan). Absorbance was measured at 0, 10, 20, 30 and 40 min. A control sample was prepared by using 0.12 ml of ethanol instead of the ethanolic extracts. Degradation rate of the extracts was calculated according to the first-order kinetics using:

$$\text{Sample degradation rate} = \ln \frac{a}{b} \times \frac{1}{t}, \quad (1)$$

where a is the initial absorbance (470 nm) at time zero; b is the absorbance (470 nm) at 40 min; t is time (min).

The antioxidant activity (AA) was expressed as % inhibition relative to the control using:

$$\text{AA} = \frac{\text{degradation rate of control} - \text{degradation rate of sample}}{\text{degradation rate of control}} \times 100. \quad (2)$$

All experiments were performed in duplicate.

2.6. Total phenolic contents

The total phenolic contents of each extract were determined using the Folin–Ciocalteu reagent (Zhou & Yu, 2006). The reaction mixture contained 50 μ l of Indian gooseberry or galangal extract, 250 μ l of the Folin–Ciocalteu reagent, 0.75 ml of 20 g/100 ml sodium carbonate and 3 ml of pure water. After 2 h of reaction at ambient temperature, the absorbance at 765 nm was measured and used to calculate the phenolic contents using gallic acid as a standard. The total phenolic contents were then expressed

as gallic acid equivalent (GAE), in mg/g dry sample. All experiments were performed in duplicate.

2.7. GC–MS analysis

The chemical compositions of the galangal extract were determined by the GC–MS analysis. The extract was dissolved in ethanol at the concentration of 10 mg/ml and the volume of the injected sample was 1 μ l. A Hewlett–Packard 6890 combined GC–MS (Hewlett–Packard Co., Wilmington, MA) was used for the analysis. The capillary column HP-5 (30 m \times 0.25 mm; phase thickness, 0.25 μ m) was used and the temperature was first held at 40 °C (2 min) and then raised to 250 °C (5 min) at a rate of 10 °C/min. The carrier gas was helium at a flow rate of 0.9 ml/min. The components of the extract were recognized by the retention time of the chromatogram peaks and by their mass spectra. The identities of the main component peaks were confirmed by comparison of their retention time with that of reference compounds using Wiley, NIST libraries as well as mass spectra databases (Nevás et al., 2004).

2.8. HPLC analysis

The HPLC analysis method that was used to isolate compounds of Indian gooseberry extract was described by Kumaran and Joel Karunakaran (2006). Indian gooseberry extract was dissolved in methanol (1 mg/ml) and filtered through a nylon syringe filter (0.45 μ m) (Filtrex Technology, Singapore) and 10 μ l aliquots of the filtrate were injected to HPLC. The standard solutions of ascorbic acid and gallic acid were prepared in methanol (1 mg/ml).

The components of Indian gooseberry extract were characterized by HPLC (Varian Chromatography Systems, model Pro Star, Walnut Creek, CA) with a Prevail™ reverse phase C₁₈ column (4.6 mm \times 250 mm; 5 μ m) (Alltech, Deerfield, IL). The HPLC system consists of a pump (ProStar, model 240, Walnut Creek, CA), a photodiode array detector (ProStar, model 335, Walnut Creek, CA) and an autosampler (ProStar, model 410, Walnut Creek, CA). A gradient elution at 1 ml/min with a gradient program was performed by varying the portion of solvent A to solvent B (0–6 min 5% B, 6–15 min 15% B, 15–35 min 20% B, 35–40 min 40% B). A 0.05% H₃PO₄ (concentrated, 85%) in water was used as solvent A and acetonitrile as solvent B in order to resolve peaks in the sample. UV detection was carried out at a wavelength of 220 nm. Injection volume was 10 μ l. Standard ascorbic acid and gallic acid were used for the identification of the components in the Indian gooseberry extract.

3. Results and discussion

3.1. Antimicrobial activities of extracts

The *in vitro* antimicrobial activities of Indian gooseberry and galangal extracts against *S. aureus* and their activity

potentials were qualitatively and quantitatively assessed by the presence or absence of inhibition zones, zone diameters, MIC and MBC values. The results given in Table 1 show that galangal extract had greater potential as an antimicrobial agent against *S. aureus* than did Indian gooseberry extract. The maximum inhibition zones, MIC and MBC values for *S. aureus* were 21.8 ± 0.6 mm, 13.97 mg/ml and 13.97 mg/ml for Indian gooseberry extract and 29 ± 0.6 mm, 0.78 mg/ml and 2.34 mg/ml for galangal extract, respectively.

The antimicrobial nature of the galangal extract is apparently related to the components shown in the GC–MS analysis as will be discussed in detail later. Several components of galangal probably acted as antimicrobial agents. 1,8-Cineole, the main component of galangal extract, has been previously reported to have an antibacterial activity against *S. aureus* (Gachkar et al., 2007).

As reported by Canillac and Mourey (2001), if the MBC/MIC ratio is found to be less than or equal to 4, the strain is considered to be susceptible; on the other hand, if this ratio is greater than 4, the strain is considered to be tolerant. From our results, MBC/MIC ratios of Indian gooseberry and galangal extracts were less than 4, so *S. aureus* was considered to be sensitive to these extracts.

3.2. Antioxidant activities of extracts

The antioxidant activity of the extracts was determined based on the coupled oxidation of β -carotene and linoleic acid. Antioxidant activity is expressed as percent inhibition relative to the control. As seen in Table 2, the antioxidant activities of Indian gooseberry and galangal extract were 86.4% and 70.3%, respectively. Indian gooseberry extract exhibited stronger antioxidant activity than did galangal extract. This is because of the different antioxidative compounds in the two extracts.

Phenolic compounds and some of their derivatives are very efficient in preventing auto-oxidation. The antioxidant

activities of phenolic compounds are mainly of redox properties, which include free radical scavenging, hydrogen donating and singlet oxygen quenching. Since Indian gooseberry is rich in tannins and phenolic compounds, these compounds acted effectively as the antioxidant agents. The better antioxidative results might also correlate to the higher total phenolic contents (see next section) in Indian gooseberry extract as well.

3.3. Total phenolic contents

The amounts of the total phenolic contents of Indian gooseberry and galangal extracts were 290.4 ± 0.7 and 40.9 ± 0.2 mg/g plant extract or 130.8 ± 0.34 and 4.7 ± 0.02 mg/g dry sample, respectively (Table 2). Indian gooseberry extract possessed much higher total phenolic contents than did galangal extract. The total phenolic contents of Indian gooseberry extract in this study are similar to the result of Kumaran and Joel Karunakaran (2007), who reported that the total phenols in *Phyllanthus* species are in the range of 171–380 mg/g plant extract (in GEA). However, the total phenolic contents data of galangal are not available elsewhere.

Phenolic compounds contribute to the overall antioxidant activities of herbs and spices. Generally, the mechanisms of phenolic compounds for antioxidant activity are inactivating lipid free radicals and preventing decomposition of hydroperoxides into free radicals. Kumar, Nayaka, Dharmesh, and Salimath (2006) found that gallic acid and tannic acid, in phenolic fraction, are major antioxidant compounds of *P. emblica*.

Antimicrobial and antioxidant activities of plant extracts correlated well with their phenolic fraction. Puupponen-Pimiä, Nohynek, Alakomi, and Oksman-Caldentey (2005) indeed reported that bioactive compounds such as phenolics and organic acids have antimicrobial activities against human pathogens, e.g., *Salmonella* and *Staphylococcus*.

3.4. Identification of galangal extract compounds

Through the use of the GC–MS, the main compounds of galangal extract were found to consist of 1,8-cineole (20.95%), β -caryophyllene (13.16%), β -bisabolene (17.95%) and β -selinene (10.56%), whereas α -selinene (9.67%), farnesene (7.47%), 1,2-benzenedicarboxylic acid (6.42%), germacrene B (6.10%) and pentadecane (2.70%) are the minor components (Table 3). Each component has different retention time; the characterization of individual components was performed with the mass spectrometry (Fig. 1). 1,8-Cineole is an oxygenated monoterpenes, while β -caryophyllene is a sesquiterpene. In addition, β -bisabolene and β -selinene are terpenes. Mallavarapu et al. (2002) also reported similar main compounds in galangal, i.e., 1,8-cineole, α -fenchyl acetate and camphor; they reported 1,8-cineole as the main component of galangal. However, the composition of galangal in this study differs from that described by other authors (Mallavarapu et al., 2002; Oonmetta-aree et al.,

Table 1
Antimicrobial activity of plant extracts against *S. aureus*

Type of plant	Inhibition zone (mm)	MIC (mg/ml)	MBC (mg/ml)
Indian gooseberry	21.8 ± 0.6	13.97	13.97
Galangal	29 ± 0.6	0.78	2.34

Table 2
Antioxidant activity and total phenolic contents of plant extracts

Type of plant	Antioxidant activity (%)	Total phenolic contents	
		mg/g extract	mg/g dry sample
Indian gooseberry	86.4 ± 1.1	290.4 ± 0.7	130.8 ± 0.34
Galangal	70.3 ± 0.8	40.9 ± 0.2	4.7 ± 0.02

Table 3
Chemical compositions of *Alpinia galanga* essential oil

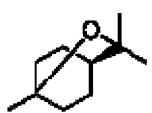
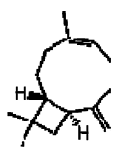

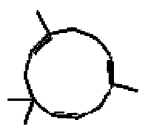
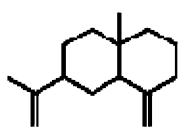

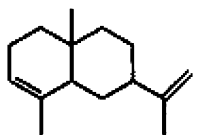
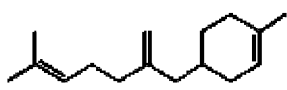
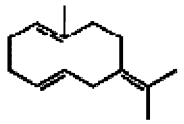
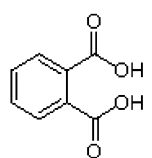
No.	Composition	% Composition	RT
1	1,8-cineole	20.95	8.81
2	 β-caryophyllene	13.16	16.68
3	 farnesene	7.47	17.19
4	 α-humulene	5.02	17.24
5	 β-selinene	10.56	17.77
6	 pentadecane	2.70	17.82
7	 α-selinene	9.67	17.90
8	 β-bisabolene	17.95	18.04
9	 germacrene B	6.10	18.86
			

Table 3 (continued)

No.	Composition	% Composition	RT
10	1,2-benzenedicarboxylic acid	6.42	19.24
			
	Total	100	

RT: retention time.

2006) because the composition of any plant essential oil is influenced by several factors such as planting, climatic, seasonal and experimental conditions (Daferera, Ziogas, & Polissiou, 2000).

The main components of galangal extract have a mechanism of action involving disruption of cytoplasmic membrane and coagulation of cell contents (Oonmetta-aree et al., 2006). 1,8-Cineole in the essential oil can inactivate against Gram-positive bacteria including *S. aureus* (Viljoen et al., 2003). Besides, the minor components might also have a critical part for action in antimicrobial activity, possibly by producing a synergistic effect between other components.

3.5. HPLC analysis of Indian gooseberry extract

The use of HPLC with UV detector at a wavelength of 220 nm along with a gradient elution program to identify compounds of the Indian gooseberry extract revealed many peaks in the chromatogram of the extract (Fig. 2). A comparison between the spectra of the sample peaks with those obtained from ascorbic acid and gallic acid standards confirmed that the retention time of ascorbic acid was 3.60 min (peak 1) while the retention time of gallic acid was 12.085 min (peak 4). The major peak (peak 3) and the second highest peak (peak 2) appeared at the retention time of 7.758 and 4.949 min, respectively. It is possible that these peaks belong to hydrolysable tannins because these compounds have high polarity due to the presence of hydroxyl group (Ghosal, Triethi, & Chauhan, 1996), which generally show as initial peaks of chromatograms.

Kumar et al. (2006) identified that gallic acid and tannic acid are the major phenolic acids of Indian gooseberry extract with 70% ethanol. Gallic acid was also found to be a major compound in the ethyl acetate extract of Indian gooseberry (Kumaran & Joel Karunakaran, 2006). These results do not agree with those of the present study, which shows that gallic acid is not the main compound of the extract, however.

In this study, it was found that the amount of ascorbic acid in Indian gooseberry extract was 11.21%, which is higher than the amount of ascorbic acid present in many Indian gooseberry products (dried fruits, processed fruits

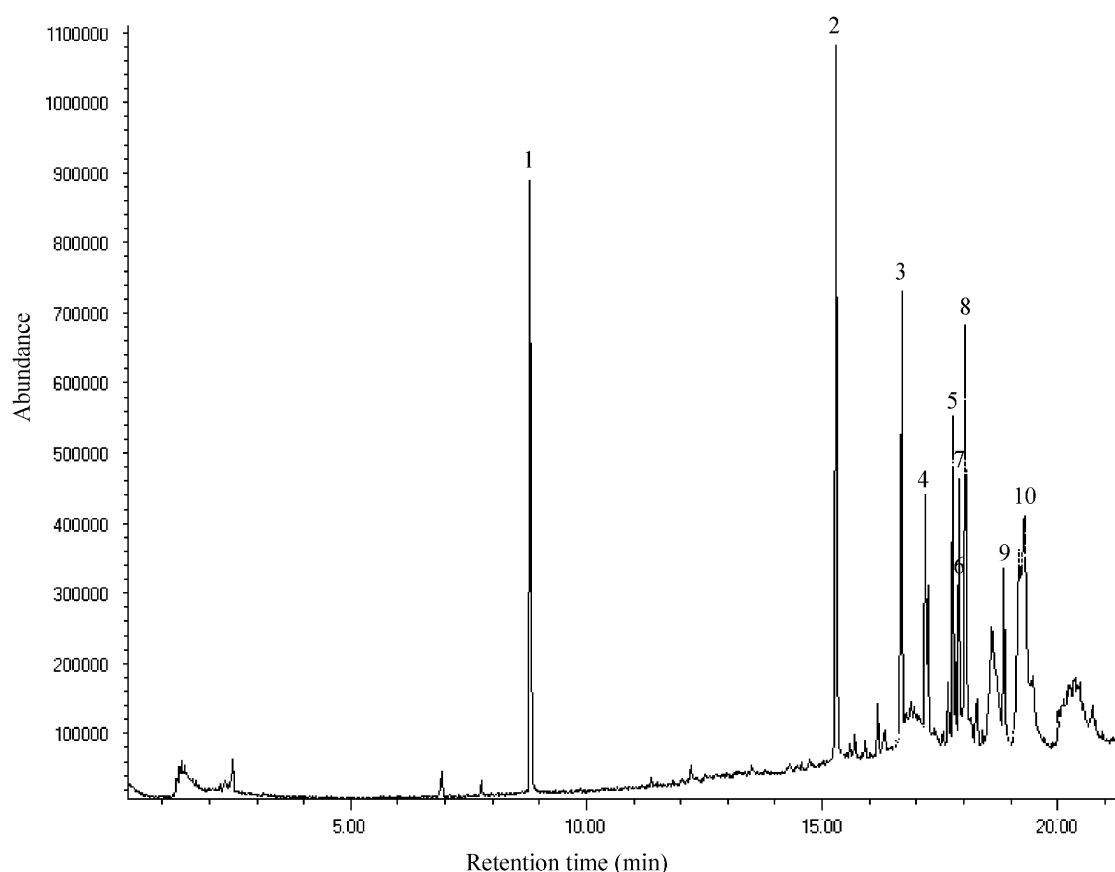


Fig. 1. Typical gas chromatograms of galangal extract: 1,8-cineole (1), β -caryophyllene (2), farnesene (3), α -humulene (4), β -selinene (5), pentadecane (6), α -selinene (7), β -bisabolene (8), germacrene B (9) and 1,2-benzenedicarboxylic acid (10).

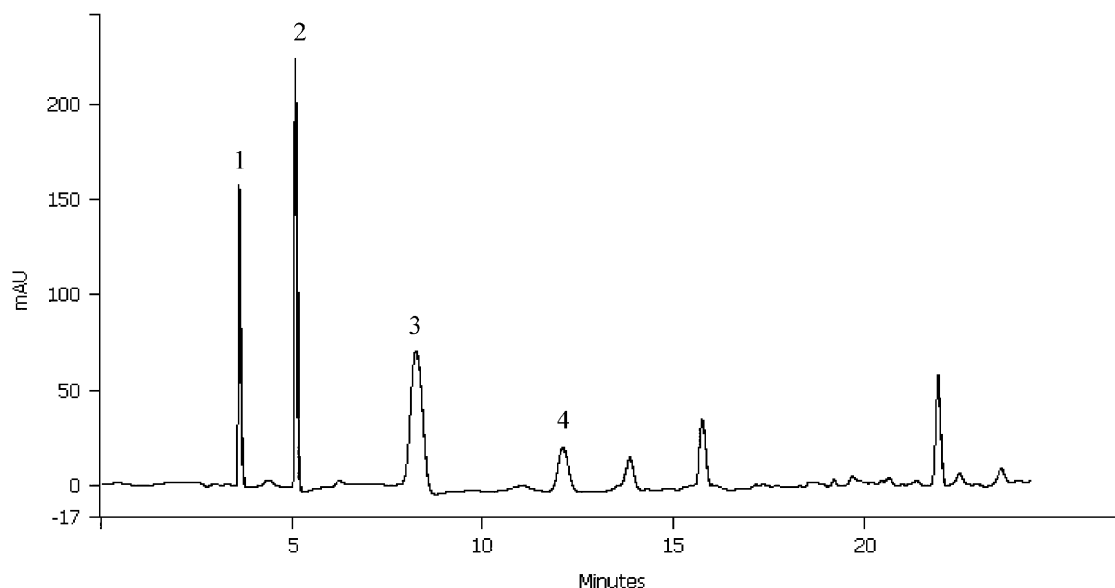


Fig. 2. HPLC chromatograms of Indian gooseberry extract at wavelength 220 nm: ascorbic acid (1), hydrolysable tannins (2, 3) and gallic acid (4).

and a commercial Merck extract); the amount of ascorbic acid is in the range of 0.37% in dried fruits to 2.0% in the Merck extract (Scartezzini, Antognoni, Raggi, Poli, & Sabbioni, 2006).

From the HPLC analysis results, it might be possible to conclude that ascorbic acid and other phenolic compounds contributed to the antioxidant activities of Indian gooseberry extract.

4. Conclusions

The antimicrobial and antioxidant activities of Indian gooseberry and galangal extracts were evaluated. These extracts showed good activity against the growth of food poisoning bacteria, *S. aureus*. In this study, both extracts were found to possess high antioxidant activities. However, Indian gooseberry extract was found to have higher total phenolic contents than did the galangal extract. The major compounds of galangal extract, which were identified by GC–MS, are 1,8-cineole, β -bisabolene, β -caryophyllene and β -selinene. Many phenolic compounds could be isolated from the Indian gooseberry extract through the use of UV-HPLC with C₁₈ column including ascorbic acid and gallic acid. The present study provides additional data for supporting the use of Indian gooseberry and galangal extracts as natural antimicrobial and antioxidant agents. Future work will be performed to encapsulate these extracts in edible films to prepare active packaging materials, which can release antimicrobial and antioxidant agents to extend the shelf life of foods.

Acknowledgments

The authors express their sincere appreciation to the Commission on Higher Education, the Thailand Research Fund (TRF) and the International Foundation for Science (IFS) in Sweden for their financial support.

References

- Ahmad, I., Mehmood, Z., & Mohammad, F. (1998). Screening of some Indian medical plants for their antimicrobial properties. *Journal of Ethnopharmacology*, 62, 183–193.
- Burt, S. (2004). Essential oils: Their antibacterial properties and potential applications in foods—A review. *International Journal of Food Microbiology*, 94, 223–253.
- Canillac, N., & Mourey, A. (2001). Antibacterial activity of the essential oil of *Picea excelsa* on *Listeria*, *Staphylococcus aureus* and coliform bacteria. *Food Microbiology*, 18, 261–268.
- Daferera, D. J., Ziogas, B. N., & Polissiou, M. G. (2000). GC–MS analysis of essential oils from Greek aromatic plants and their fungitoxicity on *Penicillium digitatum*. *Journal of Agricultural and Food Chemistry*, 48, 2576–2581.
- Delaquis, P. J., Stanich, K., Girard, S., & Mazza, G. (2002). Antimicrobial activity of individual and mixed fractions of dill, cilantro, coriander and eucalyptus essential oils. *International Journal of Food Microbiology*, 74, 101–109.
- Gachkar, L., Yadegari, D., Rezaei, M. B., Taghizadeh, M., Astaneh, S. A., & Rasooli, I. (2007). Chemical and biological characteristics of *Cuminum cyminum* and *Rosmarinus officinalis* essential oils. *Food Chemistry*, 102, 898–904.
- Ghosal, S., Triethi, V. K., & Chauhan, S. (1996). Active constituents of *Emblica officinalis*: Part 1—The chemistry and antioxidative effects of two new hydrolysable tannins, Emblicanin A and B. *Indian Journal of Chemistry*, 35, 941–948.
- Hammer, K. A., Carson, C. F., & Riley, T. V. (1999). Antimicrobial activity of essential oils and other plant extracts. *Journal of Applied Microbiology*, 86, 985–990.
- Jablonski, L. M., & Bohach, G. A. (2001). *Staphylococcus aureus*. In M. P. Doyle, L. R. Beuchat, & T. J. Montville (Eds.), *Food microbiology: Fundamentals and frontiers* (pp. 411–434). Washington, DC: ASM Press.
- Juntachote, T., & Berghofer, E. (2005). Antioxidative properties and stability of ethanolic extracts of Holy basil and Galangal. *Food Chemistry*, 92, 193–202.
- Khan, M. T. H., Lampronti, I., Martello, D., Bianchi, N., Jabbar, S., Choudhuri, M. S. K., et al. (2002). Identification of pyrogallol as an antiproliferative compound present in extracts from the medicinal plant *Emblica officinalis*: Effect on in vitro cell growth of human tumor cell lines. *International Journal of Oncology*, 20, 187–192.
- Kumar, G. S., Nayaka, H., Dharmesh, S. M., & Salimath, P. V. (2006). Free and bound phenolic antioxidants in amla (*Emblica officinalis*) and turmeric (*Curcuma longa*). *Journal of Food Composition and Analysis*, 19, 446–452.
- Kumaran, A., & Joel Karunakaran, R. (2006). Nitric oxide radical scavenging active components from *Phyllanthus emblica* L. *Plant Foods for Human Nutrition*, 61, 1–5.
- Kumaran, A., & Joel Karunakaran, R. (2007). In vitro antioxidant activities of methanol extracts of five *Phyllanthus* species from India. *Lebensmittel-Wissenschaft und-Technologie*, 40, 344–352.
- Mallavarapu, G. R., Rao, L., Ramesh, S., Dimri, B. P., Rao, B. R. R., Kaul, P. N., et al. (2002). Composition of the volatile oils of *Alpinia galanga* rhizomes and leaves from India. *Journal of Essential Oil Research*, 14, 397–399.
- Nevas, M., Korhonen, A.-R., Lindström, M., Turkki, P., & Korkeala, H. (2004). Antibacterial efficiency of Finnish spice essential oils against pathogenic and spoilage Bacteria. *Journal of Food Protection*, 67, 199–202.
- Oonmetta-aree, J., Suzuki, T., Gasaluck, P., & Eumkeb, G. (2006). Antimicrobial properties and action of galangal (*Alpinia galanga* Linn.) on *Staphylococcus aureus*. *Lebensmittel-Wissenschaft und-Technologie*, 39, 1214–1220.
- Puupponen-Pimiä, R., Nohynek, L., Alakomi, H.-L., & Oksman-Caldentey, K.-M. (2005). Bioactive berry compounds—Novel tools against human pathogens: Mini-review. *Applied Microbiology and Biotechnology*, 67, 8–18.
- Scartezzini, P., Antognoni, F., Raggi, M. A., Poli, F., & Sabbioni, C. (2006). Vitamin C content and antioxidant activity of the fruit and of the Ayurvedic preparation of *Emblica officinalis* Gaertn. *Journal of Ethnopharmacology*, 104, 113–118.
- Vardar-Ünlü, G., Candan, F., Sökmen, A., Daferera, D., Polissiou, M., Sökmen, M., et al. (2003). Antimicrobial and antioxidant activity of the essential oil and methanol extracts of *Thymus pectinatus* Fisch. et Mey. Var. *pectinatus* (Lamiaceae). *Journal of Agricultural and Food Chemistry*, 51, 63–67.
- Viljoen, A., van Vuuren, S., Ernst, E., Klepser, M., Demirci, B., Başer, H., et al. (2003). *Osmitopsis asteriscoides* (Asteraceae)—The antimicrobial activity and essential oil composition of a Cape-Dutch remedy. *Journal of Ethnopharmacology*, 88, 137–143.
- Zhou, K., & Yu, L. (2006). Total phenolic contents and antioxidant properties of commonly consumed vegetables grown in Colorado. *Lebensmittel-Wissenschaft und-Technologie*, 39, 1155–1162.

Fractal Characterization of Some Physical Properties of a Food Product under Various Drying Conditions

Soraya Kerdpi boon and Sakamon Devahastin

Department of Food Engineering, King Mongkut's University of Technology Thonburi, Bangkok, Thailand

The present work was aimed at monitoring and studying the relationship between microstructural changes of a food product and its physical property changes during two different types of drying; i.e., conventional hot air drying and low-pressure superheated steam drying, using fractal analysis. The external changes of a model food product, viz. carrot, which were represented in terms of the percentage of shrinkage and the rehydration behavior, correlated well with its microstructural changes, which were represented by the rate of change of the fractal dimension of the microstructural images. The changes of physical properties and microstructure of carrot could be divided into two periods, which are periods of uniform and nonuniform deformation. The microstructural changes of the samples undergoing different drying techniques were quite different, however. Fractal dimension of carrot undergoing drying increased with drying time for both hot air drying and low-pressure superheated steam drying cases. Fractal dimension was found to be a good indicator of the microstructural changes of a product undergoing different drying techniques and conditions.

Keywords Carrot; Fractal analysis; Hot air dryer; Low-pressure superheated steam dryer; Microstructure; Shrinkage; Structure-quality relationship

INTRODUCTION

During drying, physical properties of food change mainly because of the loss of its moisture. Attempts have been made to characterize these physical property changes in terms of such parameters as the changes in volume, area and shape.^[1–5] However, these external changes are caused by internal changes within the sample, which are directly related to the structure of the drying material.

Among many methods that could be used to describe the structural and physical changes of materials are illustrating and evaluating their microstructural changes using such optical instruments as light scanning microscope (LSM) and scanning electron microscope (SEM).^[6] These

microstructural images cannot be easily quantified without the use of other appropriate evaluation techniques, however. For example, Leonard et al.^[7] applied X-ray microtomography in combination with image analysis to evaluate the shrinkage and crack formation of a sample (wastewater sludge) during convective drying. They found a good relationship between the drying kinetics and crack development, which was caused by internal diffusion limitations leading to moisture gradients and mechanical stresses within the sample. Due to the usefulness of image analysis, some researchers have applied this technique in combination with the technique called fractals (or fractal analysis) to quantify property changes of different samples. Fractals have been used successfully to quantify, among others, the shapes of brain cells, gold colloids, sponge iron, etc.^[8,9]

Some researchers have used fractals to describe the microstructural changes and mechanical property changes of foods (via the description of the changes of images representing food surfaces) such as viscoelastic property changes of rice starch suspensions during gelatinization; stress cracks in grain kernel endosperm (corn kernel), which were caused by rapid drying at high temperatures; ruggedness of instant coffee after agglomeration; as well as ruggedness of restructured potato during deep fat frying, among others.^[10–13] Fractal dimension values are different depending on the dimension of images and equal to 1–2 if images are two-dimensional and 2–3 if images are three-dimensional.

Few attempts have been made so far in applying fractal analysis to describe or monitor the process of drying. Chanola et al.^[14] applied fractal analysis to the distributions of the surface temperature of a model food (a slab of a mixture of glucose syrup and agar gel) in order to monitor the drying kinetics of the sample. In addition, the evolution of the fractal dimension of the images of the sample surface was also monitored. Based on a fractal analysis of the surface temperature distributions, different periods of drying can be identified. It was also observed that the fractal dimension of the images of the sample surface increased with the drying time due to an increased

Correspondence: Sakamon Devahastin, Department of Food Engineering, King Mongkut's University of Technology Thonburi, 126 Pracha u-tid Road, Bangkok 10140, Thailand; E-mail: sakamon.dev@kmutt.ac.th

irregularity of the surface as drying proceeded. It was also noted that higher air temperatures and velocities led to higher values of fractal dimension of the surfaces. No attempt was made to use fractal analysis to monitor the change of physical properties of the sample, however.

This work investigated the use of fractal analysis to monitor changes of some properties; i.e., shrinkage and rehydration behavior of a food product undergoing different drying techniques, such as hot air drying and low-pressure superheated steam drying.^[15] A box counting method (BCM) was used to calculate the values of fractal dimension (FD) of microstructural images of a food product, viz. carrot. The values of FD were then related to shrinkage and rehydration behavior of carrot and to its drying kinetics. Correlations between the values of FD, in terms of the changes of FD after and before drying, and the two physical properties as well as the drying kinetics of the product were also assessed using Pearson's square correlation.

EXPERIMENTAL SETUP, MATERIALS AND METHODS

Experimental Setup

A schematic diagram of a hot air tray dryer (HAD) used in this study is presented in Fig. 1. It consists of a stainless steel drying chamber that is connected to an electric heater rated at 6.6 kW, which was used to heat up the air to the desired drying temperature. The heater was controlled by a PID temperature controller. Cubes of sample (carrot) were placed on a tray with dimensions of $30 \times 40 \text{ cm}^2$. Drying temperatures used were 60, 70, and 80°C and two air velocities of 0.5 and 1 m/s were used to dry the samples.

A schematic diagram of a low-pressure superheated steam dryer (LPSSD) and its accessories is shown in Fig. 2. The dryer consists of a stainless steel drying chamber with inner dimensions of $45 \times 45 \times 45 \text{ cm}^3$; a steam reservoir, which received the steam from the boiler and maintained its pressure at around 200 kPa (gauge); and a liquid ring vacuum pump (Nash, model ET32030, Trumbull, CT), which was used to maintain the vacuum in the drying chamber. A steam trap was installed to reduce the excess steam condensation in the reservoir. An electric

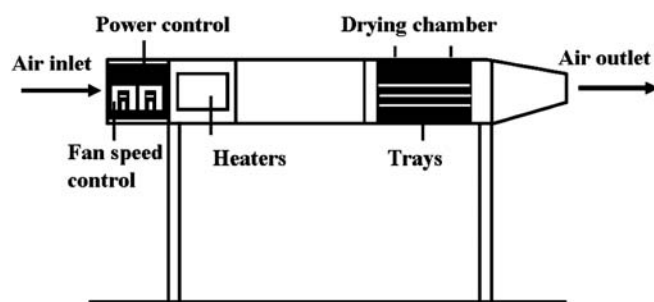


FIG. 1. A schematic diagram of a conventional hot air dryer.

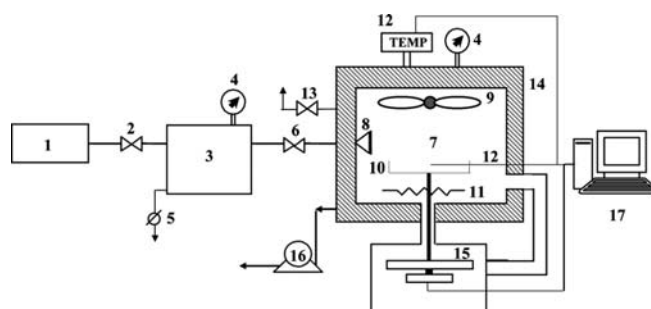


FIG. 2. A schematic diagram of low-pressure superheated steam dryer and associated units. 1, boiler; 2, steam valve; 3, steam reservoir; 4, pressure gauge; 5, steam trap; 6, steam regulator; 7, drying chamber; 8, steam inlet and distributor; 9, electric fan; 10, sample holder; 11, electric heater; 12, on-line temperature sensor and logger; 13, vacuum break-up valve; 14, insulator; 15, on-line weight indicator and logger; 16, vacuum pump; 17, PC with installed data acquisition card.

heater rated at 1.5 kW, which was controlled by a PID controller (Omron, model E5CN, Tokyo, Japan), was installed in the drying chamber to control the steam temperature and to minimize condensation of steam in the drying chamber during the start-up period. A variable-speed electric fan was used to disperse steam throughout the drying chamber. The sample holder was made of a stainless steel screen with dimensions of $12 \times 12 \text{ cm}^2$. The change of the mass of the sample was detected continuously (at 1-min intervals) using a load cell (Minebea, model Ucg-3kg, Nagano, Japan), which was installed in a smaller chamber connected to the drying chamber by a flexible hose (in order to maintain the same vacuum pressure as that in the drying chamber) and also to an indicator and recorder; A&D, model AD 4329, Tokyo, Japan). The temperatures of the steam and of the drying sample were measured continuously using type K thermocouples, which were connected to an expansion board (Omega Engineering, model no. EXP-32, Stamford, CT). Thermocouple signals were multiplexed to a data acquisition card (Omega Engineering, model no. CIO-DAS16JR., Stamford, CT) installed in a PC. Labtech Notebook software (Laboratory Technologies Corp. version 12.1, Andover, MA) was used to read and record the temperature data. Drying experiments were performed at an absolute pressure of 7 kPa and the drying temperatures of 60, 70, and 80°C .

Material

Fresh carrot (*Daucus carota* var. *sativa*) was obtained from a local supermarket and kept at 4°C . Prior to the start of each experiment, carrot was removed from the refrigerator to attain the room temperature. It was then peeled and sliced. In this work, samples were prepared using only the cortex tissues because different parts of carrot have different microstructures. The sliced carrot was diced into cubes with dimensions of $1 \times 1 \times 1 \text{ cm}^3$.

Methods

For each drying experiment, the drying process was carried out up to a predetermined sampling time; that particular experiment was terminated at that time. A new experimental run was then performed up to the next predetermined

sampling time; these steps were repeated until the complete drying curves (down to the equilibrium moisture content at each condition) were obtained. At the end of each experimental run, the sample was taken out to determine the moisture content,^[16] percentage of shrinkage, rehydration ratio, and microstructural changes. Approximately 100 cubes of carrot (about 100 g) were used in each one of the hot air drying experiments while approximately 35 cubes of carrot (about 35 g) were used in each one of the LPSSD experiments.

Measurement of Shrinkage and Rehydration Behavior

To study the physical property changes of carrot cube during drying, the percentage of shrinkage and rehydration ratio of the sample were selected as representative properties and were calculated as follows.

Shrinkage

Five carrot cubes were used for each shrinkage measurement. Shrinkage is expressed in terms of the percentage change of the volume of the sample as compared with its original volume.

$$\% \text{ shrinkage} = \left(\frac{V_i - V}{V_i} \right) \times 100 \quad (1)$$

where V_i and V are, respectively, the volumes of carrot at the beginning and at the end of each drying run. The average values of the percentage of shrinkage of five cubes were reported. All measurements were performed in duplicate.

Rehydration Ratio

The rehydration ratio (R) of the dried sample was determined by immersing the dried carrot cube in hot water at 100°C for 10 min. The sample was then drained and its masses, both before and after immersion, were measured with an electronic balance (accurate to ± 0.0001 g). The rehydration ratio of

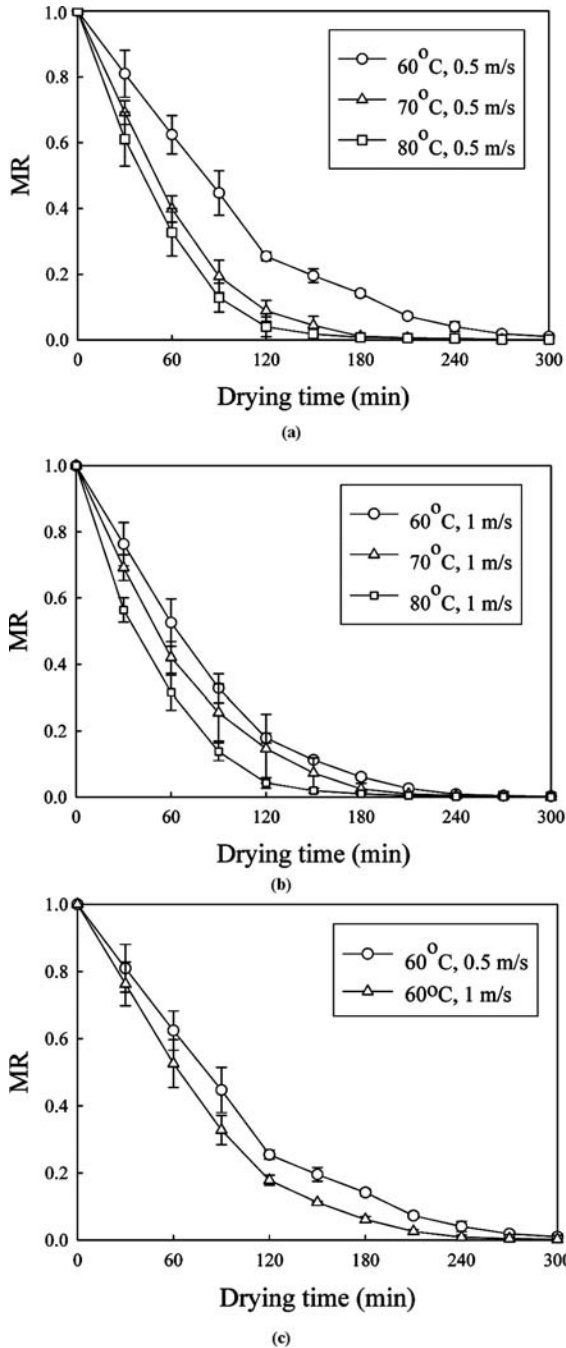


FIG. 3. Drying curves of carrot undergoing hot air drying at different drying conditions. $MR = (X - X_{eq}) / (X_i - X_{eq})$ where X = instantaneous moisture content (kg/kg, d.b.); X_{eq} and X_i are equilibrium and initial moisture contents (kg/kg, d.b.), respectively.

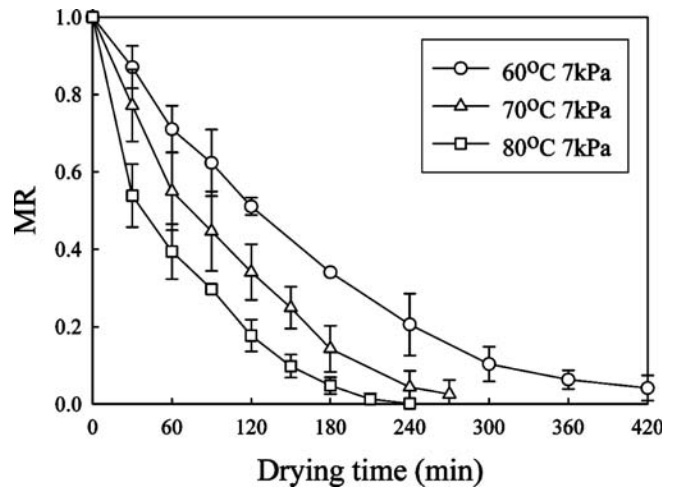


FIG. 4. Drying curves of carrot undergoing LPSSD at 7 kPa.

the dried carrot cube is calculated as:

$$R = \frac{M}{M_0} \quad (2)$$

where M_0 and M are, respectively, the masses of carrot before and after immersion in hot water. The average values of five cubes were reported and all measurements were performed in duplicate.

Measurement of Microstructural Changes and Image Processing

Microstructural Imaging

To obtain microstructural images of a drying sample the sample was taken from each type of dryer at every 30-min interval. The sample was preserved with 10% (V/V) formaldehyde prior to passing through the remaining steps. The sample was subsequently soaked with flowing distilled water for 20 min before removing the remaining moisture within the sample cells by flushing the sample with a series of isopropyl alcohol solutions of different concentrations, starting with 50, 70, 95, 95, 95, 100, 100, and 100% (V/V), respectively. The sample was flushed with isopropyl alcohol from lower to higher concentrations to prevent the damage of the cell structure, which might occur from the sudden loss of moisture. Isopropyl alcohol within the sample was then removed by flushing the sample with absolute xylene for two times. The time used for flushing the sample with each concentration of isopropyl alcohol and absolute

xylene was approximately 90 min per solution. Finally, the pores of the sample were replaced with paraffin by dipping the sample in melted paraffin at 60°C.^[17] Only the sample whose pores were fully replaced with paraffin could be sectioned by a microtome, however. If the pores of the sample were not fully replaced with paraffin, the sample must be dipped in melted paraffin at 60°C again.

Treated sample was then embedded in paraffin wax, which has a melting point in the range of 58–59°C. The steps for preparing an embedded sample started from pouring heated paraffin wax into a stainless steel box with dimensions of $30 \times 24 \times 5 \text{ mm}^3$ to about one third of the box. The sample was then placed at the middle of the stainless steel box and covered with a plastic embedded ring. Finally, liquid paraffin was poured to fully fill the box.

The embedded sample was sectioned by a microtome (Jung, model RM2025, Germany) into a 5- μm thick slice. The sliced sample was placed on a glass slide; 95% ethanol was dropped indirectly to the sliced sample to expand the cell tissue. Ethanol was then eliminated by floating the sliced sample in water at 42–43°C and removing the sliced sample immediately to the glass slide. The sliced sample was dried at room temperature and then fixed on a glass slide with the use of a hotplate set at temperature of 48–50°C for 8 h. The finished slide was dyed by haematoxylin and eosin to highlight the cell walls. Finally, the microstructural images were obtained using a light microscope (Olympus, model LH30RF200, Japan) at 10 \times magnification level.

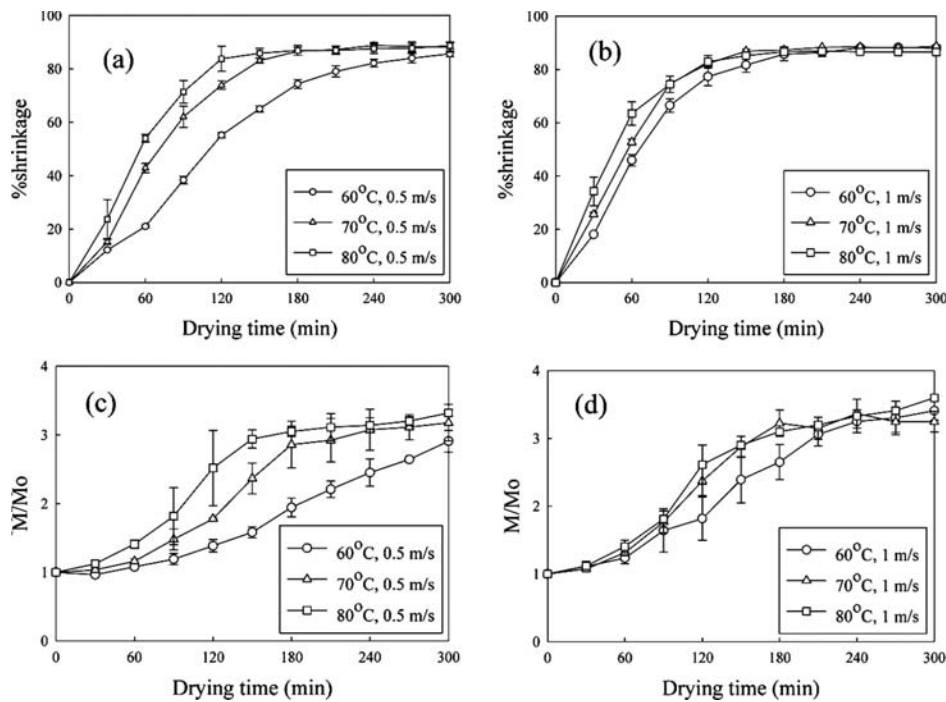


FIG. 5. Percentage of shrinkage ((a) and (b)) and rehydration ratio ((c) and (d)) of carrot undergoing conventional hot air drying.

Image Processing

A light microscopic image of the sample was captured by a Pixel View capture (Pixel View Program, Play TV/USBpro, Taiwan) at an image size of 520×520 pixels. The image was then transformed from an RGB format to a black-and-white format before a calculation of the fractal dimension (FD) was performed.

Fractal Dimension (FD) Calculation

The fractal dimension of a black-and-white image obtained as described in the previous section was calculated using the box counting method^[18] at the box sizes of 4, 5, 10, 13, 26, 65, 130, and 260 pixels and threshold values of 0.5–0.8 using Matlab[™] Software (version 6.5). The value of the threshold used for each image was chosen as the lowest value that could yield clearest the cell walls of

the sample. Ten light microscopic images were captured for one sample obtained at each sampling time.

To compare the changing values of FD of the sample undergoing drying, the normalized change of FD is reported as:

$$\Delta FD / FD_0 \quad (3)$$

$$\Delta FD = FD_t - FD_0 \quad (4)$$

where FD_0 and FD_t are, respectively, the fractal dimension of fresh sample and the fractal dimension of the sample at any instant during drying.

The correlations between FD and the drying kinetics and between FD and the physical property changes were determined by Pearson's correlation coefficient. Pearson's

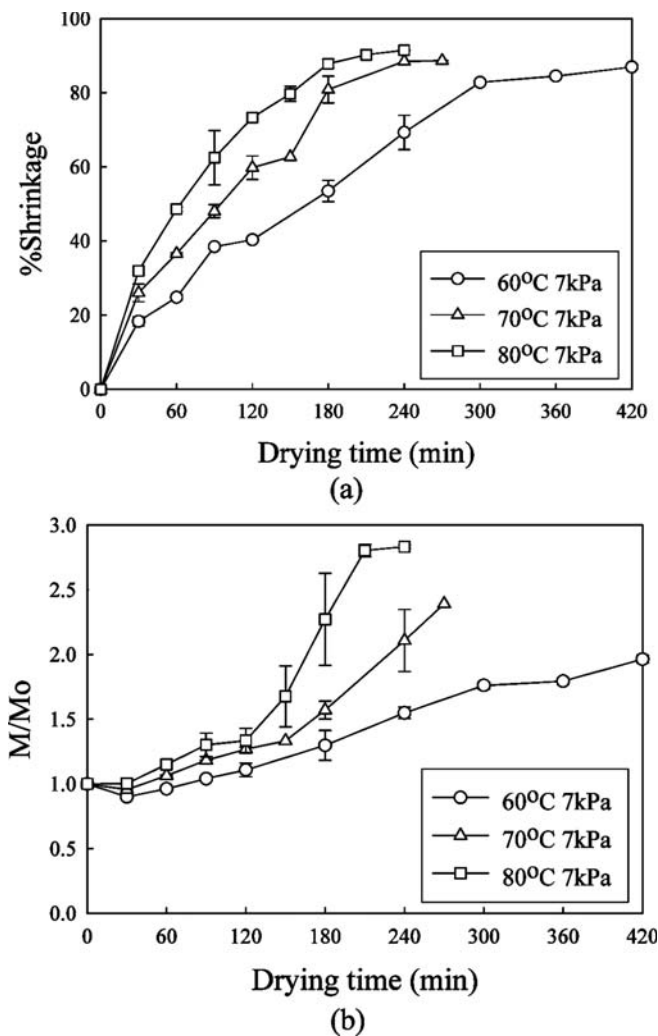


FIG. 6. Percentage of shrinkage (a) and rehydration ratio (b) of carrot undergoing LPSSD.

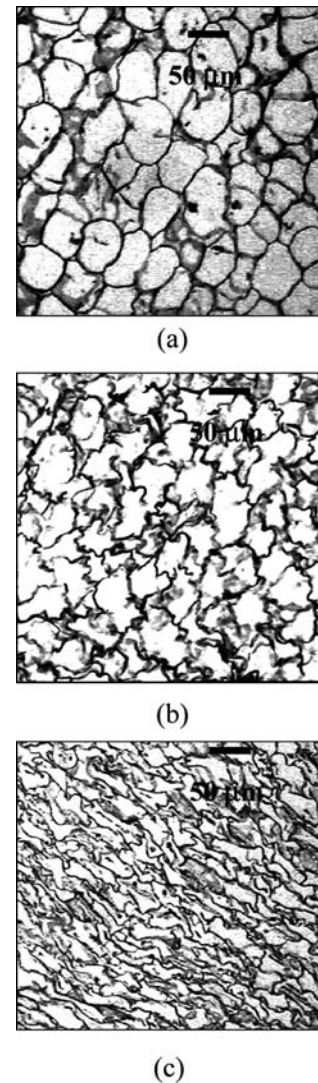


FIG. 7. Microstructure of carrot underwent hot air drying at 60°C, 0.5 m/s at 0 min (a), 150 min (b), and 300 min (c).

correlation coefficient (r) is a measure of the degree of linear relationship between two variables and the correlation coefficient may take on any values between plus and minus one; the sign of the correlation coefficient (+, -) is the direction of the relationship. A positive correlation coefficient means the values of both variables change in the same direction and vice versa. The absolute value of the coefficient illustrates the closeness of the relationship between the two variables.^[19]

RESULTS AND DISCUSSION

Drying Kinetics of Carrot Cube

Fresh carrot that had initial moisture content around 88–90% w.b. (or about 8.9–9 kg/kg d.b.) was dried until reaching its equilibrium moisture content of about 7%

w.b. (or about 0.07 kg/kg d.b.). The drying kinetics of carrot cube undergoing HAD are shown in Figs. 3a and 3b. It was found, as expected, that higher temperatures led to higher drying rates of the samples. The samples reached their equilibrium moisture contents after 300, 240, 210, 180, 180, and 150 min of drying for the cases when using drying air temperatures and velocities of 60°C, 0.5 m/s; 60°C, 1 m/s; 70°C, 0.5 m/s; 70°C, 1 m/s; 80°C, 0.5 m/s; and 80°C, 1 m/s, respectively. The effect of drying air velocity on the drying kinetics of carrot cubes is shown in Fig. 3c.

For all drying conditions tested, no constant rate period was observed; if a constant rate period existed it should be shorter than 30 min, since the first sample was taken only after 30 min. Moreover, moisture migration might be

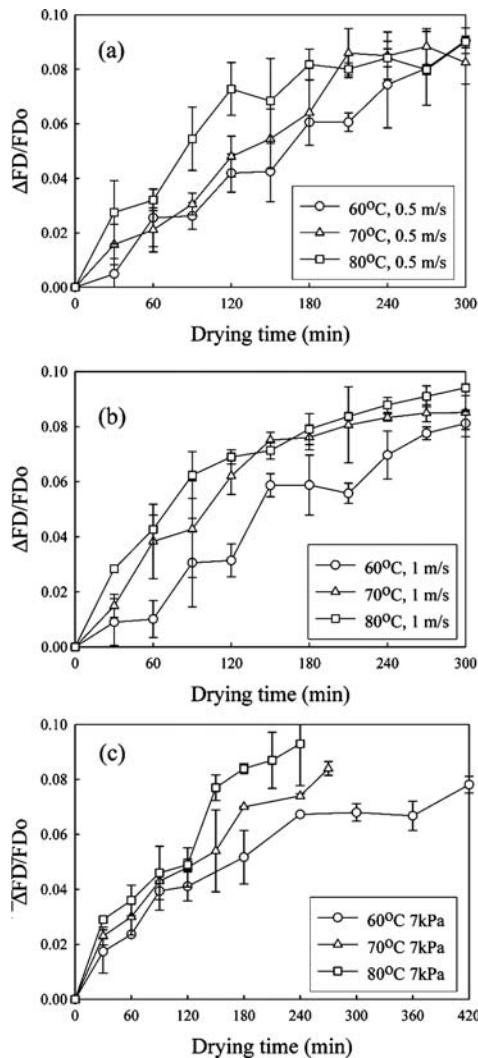


FIG. 8. $\Delta FD/FD_0$ of carrot cube undergoing hot air drying (velocity of 0.5 m/s (a) and 1 m/s (b)) and LPSSD at 7 kPa (c).

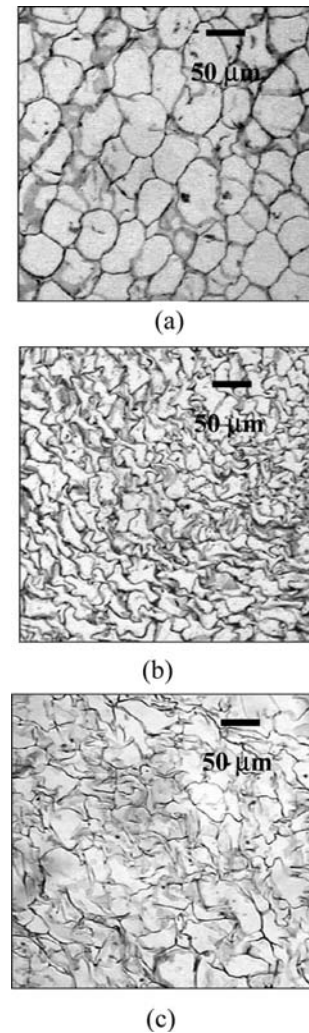


FIG. 9. Microstructure of fresh carrot (a) and of carrot dried until reaching equilibrium moisture content using hot air drying (b) and LPSSD (c).

resisted due to the collapse at the surface of the sample. Similar results were also reported by Doymaz^[20] and Prakash et al.^[21] In each case, there exist two falling rate periods. Initially, the moisture content decreased more rapidly because moisture gradients within the sample were still large and hence led to faster movement of moisture. For instance, carrot sample dried in an HAD at 60°C

and 0.5 m/s was in the first falling rate period until 120 min. Then it was in the second falling rate period until reaching equilibrium moisture content at 300 min (Fig. 3c).

Figure 4 illustrates the drying kinetics of carrot cube undergoing LPSSD. The trends of the results are the same as those of HAD; i.e., higher drying temperatures led to higher rates of drying. Carrots reached their equilibrium moisture contents after 450, 270, and 240 min when drying were performed at 60, 70, and 80°C at an absolute pressure of 7 kPa, respectively. It was found that the average drying rates over the whole period of drying in the case of LPSSD were lower than those of HAD at the same

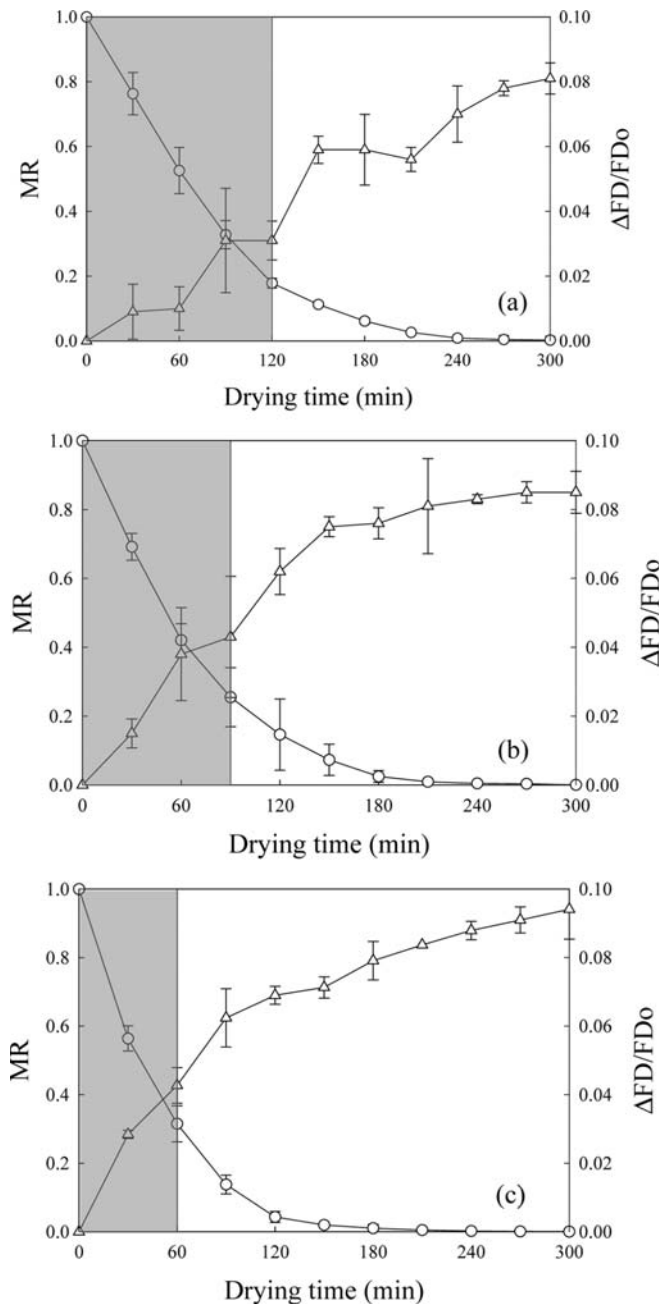


FIG. 10. Relationship between drying kinetics (o) and $\Delta FD/FD_0$ (Δ) of carrot undergoing hot air drying at velocity of 1 m/s and temperature of 60°C (a), 70°C (b), and 80°C (c).

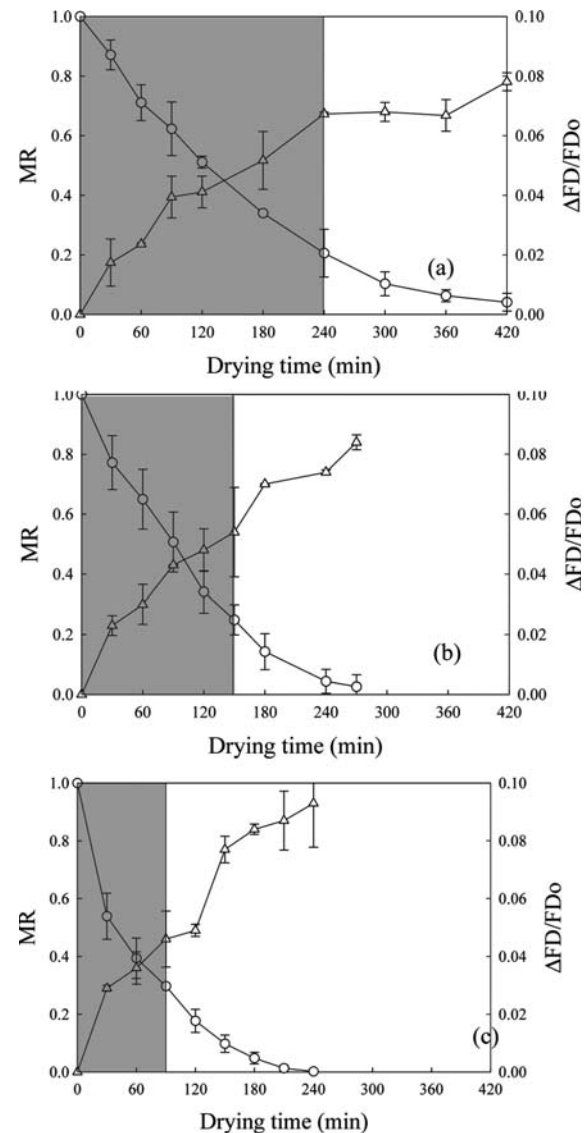


FIG. 11. Relationship between drying kinetics (o) and $\Delta FD/FD_0$ (Δ) of carrot undergoing LPSSD at temperature of 60°C (a), 70°C (b), and 80°C (c).

drying temperature. This is because the heat transfer driving forces were higher in the case of HAD than in the case of LPSSD over the range of drying temperatures investigated. The chamber of an LPSSD might also be more humid than that of an HAD and hence led to lower driving forces for mass transfer as well.

Physical Property Changes of Carrot Cube

Percentage of shrinkage and rehydration ratio of carrot cube undergoing HAD are shown in Fig. 5. As for shrinkage (Figs. 5a and 5b), it increased with the drying time. Moreover, at the same sampling time, samples undergoing drying at higher temperatures suffered more shrinkage than those undergoing drying at lower temperatures. This is because the drying temperature directly affected the shrinkage property of the product; larger moisture gradients within the sample developed when using higher drying temperatures and these larger gradients led to larger

internal stresses that in turn led to larger degrees of shrinkage.^[15] Moreover, the shape of dried carrot samples was not uniform, indicating that the deformation of the sample was not uniform.^[5]

It was observed that initially the percentage of shrinkage increased rapidly and then increased slowly until reaching the final values at the time corresponding to the point where the samples reached their equilibrium moisture contents. This trend applied to both drying techniques (Figs. 5a and 5b for HAD and Fig. 6a for LPSSD). The drying time that divided the period of shrinkage into the rapid increase and slow increase (and then constant) was the same as the time that divided the drying curves into the first falling and second falling rate periods (Figs. 3 and 4). Toward the end of drying, case-hardened skin developed and this inhibited further shrinkage of the sample.

It can be seen in Fig. 5 that the samples undergoing HAD at higher temperatures had higher rates of shrinkage

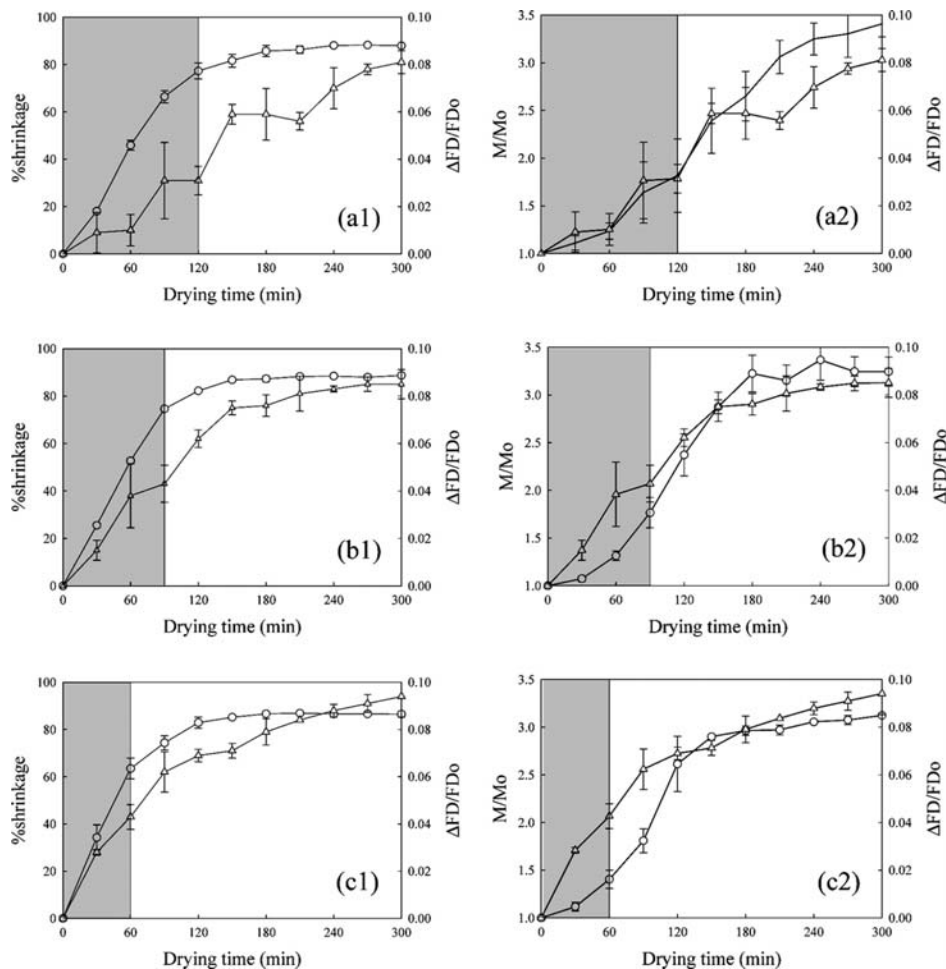


FIG. 12. Relationship between % shrinkage (o) and $\Delta FD/FD_o$ (Δ); rehydration ratio (o) and $\Delta FD/FD_o$ (Δ) of carrot undergoing hot air drying at velocity of 1 m/s temperature of 60°C (a), 70°C (b), and 80°C (c).

than those of samples undergoing drying at lower temperatures. This is because the results were compared at the same sampling periods, not at the same moisture contents. The trends of the results of LPSSD (Fig. 6a) were also the same as those of HAD.

Comparing the two drying techniques, it was found that carrot cubes dried using LPSSD had lower percentage of shrinkage than that of HAD. This is because superheated steam drying is known to have a potential to reduce the degree of shrinkage of the drying product due to evolution of water vapor inside the product that expands into cells, leading to a normally porous dried product.^[15,22,23]

As for the rehydration ratio, higher drying temperatures led to products with higher rehydration ratios. Higher rehydration ratios were observed in carrot cubes dried using either HAD or LPSSD at 80°C than those dried at lower temperatures (Figs. 5c and 5d for HAD and Fig. 6b for LPSSD). This is because the samples that were dried at lower temperatures needed a longer time to achieve their equilibrium moisture contents than those dried at higher

temperatures; the samples therefore suffered more structural damage (e.g., collapse of porous structure) than when drying at lower temperatures. The capability to reconstitute samples that underwent high-temperature drying was therefore higher than those that underwent low-temperature drying.

Microstructural Changes of Carrot Cube

The images used for microstructural analysis were observed from a light microscope at 10× magnification. After capturing the images from the light microscope, the images were used for fractal dimension calculation.

The fractal dimension of fresh carrot (Fig. 7a) was about 1.75, whereas the fractal dimension of the samples increased upon drying. Initially, the cell walls of carrot were of round shape. After some period of time, however, moisture within the cells started to migrate to the surface. Moisture gradients thus started to develop and these led to internal stresses and shrinkage of the cells (Figs. 7b

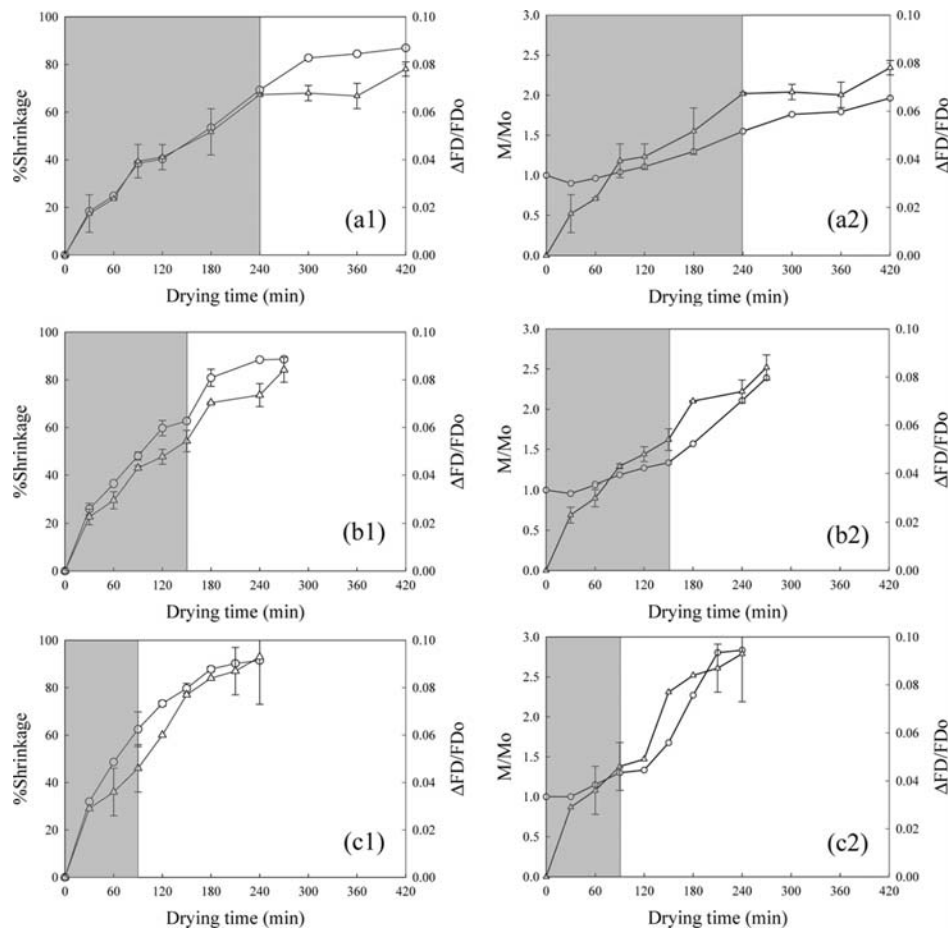
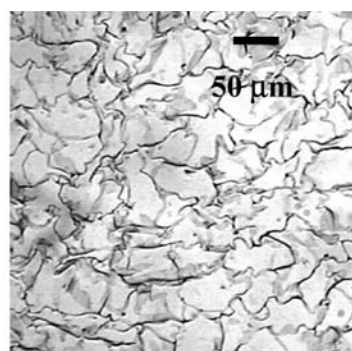


FIG. 13. Relationship between % shrinkage (o) and $\Delta FD/FD_0(\Delta)$; rehydration ratio (o) and $\Delta FD/FD_0(\Delta)$ of carrot undergoing LPSSD at temperature of 60°C (a), 70°C (b), and 80°C (c).

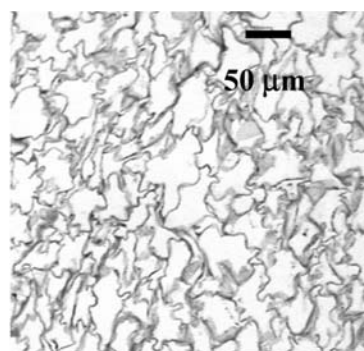
and 7c). The ruggedness of cell walls increased the fractal dimension of cell walls, as expected.

The microstructural changes of carrot cube undergoing drying are illustrated in terms of $\Delta FD/FD_0$ because this ratio represents the rate of change of fractal dimension of the sample undergoing each drying technique and hence could be used when comparing results of different drying processes and conditions.

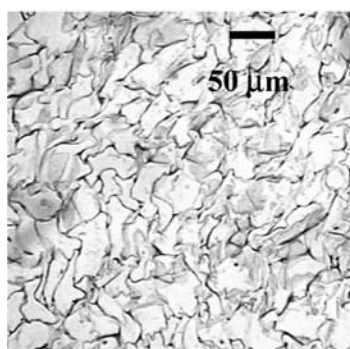
The rates of change of fractal dimension of carrot samples undergoing HAD (Figs. 8a and 8b) and LPSSD (Figure 8c) were monitored. It was found that the rates of change of the fractal dimension could be divided roughly into two periods; one is linear and the other nonlinear. The rates of fractal dimension change of carrot cubes undergoing HAD and LPSSD increased linearly during the first period of drying and increased slowly until reaching the



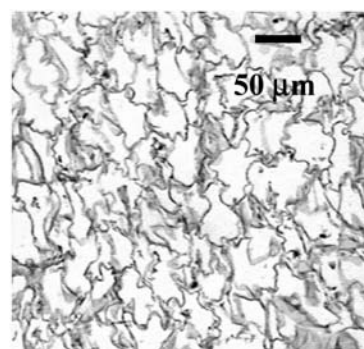
LPSSD, 60°C, 210 min



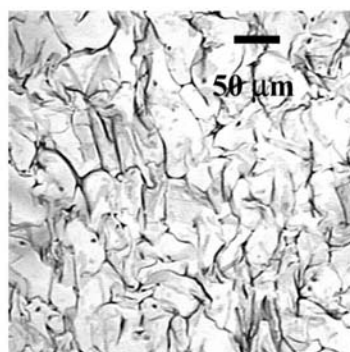
HAD, 60°C, 1 m/s, 150 min



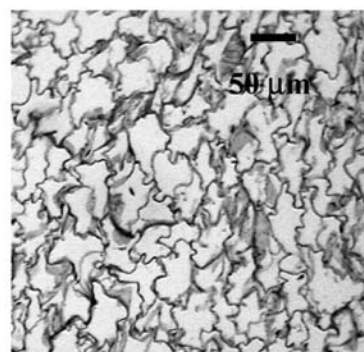
LPSSD, 70°C, 150 min



HAD, 70°C, 1m/s, 120 min



LPSSD, 80°C, 120 min



HAD, 80°C, 1m/s, 90 min

FIG. 14. Images of carrot at $\Delta FD/FD_0 = 0.06$.

constant rates of change. The drying time that identified the end point of the period where the rates of fractal dimension changed in a linear fashion was also the same as the drying time that divided the drying curves into the first and second falling rate periods and that divided the property changes (in terms of the percentage of shrinkage and rehydration ratio) into rapid increase and slow increase periods, respectively.

The microstructural changes of cell walls of carrot undergoing different drying techniques and conditions are quite different (Fig. 9). Carrots that were dried using HAD suffered more deformation of cell structure than in the case of LPSSD. This is because in HAD, cell structure was damaged directly from the hot air, whereas in LPSSD there was an evolution of vapor inside the cell structure that expanded into cells, leading to a porous dried product.^[14,15]

Relationship between FD and Physical Property Changes of Carrot Cube

As mentioned earlier, the rates of change of fractal dimension could be divided into two periods. During the first falling rate period, although the rate of moisture migration from the internal cells to the surface was not equal to the rate of moisture evaporation from the surface to the surrounding, these rates might not be much different to cause significant gradients within the sample; therefore, linear changes of fractal dimension were observed. When samples were dried further, the migration of moisture from the cells to the surface was slower than from the surface to the surrounding and this led to larger gradients, which in turn led to microstructural changes and deformation.

Drying time (Figs. 10 and 11) that divided the rates of change of fractal dimension into linear periods and nonlinear periods correlated well with the changes of physical properties, especially the percentage of shrinkage (Figs. 12 and 13). The time that the rates of change of

fractal dimension switched from the linear to nonlinear periods was the same as the point where the drying curves changed from the first falling rate period to the second falling rate period. Moreover, it was the same point where the percentage of shrinkage started to vary nonlinearly as well. The percentage of shrinkage, which represents the external changes of the samples, correlated well with the rates of change of fractal dimension, which represents the microstructural (or internal) changes of the samples.

The normalized change of fractal dimension could be used to monitor the physical property changes of carrot during drying. For example, at $\Delta FD/FD_0$ of around 0.06, the percentage of shrinkage was around 60% in all HAD and LPSSD cases (Figs. 12 and 13). This kind of relationship was also observed at other $\Delta FD/FD_0$ and percentage of shrinkage values. These results are supported by results presented in Fig. 14, which illustrates the microstructure of the samples at $\Delta FD/FD_0$ of 0.06 when drying with HAD at 60°C, 1 m/s, 150 min; 70°C, 1 m/s, 120 min; 80°C, 1 m/s, 90 min, and LPSSD at 60°C, 7 kPa, 210 min; 70°C, 7 kPa, 150 min; 80°C, 7 kPa, 90 min. All of the samples had similar levels of shrinkage although they had different microstructure. However, they all had the same $\Delta FD/FD_0$ values.

On the other hand, values of the rehydration ratio at the same $\Delta FD/FD_0$ were quite different. For instance, at $\Delta FD/FD_0$ of around 0.06, the rehydration ratio was around 2.50 at all conditions of HAD while the rehydration ratio was around 1.75 at all conditions of LPSSD (Figs. 12 and 13). However, $\Delta FD/FD_0$ could be used to correlate the rehydration behavior of samples dried using the same type of dryer.

The simple correlations between the rates of change of fractal dimension and the drying kinetics and physical property changes of carrot cube undergoing different drying techniques and conditions are shown in Table 1. The symbols (+, −) represent the direction of the relationship. It is

TABLE 1

Pearson's square correlation between $\Delta FD/FD_0$ and drying kinetics and $\Delta FD/FD_0$ and physical properties of carrot undergoing different drying techniques and conditions

Drying technique	Conditions	Parameter of interest		
		Drying kinetics	% Shrinkage	Rehydration ratio
Hot air drying	60°C, 0.5 m/s	−0.941	0.961	0.954
	60°C, 1 m/s	−0.883	0.872	0.964
	70°C, 0.5 m/s	−0.844	0.913	0.966
	70°C, 1 m/s	−0.981	0.955	0.972
	80°C, 0.5 m/s	−0.979	0.964	0.954
	80°C, 1 m/s	−0.962	0.959	0.945
LPSSD	60°C, 7 kPa	−0.970	0.976	0.885
	70°C, 7 kPa	−0.984	0.985	0.859
	80°C, 7 kPa	−0.947	0.947	0.901

seen from the table that the changes of the fractal dimension correlated well with the drying kinetics and the changes of physical properties during drying. The Pearson's square correlation coefficients between the fractal dimension and the physical property changes were between 0.86 and 0.99 depending on the tested conditions and techniques of drying. These close-to-unity coefficients imply that $\Delta FD/FD_0$ and other observed variables correlated well with each other.

CONCLUSION

Fractal dimension was used to relate the physical property changes to the microstructural changes of carrot undergoing two different types of drying at various conditions. The external changes of carrot, which were represented in terms of percentage of shrinkage, correlated well with the changes of fractal dimension, which were used to represent the microstructural changes. Fractal dimension was proved to be capable of being a structure-quality index of food undergoing drying. Further work is now underway to develop an approach (via the use of neural network simulation) to predict the physical properties of products when the values of fractal dimension are given.

ACKNOWLEDGEMENTS

The authors express their sincere appreciation to the Commission on Higher Education, the Thailand Research Fund (TRF), the National Research Council of Thailand, and the International Foundation for Science (IFS), Sweden, for financial support. Our appreciation also goes to the Faculty of Fishery, Kasetsart University, for their help with the microstructural imaging of the samples.

REFERENCES

1. Ratti, C. Shrinkage during drying of foodstuffs. *Journal of Food Engineering* **1994**, *23*, 91–105.
2. Khraisheh, M.A.M.; Cooper, T.J.R.; Magee, T.R.A. Shrinkage characteristics of potatoes dehydrated under combined microwave and convective air conditions. *Drying Technology* **1997**, *15*, 1003–1022.
3. Ochoa, M.R.; Kessler, A.G.; Pirone, B.N.; Marquez, C.A.; De Michelis, A. Volume and area shrinkage of whole sour cherry fruits (*Prunus cerasus*) during dehydration. *Drying Technology* **2002**, *20*, 147–156.
4. Madamba, P.S. Physical changes in bamboo (*Bambusa phyllostachys*) shoot during hot air drying: Shrinkage, density, and porosity. *Drying Technology* **2003**, *21*, 555–568.
5. Panyawong, S.; Devahastin, S. Determination of deformation of a food product undergoing different drying methods and conditions via evolution of a shape factor. *Journal of Food Engineering* **2007**, *78*, 151–161.
6. Aguilera, J.M.; Stanley, D.W. *Microstructural Principles of Food Processing and Engineering*; 2nd edition, Aspen Publishers: Gaithersburg, 1999.
7. Leonard, A.; Blacher, S.; Marchot, P.; Pirard, J.P.; Crine, M. Measurement of shrinkage and cracks associated to convective drying of soft materials by X-ray microtomography. *Drying Technology* **2004**, *22*, 1695–1708.
8. Graf, J.C. The importance of resolution limits to the interpretation of fractal descriptions of fine particles. *Powder Technology* **1991**, *67*, 83–85.
9. Mandelbrot, B.M. *The Fractal Geometry of Nature*; Freeman Press: New York, 1983.
10. Hsu, S.; Lu, S.; Huang, C. Viscoelastic changes of rice starch suspensions during gelatinization. *Journal of Food Science* **2000**, *65*, 215–220.
11. Peleg, M.; Normand, M.D. Characterization of the ruggedness of instant coffee particle shape by natural fractals. *Journal of Food Science* **1985**, *50*, 829–831.
12. Zhu, W.; Dong, T.; Cao, C.; Li, D. Fractal modeling and simulation of the developing process of stress cracks in corn kernel. *Drying Technology* **2004**, *22*, 59–69.
13. Rubnov, M.; Saguy, I.S. Fractal analysis and crust water diffusivity of a restructured potato product during deep-fat frying. *Journal of Food Science* **1997**, *62*, 135–154.
14. Chanola, P.J.J.; Alamilla, B.L.; Farrera, R.R.R.; Quevedo, R.; Aguilera, J.M.; Gutierrez, L.G.F. Description of the convective air-drying of a food model by means of the fractal theory. *Food Science and Technology International* **2003**, *9*, 207–213.
15. Devahastin, S.; Suvarnakuta, P.; Soponronnarit, S.; Mujumdar, A.S. A comparative study of low-pressure superheated steam and vacuum drying of a heat-sensitive material. *Drying Technology* **2004**, *22*, 1854–1867.
16. Association of Official Analytical Chemists. *Official Methods of Analysis*, 14th Ed.; AOAC: Washington, DC, 1984.
17. Humason, G.L. *Animal Tissue Techniques*, 4th Ed.; W.H. Freeman and Company: San Francisco, 1979.
18. Quevedo, R.; Calos, L.G.; Aguilera, J.M.; Cadoche, L. Description of food surfaces and microstructural changes using fractal image texture analysis. *Journal of Food Engineering* **2002**, *53*, 361–371.
19. Downie, N.M.; Health, R.W. *Basic Statistical Methods*, 4th Ed.; Harper & Row Publishers: New York, 1974.
20. Doymaz, I. Convective air drying characteristics of thin layer carrots. *Journal of Food Engineering* **2004**, *61*, 359–364.
21. Prakash, S.; Jha, S.K.; Datta, N. Performance evaluation of blanched carrot dried by three different driers. *Journal of Food Engineering* **2004**, *62*, 305–313.
22. Elustondo, D.M.; Mujumdar, A.S.; Urbicain, M.J. Optimum operating conditions in drying foodstuffs with superheated steam. *Drying Technology* **2002**, *20*, 381–402.
23. Moreira, R.G. Impingement drying of foods using hot air and superheated steam. *Journal of Food Engineering* **2001**, *49*, 291–295.

Comparative fractal characterization of physical changes of different food products during drying

Soraya Kerdpi boon^a, Sakamon Devahastin^{a,*}, William L. Kerr^b

^a Department of Food Engineering, King Mongkut's University of Technology Thonburi, 126 Pracha u-tid Road, Bangkok 10140, Thailand

^b Department of Food Science and Technology, University of Georgia, Athens, GA, USA

Received 12 February 2007; received in revised form 12 March 2007; accepted 30 March 2007

Available online 14 April 2007

Abstract

The development of a relationship between microstructural changes of model food products (carrot and potato cubes) and their physical changes during conventional hot air drying (HAD) using combined fractal and image analysis was performed in this study. Dried carrot and potato sections were examined by light microscopy and the fractal dimension (FD) of the microscopic images was determined using a box counting technique. The apparent physical changes of the samples undergoing HAD were represented in terms of the percentage of shrinkage and rehydration ratio. These apparent changes correlated well with their microstructural changes represented by the normalized changes of fractal dimension ($\Delta FD/FD_0$) of the microstructural images. Although the microstructural changes of the samples undergoing HAD were quite different, the changes of $\Delta FD/FD_0$ of the samples undergoing drying were in the same trend. FD has thus proved to be a good indicator of microstructural changes of products undergoing drying.

© 2007 Elsevier Ltd. All rights reserved.

Keywords: Carrot; Conventional hot air drying; Deformation; Fractal analysis; Physical properties; Potato; Structure-quality relationship

1. Introduction

Physical properties are those properties that provide descriptive quantification of foods by physical rather than chemical means. During drying physical properties of foods change primarily due to the loss of moisture from the interior regions to the surfaces and surrounding air. Numerous studies have attempted to characterize these physical changes in terms of such parameters as changes in volume, area, size and shape (Khraisheh, Cooper, & Magee, 1997; Madamba, 2003; Ochoa, Kessler, Pirone, Marquez, & De Michelis, 2002; Panyawong & Devahastin, 2007; Ratti, 1994). However, these external or apparent changes are primarily caused by internal changes, which are directly related to the microstructure of drying materials.

Structural changes of drying materials can be observed using microscopy. However, it is not easy to describe changes

of these microstructural images quantitatively. One technique, called fractal analysis, could be used to quantify these microstructural images. Fractal analysis has been applied successfully to quantify irregular fragments or complex particles such as shorelines, clouds, plants, brain cells, gold colloids and sponge iron (Graf, 1991; Mandelbrot, 1983). Fractal analysis has also been used to study surface and morphology of food materials after processing. Barletta and Canovas (1993) characterized the ruggedness of food powders, which were commercial instant coffee and instant skim milk, exposing to attrition in a tap density tester. It was shown that the calculated fractal dimension (FD) was sensitive enough to detect the ruggedness of the agglomerates when exposing to small amount of tapping. FD can also be used to describe the surface and morphology of food products such as chocolate, bread, and potato, among others (Pedreschi & Aguilera, 2000; Quevedo, Carlos, Aguilera, & Cadoche, 2002).

Recently, Kerdpi boon and Devahastin (2007) developed a relationship between microstructural changes of carrot

* Corresponding author. Tel.: +66 2 470 9246; fax: +66 2 470 9240.
E-mail address: sakamon.dev@kmutt.ac.th (S. Devahastin).

cubes and their physical changes during conventional hot air drying (HAD) and low-pressure superheated steam drying (LPSSD) using combined fractal and image analysis. The apparent changes of carrot cubes, which were represented in terms of the percentage of shrinkage and rehydration behavior, correlated well with their microstructural changes, which were represented by the normalized changes of fractal dimension ($\Delta FD/FD_0$) of the microstructural images. In addition, the use of artificial neural networks (ANN) to predict the percentage of shrinkage and rehydration ratio of dried carrots based on the inputs of moisture content and $\Delta FD/FD_0$ of the cell structure was implemented (Kerdpiroon, Kerr, & Devahastin, 2006). ANN models were developed and the measured values of the percentage of shrinkage and rehydration ratio were predicted with $R^2 > 0.95$ in all cases.

To investigate if the above correlations can also be extended to other products the application of fractal analysis to monitor physical changes of various kinds of foods during drying is of interest. This work aimed at studying apparent physical changes (in terms of shrinkage and rehydration ratio) of food products (which are carrot and potato cubes) during conventional hot air drying. The normalized changes of fractal dimension of different microstructural images of carrot and potato cubes undergoing drying were compared. Simple correlations between apparent and microstructural changes of samples were also calculated.

2. Materials and methods

2.1. Experimental set-up

A schematic diagram of the hot air tray dryer (HAD) used in this study is presented in Fig. 1. The HAD consists of a stainless steel drying chamber that is connected to an electric heater rated at 6.6 kW, which was used to heat up the air to the desired drying temperature. The heater was controlled by a PID temperature controller. The cubes of sample were placed on trays with dimensions of $30 \times 40 \text{ cm}^2$.

2.2. Materials

Fresh carrots (*Daucus carota* var. *sativa*) and potatoes (*Solanum tuberosum* Linn.) were obtained from a local supermarket and stored at 4°C . Prior to the start of each

experiment the samples were removed from the refrigerator to attain room temperature. The carrots and potatoes were then peeled and sliced. In this study, carrots were prepared using only the cortex tissues since different parts of carrots may have different microstructures. Moreover, the samples were used immediately after preparation, especially in the case of potatoes, which could suffer browning reactions on their surfaces. The sliced carrots and potatoes were then diced into cubes with dimensions of $1 \times 1 \times 1 \text{ cm}^3$.

2.3. Methods

2.3.1. Drying experiments

The samples were dried using HAD at drying temperatures of 60 , 70 and 80°C and two air velocities of 0.5 and 1 m/s in the case of carrot cubes and one air velocity of 1 m/s in the case of potato cubes. Carrot and potato cubes were dried by HAD to compare the differences in their physical and microstructural changes.

Approximately 100 cubes of sample (about 100 g) were used in each HAD experiment. In each drying experiment the drying process was carried out up to a predetermined sampling time and ended at that time. A new experimental run was then performed up to the next predetermined sampling time. These steps were repeated until a complete drying curve (down to the equilibrium moisture content at each condition) was obtained. At the end of each experimental run the samples were taken out to determine the moisture content (AOAC, 1984), percentage of shrinkage, rehydration ratio and microstructural changes.

2.3.2. Measurement of shrinkage and rehydration ratio

To study the physical changes of carrot cubes and potato cubes during drying the percentage of shrinkage and rehydration ratio of the samples were selected as representative properties and were calculated as follows.

2.3.2.1. Percentage of shrinkage. Five sample cubes were used for each shrinkage measurement. Shrinkage is expressed in terms of the percentage change of the volume of the sample as compared with its original volume.

$$\%S = \left(\frac{V_i - V}{V_i} \right) \times 100, \quad (1)$$

where V_i and V are the volumes of the sample at the beginning and at the end of each drying run, respectively. The average values of the percentage of shrinkage of five samples were reported. All measurements were performed in triplicate.

2.3.2.2. Rehydration ratio. The rehydration ratio (R) of the dried sample was determined by immersing the dried sample in hot water at 100°C for 10 min. The sample was then drained and its mass, both before and after immersion, was measured by using an electronic balance (accurate to 0.001 g). The rehydration ratio of the sample was calculated by

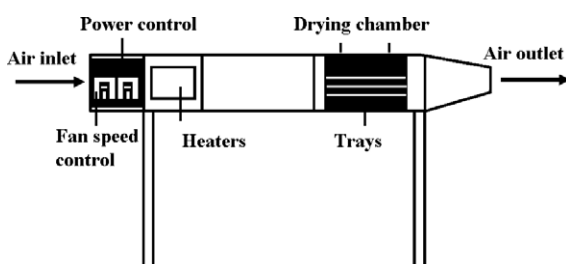


Fig. 1. Conventional hot air dryer.

$$R = \frac{M}{M_0} \quad (2)$$

where M_0 and M are the masses of sample before and after immersion in hot water, respectively. The average values of five samples were reported and all measurements were performed in duplicate.

2.3.3. Microstructural analysis

2.3.3.1. Microstructural imaging. The process of microstructural imaging consists of fixation, in which the sample was preserved with 10% (V/V) formaldehyde prior to passing through the remaining steps. The objective of the fixation step is to immobilize cellular components in order to ensure that the structure and tissue shown in the microstructural images reflect as closely as possible the living state of the sample. After fixation the sample was soaked with flowing distilled water for 20 min before removing the remaining moisture within the sample cells by flushing the sample with a series of isopropyl alcohol solutions at different concentrations starting with 50%, 70%, 95%, 95%, 95%, 100%, 100% and 100% (V/V), respectively. The sample was flushed with isopropyl alcohol from the lower to higher concentrations to prevent the damage of the cell structure, which might occur from the sudden loss of moisture. Isopropyl alcohol within the sample was subsequently removed by flushing the sample with absolute xylene for two times. The time used for flushing the sample with each concentration of isopropyl alcohol and absolute xylene was approximately 90 min per solution. Finally, the pores of the sample were replaced with paraffin by dipping the sample in melted paraffin at 60 °C (Humason, 1979; Aguilera & Stanley, 1999).

The treated sample was embedded in paraffin wax, which has a melting point in the range of 58–59 °C. The steps for preparing an embedded sample started from pouring heated paraffin wax into a stainless steel box with dimensions of $30 \times 24 \times 5 \text{ mm}^3$ to cover approximately one-third of the depth of the box. The sample was then placed at the middle of the stainless steel box and covered with a plastic embedded ring. Finally, additional liquid paraffin was poured to fully fill the box. The paraffin within the embedded sample could be set at room temperature and kept in a refrigerator at 4 °C. The cool embedded sample was easier to be sectioned than the sample at room temperature.

Each embedded sample was sectioned by a microtome (Jung, model RM2025, Germany) into a 5 µm thick slice. As the deformation of the sample occurred from the outside to inside, the samples were sliced at their center. For example, fresh sample was sectioned at $0.5 \text{ cm} \pm 2.5 \text{ µm}$. Sliced sample was placed on a glass slide and 95% ethanol was dropped indirectly to the sliced sample to expand the cell tissue. Ethanol was then eliminated by floating the sliced sample in water at 42–43 °C and removing the sliced sample immediately to the glass slide. The sliced sample was dried by placing at room temperature and then fixed

on the glass slide with the use of a hotplate set at temperature of 48–50 °C for 8 h. The finished slide was then dyed using haematoxylin and eosin to highlight the cell walls. Finally, the microstructural images were obtained using a light microscope (Olympus, model LH30RF200, Japan) at a 10× magnification level.

Although the microstructure of sample cells might change during the fixation step, the normalized fractal dimension of a sample undergoing drying was determined from the difference between the fractal dimension of the fresh sample and of the sample undergoing drying. All of the samples were fixed with paraffin and sectioned with a microtome in the same fashion. Therefore, the sample characteristic change was expected to be similar.

2.3.3.2. Image analysis. A light microscopic image of the sample was captured by a Pixel View capture (Pixel View Program, Play TV/USBpro, Taiwan) at an image size of 520×520 pixels (one pixel has the resolution of 0.71 µm). The image was then transformed from an RGB format to a black and white format before a calculation of the fractal dimension (FD) was performed.

2.3.4. Fractal dimension (FD) calculation

The fractal dimension of a black and white image obtained as described in the previous section was calculated using the box counting method (Quevedo et al., 2002). Cubic boxes with different sizes (r) were mounted into the images. The number of boxes (N_r), which were formed on the image was then counted. Fractal dimension was calculated by

$$FD = \frac{\log(N_r)}{\log(1/r)} \quad (3)$$

The sizes of boxes are composed of 4, 5, 10, 13, 26, 65, 130 and 260 pixels and the threshold values used were between 0.5 and 0.8. Fractal dimension calculation was performed using Matlab™ Software (version 6.5). Ten light microscopic images were captured for each sample obtained at each sampling time.

To compare the changing values of FD of the sample undergoing drying the normalized changes of FD is reported as

$$\frac{\Delta FD}{FD_0}, \quad (4)$$

$$\Delta FD = FD_t - FD_0, \quad (5)$$

where FD_0 and FD_t are the fractal dimensions of fresh sample and of the sample at any instant during drying, respectively.

2.4. Structure-quality relationship determination

The correlations between normalized changes of FD and the drying kinetics as well as between normalized changes of FD and the physical changes were determined by the

Pearson's correlation coefficient. Pearson's correlation coefficient (r) is a measure of the degree of the linear relationship between two variables and the correlation coefficient may take on any values between plus and minus one. The sign of this correlation coefficient (+, -) represents the direction of the relationship. A positive correlation coefficient indicates that the values of both variables change in the same direction and a negative r indicates that the values change in opposite directions. The absolute value of the coefficient illustrates the closeness of the relationship between the two variables.

Pearson's correlation coefficient was calculated by Eq. (6).

$$r = \frac{\sum XY - \frac{\sum X \sum Y}{N}}{\sqrt{\left(\sum X^2 - \frac{(\sum X)^2}{N}\right) \left(\sum Y^2 - \frac{(\sum Y)^2}{N}\right)}}, \quad (6)$$

where X , Y and N represent the data of variables X , Y and the number of data X and Y , respectively.

3. Results and discussion

3.1. Drying kinetics of carrot and potato cubes

Fresh carrots with an initial moisture content around 88–90% (w.b.) (or about 8.8–9 kg/kg (d.b.)) were dried until reaching an equilibrium moisture content of approximately 7% (w.b.) (or about 0.075 kg/kg (d.b.)). The drying kinetics of carrot cubes undergoing HAD are shown in Fig. 2. As expected, higher temperatures led to higher drying rates of the samples. Carrot cubes reached their equilibrium moisture contents after 300, 240, 210, 180, 180 and 150 min of drying with air temperatures and air velocities of 60 °C, 0.5 m/s; 60 °C, 1 m/s; 70 °C, 0.5 m/s; 70 °C, 1 m/s; 80 °C, 0.5 m/s and 80 °C, 1 m/s, respectively. The effect of drying air velocity on the drying kinetics of carrot cubes is shown in Fig. 2c.

For all drying conditions tested no constant rate period was observed; a constant rate period might be shorter than 30 min, which was the first sampling time. Moreover, moisture migration might be resisted due to the collapse at the surface of the sample. Similar results were also reported by Doymaz (2004). In each case, two falling rate periods were noted. Initially, the moisture content decreased more rapidly due to large moisture gradients within the sample, leading to faster movement of moisture. For example, carrot dried in an HAD at 60 °C and 0.5 m/s remained in the first falling rate period for 120 min. It was subsequently in the second falling rate period until reaching an equilibrium moisture content at 300 min (Fig. 2c).

The drying kinetics of potato cubes undergoing HAD at temperatures of 60, 70 and 80 °C and air velocity of 1 m/s are shown in Fig. 3. Potato cubes were dried until reaching an equilibrium moisture content of 8–9% (w.b.) (or about 0.087–0.099 kg/kg (d.b.)). Potato cubes reached their equi-

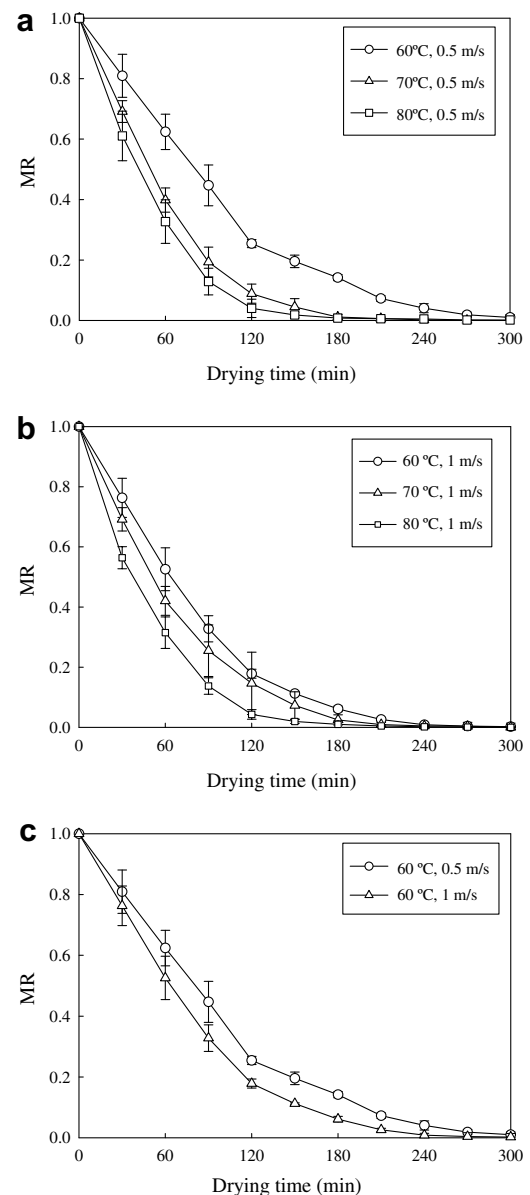


Fig. 2. Drying kinetics of carrot cubes undergoing hot air drying at different drying conditions. $MR = (X - X_{eq}) / (X_i - X_{eq})$, where X = instantaneous moisture content (kg/kg, d.b.); X_{eq} and X_i are equilibrium and initial moisture contents (kg/kg, d.b.), respectively.

librium moisture contents after 420, 390 and 300 minutes of drying at air temperatures of 60, 70 and 80 °C, respectively. Similar results were found for both potato and carrot cubes; there was no constant rate period at all conditions tested.

3.2. Physical changes of carrot and potato cubes

Physical changes of carrot cubes and potato cubes undergoing HAD are shown in Figs. 4 and 5, respectively. As for shrinkage (Fig. 4a and b for carrot cubes and Fig. 5a for potato cubes), it increased with the drying time. In addition, at the same sampling time, samples undergoing

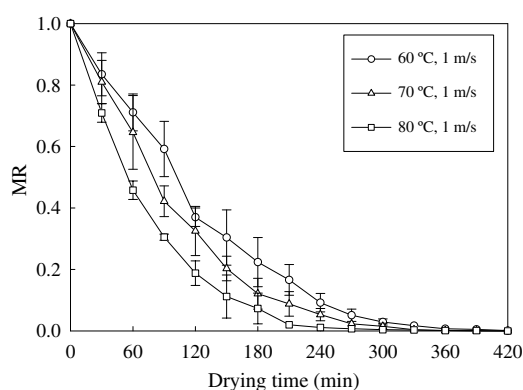


Fig. 3. Drying kinetics of potato cubes undergoing hot air drying at different drying conditions.

drying at an air velocity of 0.5 m/s and higher temperatures suffered more shrinkage than those undergoing drying at lower temperatures. This is because the drying temperature directly affected shrinkage (or deformation) of the product; larger moisture gradients within the samples developed when using higher drying temperatures and these larger gradients led to increased internal stresses, which in turn led to larger degrees of shrinkage (Devahastin, Suvarnaku-ta, Soponronnarit, & Mujumdar, 2004). Moreover, the shape of the drying samples was not uniform indicating that deformation of the samples was not symmetrical

(Panyawong & Devahastin, 2007). However, the samples undergoing drying at an air velocity of 1 m/s at different temperatures (Fig. 4b) were not much different in terms of the percentage of shrinkage. This is because case-hardening occurred more at the surface and limited shrinkage of the samples.

Initially, the percentage of shrinkage increased rapidly. This was followed by a period of slow increase until reaching the final values at the time corresponding to the points where the samples reached their equilibrium moisture contents. The drying time that divided the periods of shrinkage into the rapid increase and slow increase (followed by constant) periods was the same as the time that divided the drying curves into the first falling and second falling rate periods (Figs. 2 and 4 for carrot cubes and Figs. 3 and 5 for potato cubes). Towards the end of drying case hardened skin developed, which inhibited further shrinkage of the samples. It can be seen in Figs. 4 and 5 that the samples undergoing HAD at higher temperatures possessed higher rates of shrinkage than those of samples undergoing drying at lower temperatures. This is because the results were compared at the same sampling periods rather than at the same moisture contents.

Higher drying temperatures led to products with higher rehydration ratios. Higher rehydration ratios were observed with both carrot and potato cubes dried using HAD at 80 °C as compared to those dried at lower temperatures (Fig. 4c

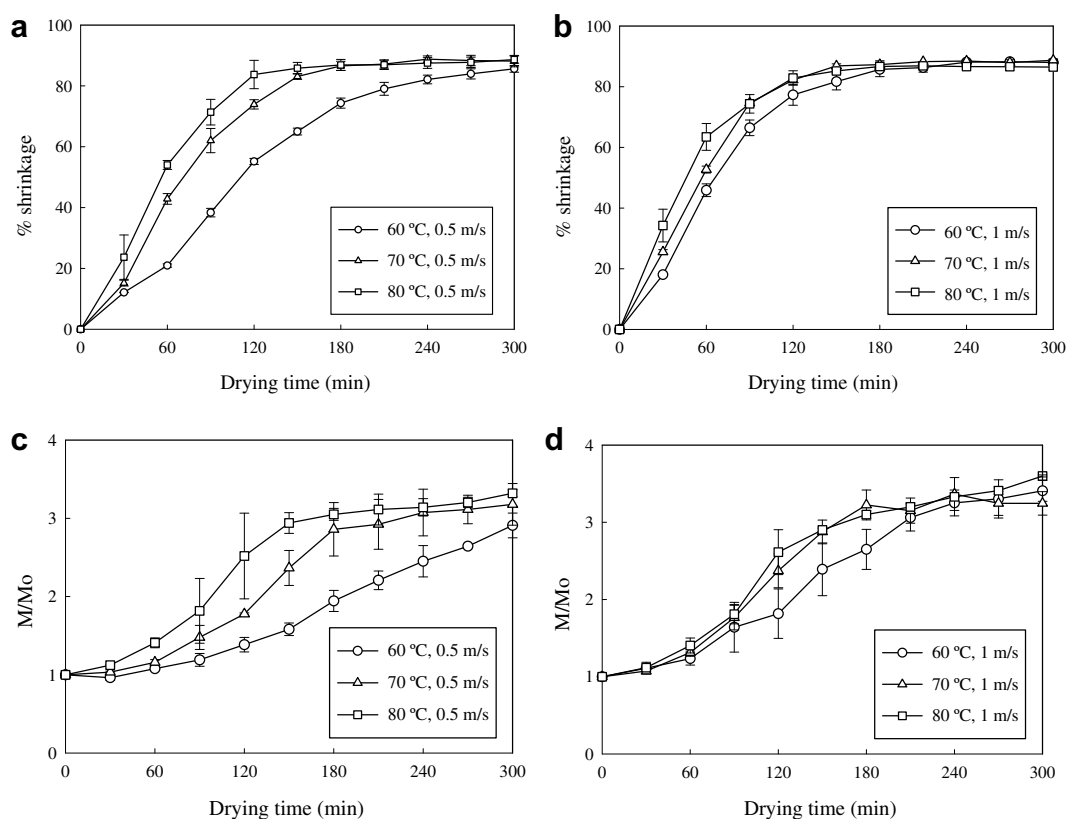


Fig. 4. Percentage of shrinkage ((a) and (b)) and rehydration ratio ((c) and (d)) of carrot cubes undergoing hot air drying.

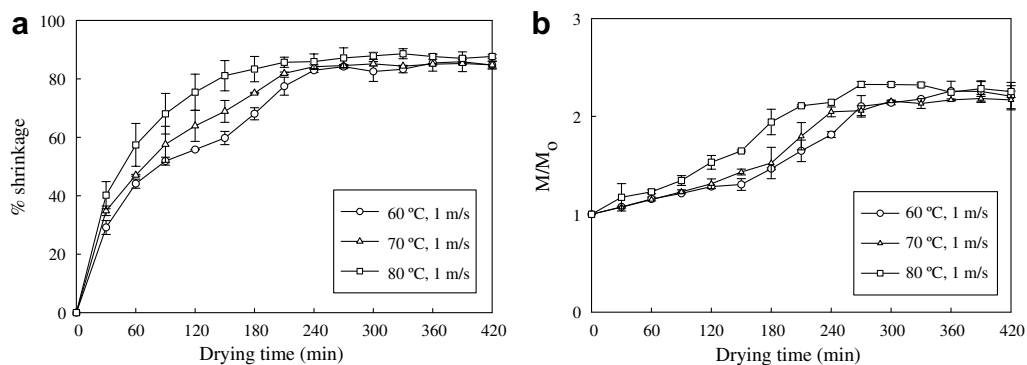


Fig. 5. Percentage of shrinkage (a) and rehydration ratio (b) of potato cubes undergoing hot air drying.

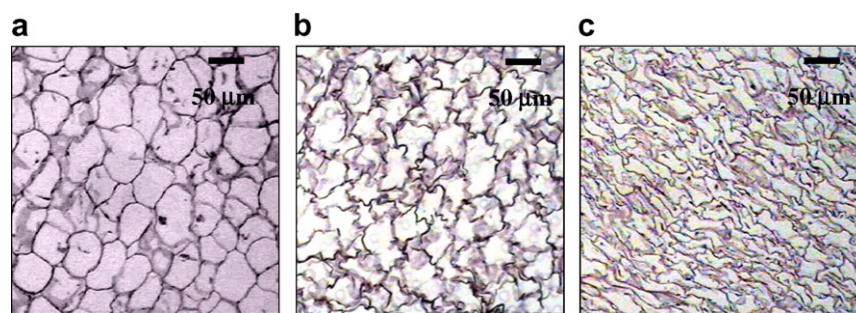


Fig. 6. Microstructure of carrot cubes undergoing hot air drying at 60 °C, 0.5 m/s after 0 min (a), 150 min (b) and 300 min (c).

and d for HAD carrot and Fig. 5b for HAD potato). This is because the samples, which were dried at lower temperatures, needed more time to achieve their equilibrium moisture contents than those dried at higher temperatures; the samples therefore suffered more structural damage (e.g., collapse of porous structure) than when drying at lower temperatures. As a result, the reconstitution capability of the sample undergoing high-temperature drying was higher than those undergoing low-temperature drying.

3.3. Microstructural changes of carrot and potato cubes

The images for microstructural analysis were observed with a light microscope at 10 \times magnification. After capturing the images these images were used for fractal dimension calculation.

The fractal dimension of fresh carrot (Fig. 6a) was approximately 1.75 whereas the fractal dimension of the samples increased upon drying. Initially, the cell walls of carrots were of round shape. After some period of time, however, moisture within the cells started to migrate to the surface. As a result, moisture gradients started to develop, which led to internal stresses and shrinkage of the cells (Fig. 6b and c). The ruggedness of cell walls increased leading to an increase in the fractal dimension of the cells, as expected.

The microstructural changes of carrot cubes undergoing drying are illustrated in terms of $\Delta FD/FD_0$ because this ratio represents the rates of change of fractal dimension

of the samples and hence could be used to compare the results of different drying conditions.

The rates of change of fractal dimension of carrot cubes undergoing HAD (Fig. 7) were monitored. The rates of change of fractal dimension were observed to be divided roughly into two periods, consisting of linear and non-linear rates of change. The drying time that identified the end point of the period where the rates of change of fractal dimension were linear was the same as the time that divided the drying curves into the first and second falling rate periods and that divided the physical changes (in terms of the percentage of shrinkage and rehydration ratio) into rapid increase and slow increase periods, respectively.

The light microscopic images of potato were also captured at 10 \times magnification. Each image represents both cell walls and starch granules. However, it was not easy to describe the changes of starch granules using a light microscope. The starch granules were therefore eliminated from every image. Thus, only cell walls of potato are displayed within the images. Fig. 8 represents the steps in processing the images starting from an original image (Fig. 8a), deleting the starch granules via the use of MatlabTM (version 6.5) (Fig. 8b) and converting the image without starch granules into a black and white format (Fig. 8c). Some starch granules that could not be deleted via the use of the program could be deleted manually to allow better analysis of the image (Aguilera & Stanley, 1999). In this research, starch granules were deleted manually using Adobe PhotoshopTM (version 6.0).

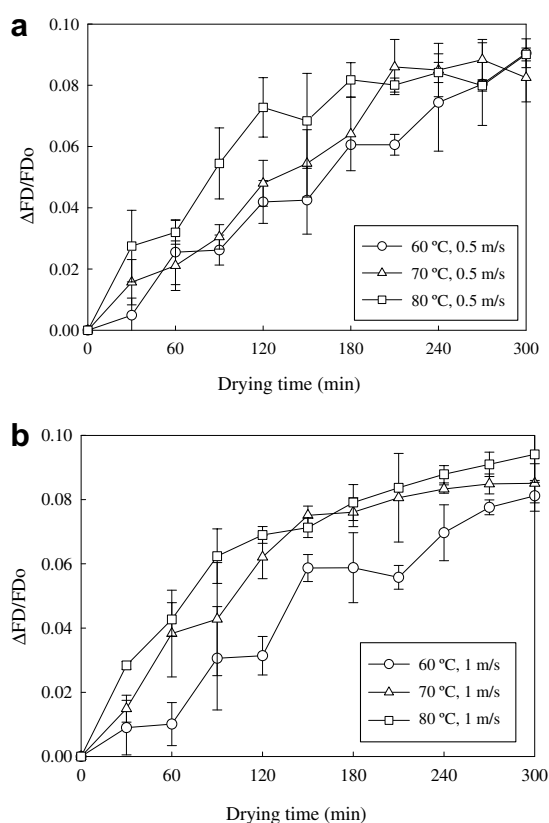


Fig. 7. $\Delta FD/FD_0$ of carrot cubes undergoing hot air drying (velocities of 0.5 m/s (a) and 1 m/s (b)).

Fractal dimension (FD) of fresh potato (Fig. 9a) was approximately 1.61. Again, FD of potato increased as drying time increased. For example, FD of potato cubes undergoing drying at an air temperature of 60 °C and air velocity of 1 m/s was approximately 1.70 (Fig. 9b) and 1.73 (Fig. 9c) at 180 and 240 min, respectively. However, fractal dimension of potato cubes did not change much comparing with that of carrot cubes undergoing hot air drying at the same condition; for carrot FD varied between 1.75 and 1.91. This is because the structures of potatoes and carrots are quite different. Carrot structure is composed mainly of cellulose and water. When carrots were dried water migrate from inside to the outside of cell walls. In contrast, potato structure consists mainly of cell walls, water and starch granules, which might have limited changes during drying. Moreover, initial moisture content of carrot (89–90% (w.b.)) was higher than that of potato (85–86% (w.b.)). This led carrots to have higher moisture gradients and larger changes in their structure during drying than potatoes.

Fractal dimension changes of potatoes were again presented in terms of the normalized changes of fractal dimension ($\Delta FD/FD_0$). It was found that $\Delta FD/FD_0$ increased with the drying time (Fig. 10). The results were in the same trend as those of carrots undergoing HAD.

3.4. Structure-quality relationship of carrot and potato cubes

As mentioned earlier, the rates of change of the fractal dimension could be divided into two periods, consisting

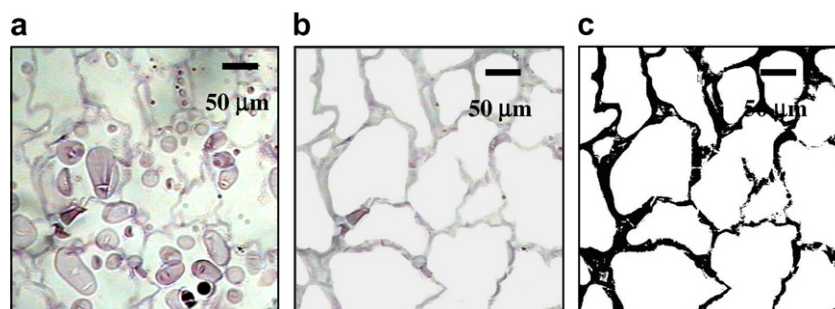


Fig. 8. Image processing of potato cubes; original image (a), image after deleting of starch granules (b) and black and white image (c).

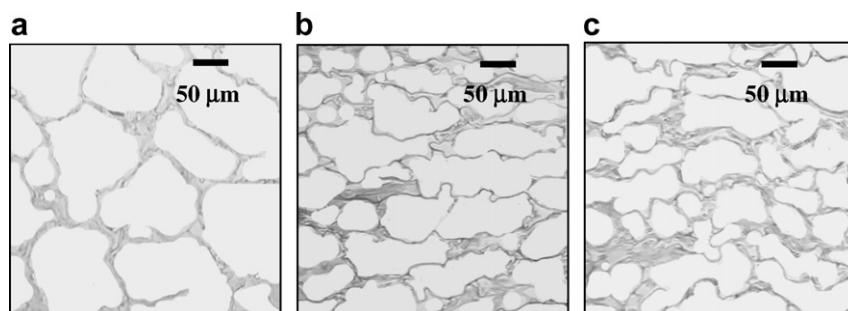


Fig. 9. Microstructure of potato cubes undergoing hot air drying at 60 °C, 1 m/s after 0 min (a), 150 min (b) and 300 min (c).

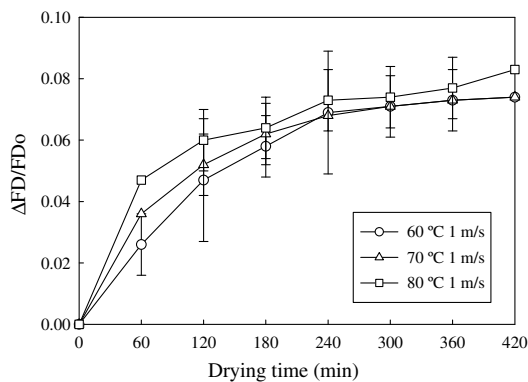


Fig. 10. $\Delta FD/FD_0$ of potato cubes undergoing hot air drying.

of periods of linear and non-linear changes. During the first falling rate period, although the rate of moisture migration from the internal cells to the surface was not equal to the rate of moisture evaporation from the surface to the surrounding, these rates might not be much different to cause large gradients within the sample and therefore linear changes of fractal dimension were observed. When samples were further dried the migration of moisture from the cells to the surface was slower than from the surface to the surroundings leading to larger gradients, which in turn led to more severe microstructural changes and deformation.

The drying time (Fig. 11) that divided the rates of change of the fractal dimension into linear period and non-linear period correlated well with the physical changes, especially the percentage of shrinkage (Fig. 12). The time at which the rates of change of fractal dimension switched from the linear to non-linear periods was the same as the point where the drying curves changed from the first falling rate period to the second falling rate period. Moreover, these were the same points where the percentage of shrinkage started to vary non-linearly as well. The percentage of shrinkage, which represents the apparent changes of the samples, correlated well with the normalized changes of fractal dimension, which represents the microstructural changes of the samples.

The normalized changes of fractal dimension could be used to monitor the physical changes of carrot and potato during drying (Figs. 12 and 13). For example, at $\Delta FD/FD_0$ of approximately 0.06 the percentage of shrinkage of carrot and potato cubes was around 70–80% in all cases. This type of relationship was also observed at other $\Delta FD/FD_0$ and percentage of shrinkage values. This has therefore proved that $\Delta FD/FD_0$ could be used to monitor shrinkage (deformation) of both potatoes and carrots undergoing HAD and thus has the potential of being an indicator for describing deformation of other products undergoing drying as well. Further investigation is certainly needed to confirm this hypothesis.

The ability to predict the percentage of shrinkage was better than that for rehydration ratio. This is likely due to the fact that shrinkage is more dependent on cellular changes throughout the volume of the dried samples and

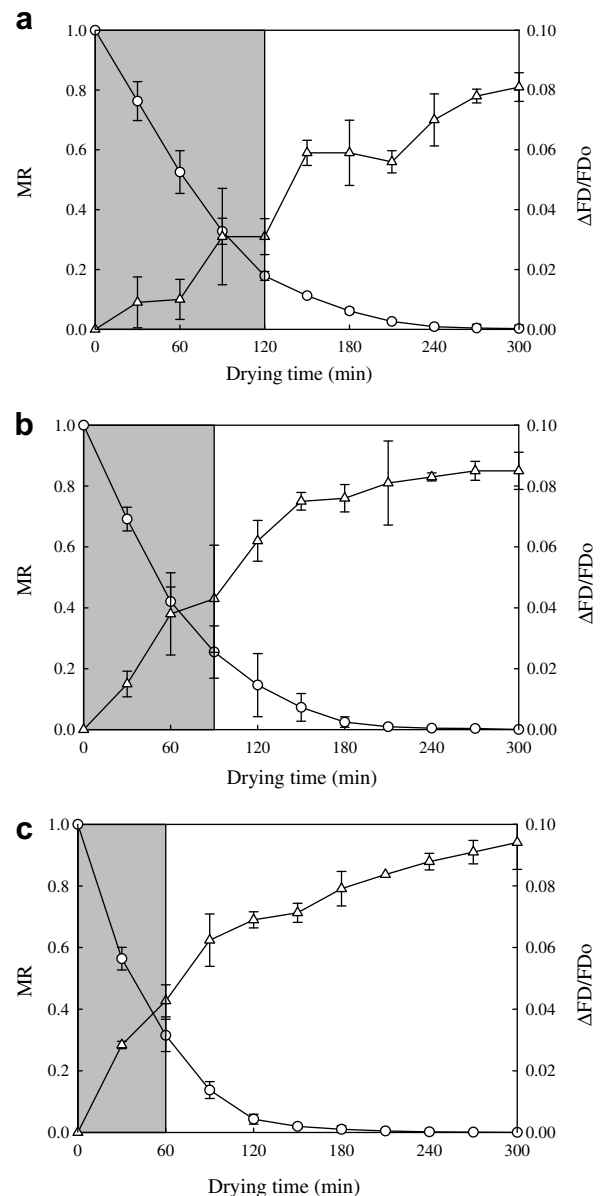


Fig. 11. Relationship between drying kinetics (○) and $\Delta FD/FD_0$ (Δ) of carrot cubes undergoing hot air drying at velocity of 1 m/s and temperature of 60 °C (a), 70 °C (b) and 80 °C (c).

these are well-characterized by the changes in the normalized fractal dimension. While rehydration is also dependent on internal structural changes and the ability for water to diffuse within the sample matrix, it may also depend on limiting factors at the surface such as case-hardening as well as the presence of some chemical constituents such as pectin, as in the case of carrot.

The relationship between the normalized changes of fractal dimension and rehydration ratio of carrots and potatoes undergoing HAD at different conditions are shown in Figs. 12 and 14, respectively. $\Delta FD/FD_0$ could somehow be used to monitor the changes in rehydration ratio. For example, $\Delta FD/FD_0$ of approximately 0.06 referred to the rehydration ratio of potato of around 1.50

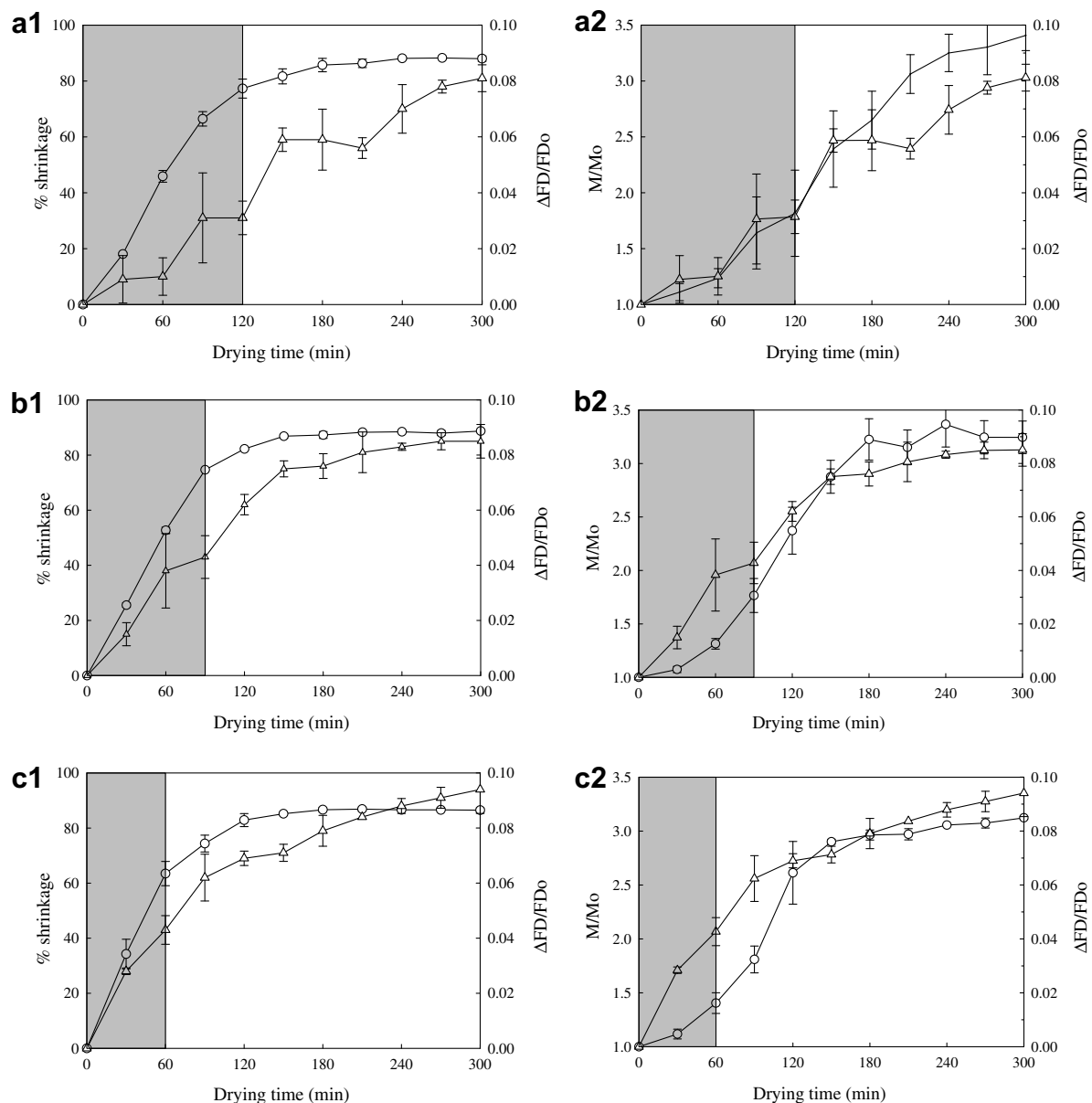


Fig. 12. Relationship between % shrinkage (\circ) and $\Delta FD/FD_0$ (Δ); rehydration ratio (\circ) and $\Delta FD/FD_0$ (Δ) of carrot cubes undergoing hot air drying at velocity of 1 m/s and temperatures of 60 °C (a), 70 °C (b) and 80 °C (c).

at all conditions tested. However, the same value of $\Delta FD/FD_0$ of carrot cubes undergoing HAD referred to the rehydration ratio of around 2.0–3.0.

The simple correlations between the rates of change of fractal dimension and the drying kinetics and physical changes of carrot and potato cubes undergoing different drying techniques and conditions are shown in Table 1. The results illustrated that the changes of fractal dimension correlated well with both the drying kinetics and physical changes. The Pearson's correlation coefficients representing the fractal dimension and the physical changes were between 0.86 and 0.99, depending on the tested conditions. These close-to-unity coefficients imply that $\Delta FD/FD_0$ and other observed variables correlated well with each other. However, the normalized changes of fractal dimension cor-

related better with shrinkage compared to the correlations with the rehydration ratio.

4. Conclusions

Fractal dimension was used in the present study to relate the apparent physical changes to the microstructural changes of food products (carrot and potato cubes) undergoing conventional hot air drying at various conditions. The apparent changes of the foods, which were represented in terms of the percentage of shrinkage correlated well with the normalized changes of fractal dimension, which were used to represent the microstructural changes. Fractal dimension (or more exactly, the normalized changes of fractal dimension) was thus proved to be capable of being

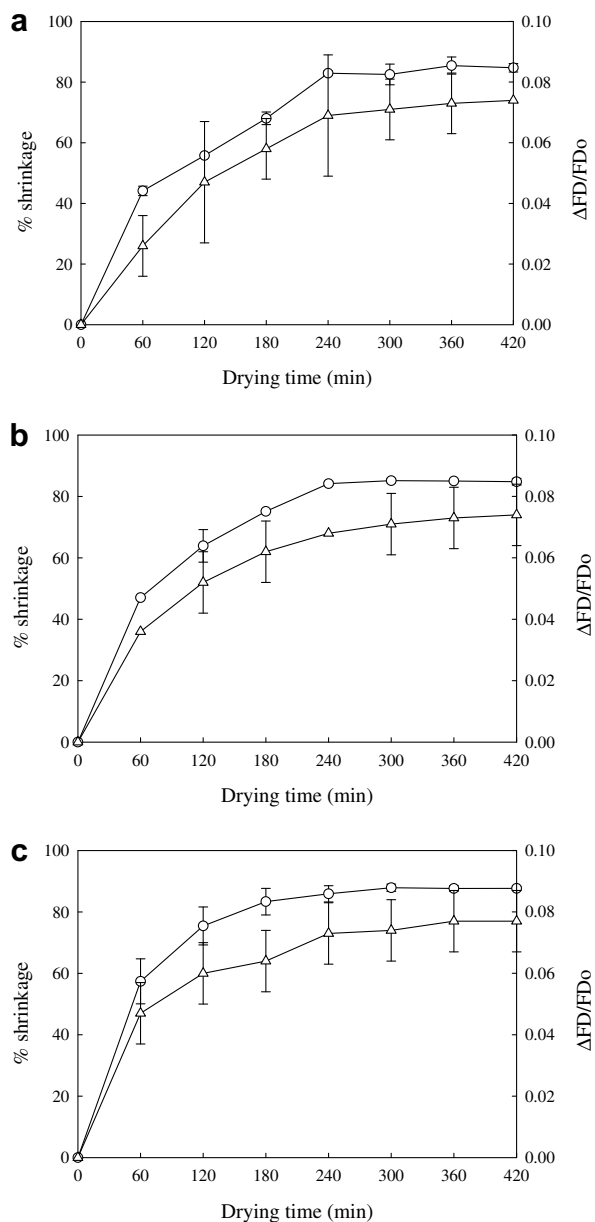


Fig. 13. $\Delta FD/FD_0$ (Δ) and % shrinkage (\circ) of potato cubes undergoing hot air drying at 60 °C, 1 m/s (a), 70 °C, 1 m/s (b) and 80 °C, 1 m/s (c).

Table 1

Pearson's correlation coefficients between $\Delta FD/FD_0$ and drying kinetics as well as between $\Delta FD/FD_0$ and physical changes of samples undergoing hot air drying

Sample	HAD conditions	Parameter of interest		
		Drying kinetics	% Shrinkage	Rehydration ratio
Carrot cubes	60 °C, 0.5 m/s	−0.941	0.961	0.954
	60 °C, 1 m/s	−0.883	0.872	0.964
	70 °C, 0.5 m/s	−0.844	0.913	0.966
	70 °C, 1 m/s	−0.981	0.955	0.972
	80 °C, 0.5 m/s	−0.979	0.964	0.954
	80 °C, 1 m/s	−0.962	0.959	0.945
Potato cubes	60 °C, 1 m/s	−0.998	0.988	0.894
	70 °C, 1 m/s	−0.990	0.997	0.876
	80 °C, 1 m/s	−0.992	0.993	0.893

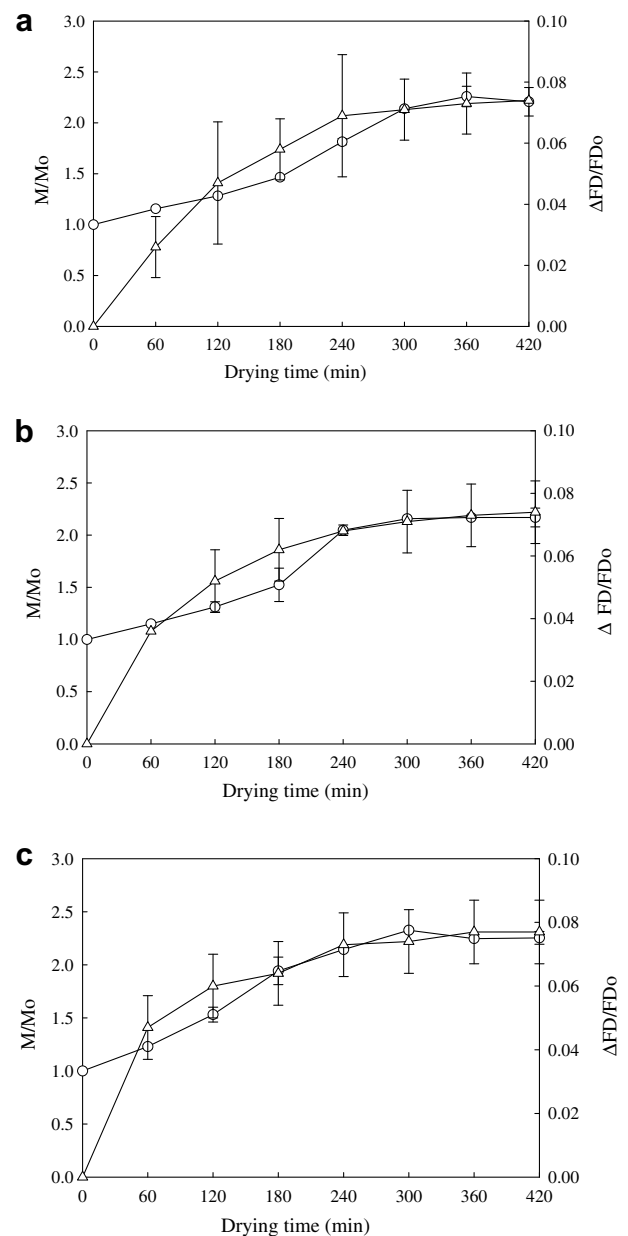


Fig. 14. $\Delta FD/FD_0$ (Δ) and rehydration ratio (\circ) of potato cubes undergoing hot air drying at 60 °C, 1 m/s (a), 70 °C, 1 m/s (b) and 80 °C, 1 m/s (c).

a generalized structure-quality index of foods undergoing drying. A comparison between the use of microstructural and apparent changes to monitor and/or evaluate physical properties of a sample should be made. This would allow the selection of an appropriate technique for an industrial use.

Acknowledgements

The authors express their sincere appreciation to the Commission on Higher Education, the Thailand Research Fund (TRF) and the International Foundation for Science (IFS), Sweden for financial support. Our appreciation also

goes to the Faculty of Fishery, Kasetsart University, Bangkok, Thailand for their help with the microstructural imaging of the samples.

References

- Aguilera, J. M., & Stanley, D. W. (1999). *Microstructural principles of food processing and engineering* (2nd ed.). Gaithersburg: Aspen Publishers.
- AOAC (1984). *Official methods of analysis* (14th ed.). Washington, DC: Association of Official Analytical Chemists.
- Barletta, B. J., & Canovas, V. B. (1993). An attrition index to assess fines formation and particle size reduction in tapped agglomerated food powders. *Powder Technology*, 77, 89–93.
- Devahastin, S., Suvarnakuta, P., Soponronnarit, S., & Mujumdar, A. S. (2004). A comparative study of low-pressure superheated steam and vacuum drying of a heat-sensitive material. *Drying Technology*, 22, 1845–1867.
- Doymaz, I. (2004). Convective air drying characteristics of thin layer carrots. *Journal of Food Engineering*, 61, 359–364.
- Graf, J. C. (1991). The importance of resolution limits to the interpretation of fractal descriptions of fine particles. *Powder Technology*, 67, 83–85.
- Humason, G. L. (1979). *Animal tissue techniques*. San Francisco: Freeman Press.
- Kerdpi boon, S., & Devahastin, S. (2007). Fractal characterization of some physical properties of a food product under various drying conditions. *Drying Technology*, 25, 135–146.
- Kerdpi boon, S., Kerr, W. L., & Devahastin, S. (2006). Neural network prediction of physical property changes of dried carrot as a function of fractal dimension and moisture content. *Food Research International*, 39, 1110–1118.
- Khraisheh, M. A. M., Cooper, T. J. R., & Magee, T. R. A. (1997). Shrinkage characteristics of potatoes dehydrated under combined microwave and convective air conditions. *Drying Technology*, 15, 1003–1022.
- Madamba, P. S. (2003). Physical changes in bamboo (*Bambusa Phyllostachys*) shoot during hot air drying: shrinkage, density, and porosity. *Drying Technology*, 21, 555–568.
- Mandelbrot, B. M. (1983). *The fractal geometry of nature*. New York: Freeman Press.
- Ochoa, M. R., Kessler, A. G., Pirone, B. N., Marquez, C. A., & De Michelis, A. (2002). Volume and area shrinkage of whole sour cherry fruits (*Prunus cerasus*) during dehydration. *Drying Technology*, 20, 147–156.
- Panyawong, S., & Devahastin, S. (2007). Determination of deformation of a food product undergoing different drying methods and conditions via evolution of a shape factor. *Journal of Food Engineering*, 78, 151–161.
- Pedreschi, F., & Aguilera, J. M. (2000). Characterization of food surfaces using scale-sensitive fractal analysis. *Journal of Food Process Engineering*, 23, 127–143.
- Quevedo, R., Carlos, L. G., Aguilera, J. M., & Cadoche, L. (2002). Description of food surfaces and microstructural changes using fractal image texture analysis. *Journal of Food Engineering*, 53, 361–371.
- Ratti, C. (1994). Shrinkage during drying of foodstuffs. *Journal of Food Engineering*, 23, 91–105.



Determination of deformation of a food product undergoing different drying methods and conditions via evolution of a shape factor

Sawitree Panyawong, Sakamon Devahastin *

Department of Food Engineering, King Mongkut's University of Technology Thonburi, 91 Pracha u-tid Road, Bangkok 10140, Thailand

Received 5 August 2005; accepted 14 September 2005

Available online 2 November 2005

Abstract

Shrinkage is a phenomenon that is common during drying of foods and other bio-products. Attempts have been made to describe shrinkage of different products undergoing different drying processes and conditions. However, most works describe shrinkage only in terms of its magnitude but fail to describe it in terms of pattern or, in other words, of how the drying material deforms during drying. Although the degree of shrinkage of a product undergoing different drying processes and conditions may not be significantly different, the shrinkage pattern may not be the same. Using only the degree of shrinkage to describe shrinkage (and deformation) is therefore not adequate. The present study proposed and investigated the use of a shape factor viz. Heywood shape factor to describe the deformation of a food product (carrot cube) undergoing different drying techniques viz. low-pressure superheated steam drying and vacuum drying at different conditions. It was found that the evolution of Heywood shape factor agreed reasonably well with the deformation kinetics of carrot cube as observed visually. It was possible, to some extent, to use this shape factor to describe the effects of drying methods and conditions on the deformation of carrot cube.

© 2005 Elsevier Ltd. All rights reserved.

Keywords: Carrot; Drying kinetics; Low-pressure superheated steam drying; Heywood shape factor; Shrinkage; Shrinkage pattern; Vacuum drying

1. Introduction

During drying water migrates from the inner cells of food via the cell membrane and the surrounding wall and then across the porous structure to the environment. Moisture gradients within the product induce microstructural stresses leading to shrinkage of the product, which in turn reflects the amount of water removed. Shrinkage may occur due to two reasons. Firstly, the tissue is unable to hold its structural network when the space taken by water is continuously emptied and air-filled. Secondly, the outside skin structure collapses and leads to shrinkage. In this case, case hardening at the skin surface also influences the shrinkage properties of the product as well (Achanta & Okos, 2000). Mostly, shrinkage of a food product is reported as a func-

tion of its moisture content. Shrinkage is generally quantified in terms of a shrinkage ratio, V/V_0 , i.e., the ratio of the volume of the product at any instant to its initial volume. However, drying does not cause only the volume change but also the change of the shape of the product. Therefore, expressing deformation of the product by indicating only the change of volume is inadequate.

It is well known that different drying methods and conditions affect the quality of the drying product, including volume and shape changes, differently. Ratti (1994) proposed the shrinkage characteristics as a function of water content for potato, apple and carrot of different geometries and under various drying conditions. Volumetric shrinkage of individual samples was affected mainly by air velocity; other drying variables had negligible effects. Changes in the ratio of the surface area to the volume with water content were practically independent of drying conditions but dependent on the sample geometry and the type of foodstuff. Khraisheh, Cooper, and Magee (1997) studied

* Corresponding author. Tel.: +66 2 470 9246; fax: +66 2 470 9240.
E-mail address: sakamon.dev@kmutt.ac.th (S. Devahastin).

the physical structure of potato during microwave and hot air drying and found that the shrinkage of potato undergoing both drying techniques was a linear function of the moisture content level. Shrinkage was reduced by the use of microwave drying but was rather independent on the sample geometry and air temperature. Ochoa, Kessler, Pirone, Marquez, and De Michelis (2002) investigated the volume and area shrinkage of whole sour cherry fruits during drying. It was observed that volume and area changes did not depend on the drying parameters. The linear relationship was again found between the dimensionless volume change and the dimensionless moisture content of the dehydrated fruits. Similar results were also reported for carrot drying in a mechanically agitated fluidized bed dryer (Reyes, Alvarez, & Marquardt, 2002).

On the other hand, Devahastin, Suvarnakuta, Soponronnarit, and Mujumdar (2004) reported that although the degrees of shrinkage of carrot cube underwent vacuum drying and low-pressure superheated steam drying (LPSSD) were similar, the changes of shape of carrot cube underwent these two drying processes were much different. Madamba (2003) also reported that although a linear relationship between the dimensionless volume change and the dimensionless moisture content was observed during hot air drying of bamboo shoot, shrinkage of bamboo shoot parallel to its fibers was different from that occurring perpendicular to its fibers. Thus, expressing the deformation of the drying material using only the degree of shrinkage (or volume shrinkage ratio) is not adequate.

Since experimental shrinkage results are product-specific and limited to the operating conditions tested, the use of a mathematical model to predict shrinkage as well as deformation and their effects on the rates of heat and mass transfer and drying kinetics of the drying material is desirable. Such models have indeed been proposed and tested with various products (Chemkhi, Zagrouba, & Bellagi, 2004; Mihoubi, Zagrouba, Vaxelaire, Bellagi, & Roques, 2004; Yang, Sakai, & Watanabe, 2001). Although these models

could predict the deformation of shrinkable materials to some extents, they are rather sophisticated and contain many parameters that must be known prior to the simulation. In addition, the need for a rapid and simple identification of deformation still exists.

The objective of the present study was to find a simple way to describe the deformation of a food product undergoing drying more precisely. Vacuum drying and LPSSD were chosen as the representative drying techniques and carrot cube was chosen as the representative product. The so-called Heywood shape factor, or the volume shape factor, was chosen to represent the shape of the drying product in this study.

2. Experimental set-up, material and methods

2.1. Experimental set-up

A schematic diagram of the low-pressure superheated steam dryer and its accessories is shown in Fig. 1. The dryer consists of a stainless steel drying chamber, insulated carefully with rock wool, with an inner dimension of $45 \times 45 \times 45 \text{ cm}^3$; a steam reservoir, which received the steam from the boiler and maintained its pressure at around 200 kPa (gauge); and a liquid ring vacuum pump (model ET32030, Nash, Trumbull, CT), which was used to maintain the vacuum in the drying chamber. Steam trap was installed to reduce the excess steam condensation in the reservoir. An electric heater, rated at 1.5 kW, which was controlled by a proportional-integral-derivative controller (model E5CN, Omron, Tokyo, Japan) was installed in the drying chamber to control the steam temperature and to minimize the condensation of steam in the drying chamber during the start-up period. A variable-speed electric fan was used to disperse steam throughout the drying chamber. The steam inlet was made into a conical shape and was covered with a screen to also help distributing steam in the chamber. The sample holder was made of

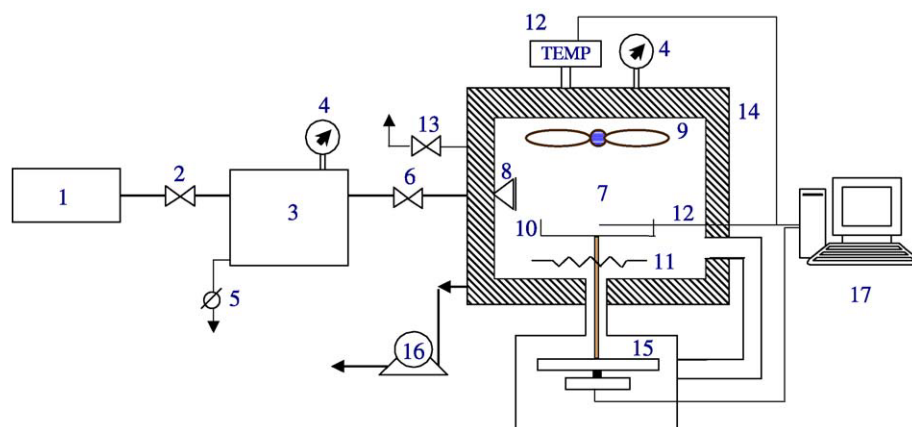


Fig. 1. A schematic diagram of low-pressure superheated steam dryer and associated units. (1) Boiler; (2) steam valve; (3) steam reservoir; (4) pressure gauge; (5) steam trap; (6) steam regulator; (7) drying chamber; (8) steam inlet and distributor; (9) electric fan; (10) sample holder; (11) electric heater; (12) on-line temperature sensor and logger; (13) vacuum break-up valve; (14) insulator; (15) on-line weight indicator and logger; (16) vacuum pump; (17) PC with installed data acquisition card.

stainless steel with a dimension of $12 \times 12 \text{ cm}^2$. The change of the mass of the sample was detected continuously (at 30 s interval) using a load cell (model Ucg-3 kg, Minebea, Nagano, Japan), which was installed in a smaller chamber connected to the drying chamber by a flexible hose (in order to maintain the same vacuum pressure as that in the drying chamber), and also to an indicator and recorder (model AD 4329, A&D Co., Tokyo, Japan). The temperatures of the steam and of the drying sample were measured continuously using type K thermocouples, which were connected to an expansion board (model no. EXP-32, Omega Engineering, Stamford, CT). Thermocouple signals were multiplexed to a data acquisition card (model no. CIO-DAS16Jr, Omega Engineering, Stamford, CT) installed in a PC. LABTECH NOTEBOOK software (version 12.1, Laboratory Technologies Corp., MA) was used to read and record the temperature data. For vacuum drying experiments the same experimental set-up was used but without an application of steam to the drying chamber.

2.2. Material

Fresh carrot was purchased from a local supermarket and stored in a refrigerator at 4°C . Prior to the start of each experiment carrot was removed from the refrigerator to attain the room temperature. It was then peeled and sliced. In this work, samples were prepared using only the cortex tissues because different microstructure of material may affect the degree and pattern of shrinkage. The sliced carrot was cut into cubes with the dimension of $1 \times 1 \times 1 \text{ cm}^3$.

2.3. Methods

To perform a drying experiment approximately 30 cubes of carrot (about 30 g) were placed in the sample holder. Each drying experiment was carried out up to a pre-determined sampling time; that particular experiment was ended at that time. The moisture content (AOAC, 1984), volume and area of the dried product were then measured. These properties were used to calculate the degree and pattern of shrinkage of carrot cube undergoing each drying condition. A new experiment was then performed until the next pre-determined sampling time was reached.

2.4. Measurement of degree of shrinkage

Five carrot cubes taken at any sampling time were used to determine the degree of shrinkage in terms of the volume change ratio. The degree of shrinkage was calculated using the volume of the sample at any sampling time along with its initial volume as shown in Eq. (1). The average values of five samples were then reported.

$$\text{Degree of shrinkage} = \frac{V}{V_0} \quad (1)$$

where V is the volume of carrot cube after drying (m^3); V_0 is the volume of carrot cube before drying (m^3). The sample

volume (V) was determined by n -heptane displacement. The weight of the sample displaced in n -heptane was measured using a digital balance (model RC 250S, Sartorius, Goettingen, Germany).

2.5. Measurement of shrinkage pattern

Many attempts have been made in the field of powder and particle technology to define the particle shape using one single parameter. Among many proposed parameters is the Heywood shape factor (k), which uses measurements of surface area and volume to characterize the shape of material. In the present study the shrinkage pattern of carrot cube was determined in terms of this shape factor, which is calculated as follows (Yang, 2003):

$$k = \frac{V_p}{d_a^3} \quad (2)$$

where V_p is the volume of the cube (m^3); A_p is the projected area of the cube (m^2); and d_a is the equivalent projected-area diameter of the cube (m), $d_a = \sqrt{4A_p/\pi}$.

The volume of each carrot cube was measured by n -heptane displacement. The projected area of six sides of the cube was determined by a planimeter (model X-plan360dII, Ushikata Manufacturing, Tokyo, Japan). The maximum projected area of the cube was then selected to calculate the equivalent diameter of the cube. This is because the equivalent diameter is defined as the diameter of a sphere having the same projected area as the cube viewed in a direction perpendicular to the plane of the greatest stability of the cube (Seville, Tüzün, & Clift, 1997).

The effects of two factors, i.e., drying method and temperature, on the deformation kinetics of carrot cube were investigated in this study. Drying was conducted at three levels of temperature, i.e., 60, 70 and 80°C ; the chamber pressure was maintained at 7 kPa. The drying samples were taken out at 0.5-h interval during the first 2.5 h and then at 1 h interval until the sample achieved the final moisture content of 0.07 kg/kg (d.b.).

2.6. Statistical analysis

The experiments were designed in complete random. The data were analyzed and presented as mean values with standard deviations. Differences between mean values were established using Tukey's HSD comparisons. Values were considered at 95% confidence level ($p < 0.05$). All experiments were performed in duplicate.

3. Results and discussion

3.1. Drying kinetics of carrot cube

Carrot cube that had an initial moisture content of about 9.2 kg/kg (d.b.) (or about 90% w.b.) was dried and sampled out at every 0.5 h interval during the first 2.5 h

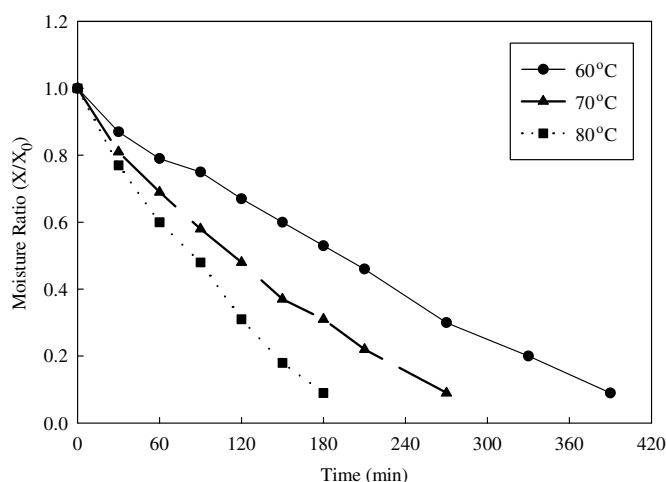


Fig. 2. Drying curves of carrot cube undergoing LPSSD.

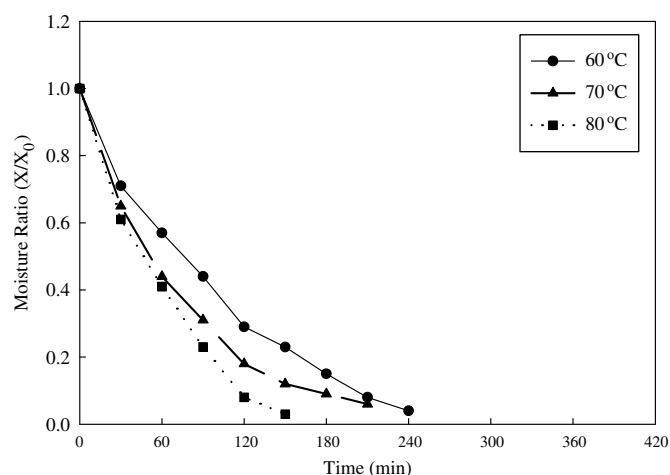


Fig. 3. Drying curves of carrot cube undergoing vacuum drying.

and every 1 h afterwards until the final moisture content of 0.07 kg/kg (d.b.) was reached in LPSSD and vacuum dryer. Figs. 2 and 3 show the drying curves of carrot cube undergoing LPSSD and vacuum drying, respectively. As

expected, higher drying temperatures led to higher rates of moisture removal due to higher temperature differences between the sample and the drying medium at higher drying temperatures. Moisture diffusivity is also higher at a

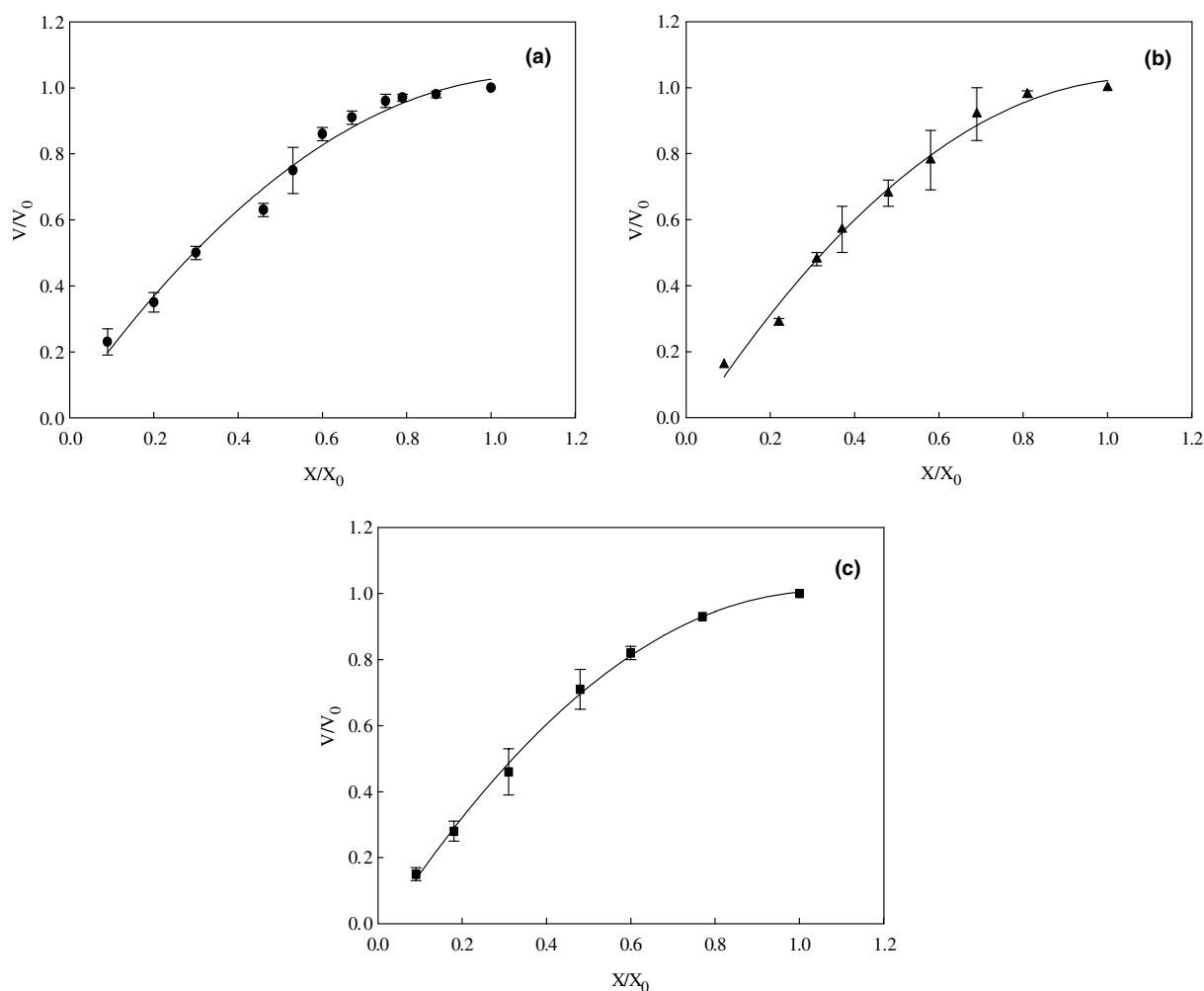


Fig. 4. Shrinkage of carrot cube during LPSSD as a function of moisture ratio at temperature: (a) 60 °C, (●) experimental data, (—) model (b) 70 °C, (▲) experimental data, (—) model (c) 80 °C, (■) experimental data, (—) model.

higher drying temperature leading to a greater mobility of water through the drying product.

Comparison between the two drying methods revealed that the drying time of vacuum drying was shorter than that of LPSSD at the same drying temperature. This is probably due to the fact that the electric heater was used more often during vacuum drying since it was the only source of energy for drying. This might increase the amount of radiation absorbed by the carrot surfaces, thus explaining the higher drying rate during vacuum drying (Devahastin et al., 2004). In addition, the chamber of the vacuum dryer was less humid and hence led to larger moisture gradients between the product and the surrounding, which facilitated drying. The driving force for heat transfer in the case of vacuum dryer might also be higher in this tested range of drying temperatures as well (Suvarnakuta, Devahastin, Soponronnarit, & Mujumdar, 2005).

3.2. Degree of shrinkage of carrot cube

Fig. 4 shows the degree of shrinkage (V/V_0) of carrot cube during LPSSD at 60, 70 and 80 °C as a function of

the moisture ratio. Generally, the literature reports the shrinkage of a food product as a linear function of moisture ratio (Corzo & Bracho, 2004; Ochoa et al., 2002; Raghavan & Silveira, 2001; Ratti, 1994). However, in this work, it was found that the relation between the volume ratio and the moisture ratio was almost second-order. However, if the data during the first period of drying were neglected, the trend of the volume ratio and the moisture ratio would be almost linear as reported by other researchers.

The degree of shrinkage of carrot cube during vacuum drying as a function of moisture ratio at 60, 70 and 80 °C is shown in Fig. 5. The result is similar to that of LPSSD, i.e., the relationship between the volume ratio and the moisture ratio is almost second-order in nature. The following equation may thus be used to represent the relationship between the volume ratio and the moisture ratio of carrot cube undergoing both LPSSD and vacuum drying

$$\frac{V}{V_0} = a \left(\frac{X}{X_0} \right)^2 + b \left(\frac{X}{X_0} \right) + c \quad (3)$$

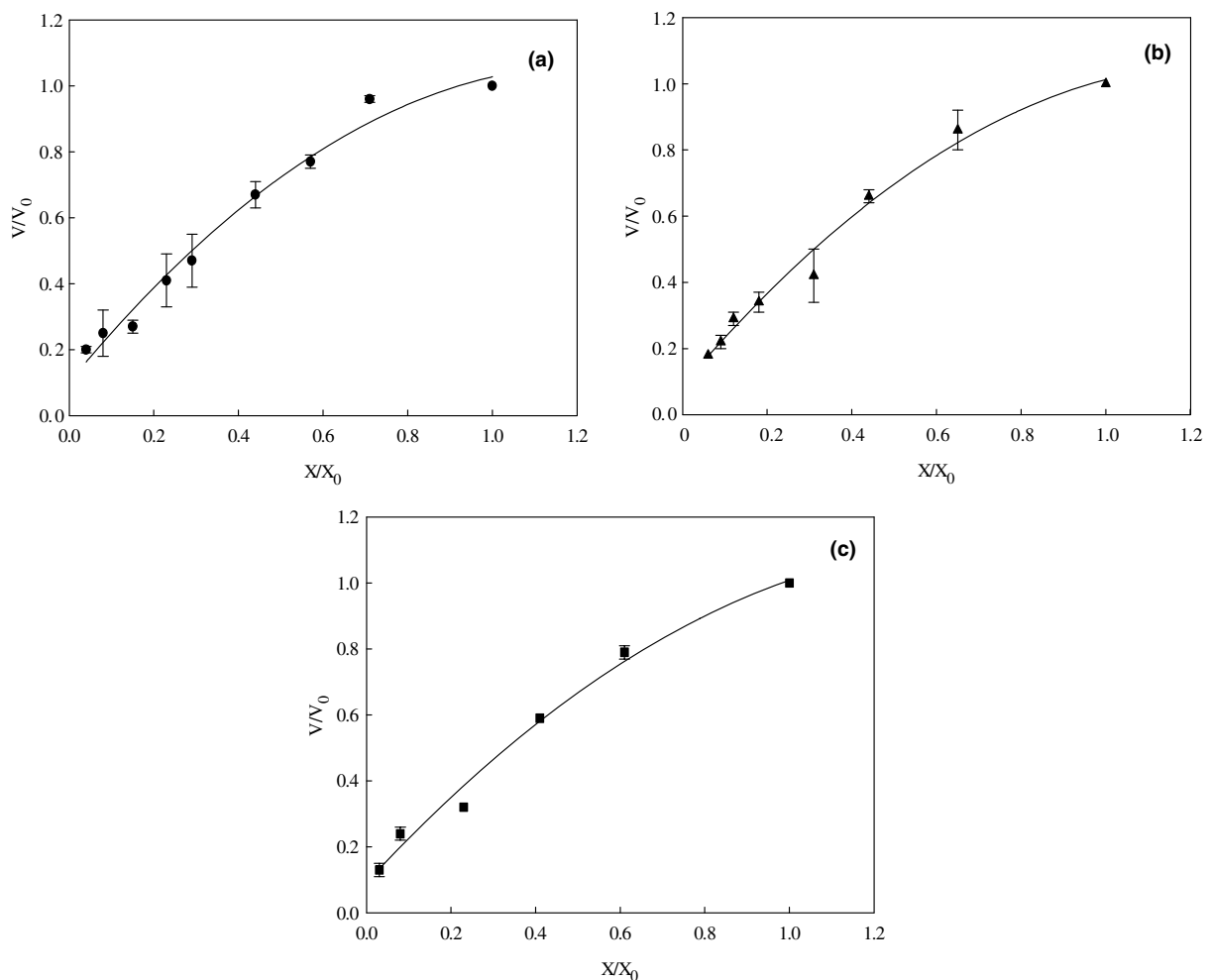


Fig. 5. Shrinkage of carrot cube during vacuum drying as a function of moisture ratio at temperature: (a) 60 °C, (●) experimental data, (—) model; (b) 70 °C, (▲) experimental data, (—) model; (c) 80 °C, (■) experimental data; (—) model.

a, *b* and *c* are constants obtained by fitting the equation to the experimental results at various drying conditions; the values of these constants are listed in Table 1. It can be observed nevertheless that the relationship between the volume ratio and the moisture ratio in the case of vacuum drying is slightly more linear than that of LPSSD due probably to its higher rate of water removal.

The comparison of the degree of shrinkage of carrot cube undergoing LPSSD and vacuum drying at various temperatures is shown in Fig. 6. During an early stage of drying shrinkage of carrot undergoing LPSSD was less than that of vacuum drying due probably to the steam

evolution and less moisture gradient induced stresses within carrot cube. However, towards the end of drying, at moisture ratios of less than 0.4, the results were opposite. Towards the end carrot cube undergoing vacuum drying shrank less than carrot cube undergoing LPSSD. This is because at this point the surface of vacuum dried carrot was much drier and some case hardening occurred; this case hardened skin acted to preserve the final size of carrot cube better than in the case of LPSSD dried carrot, which had much less case hardened skin. However, the differences of the results of the two drying methods were not significantly different at 95% confidence level.

Table 1
The *a*, *b* and *c* values at different drying methods and drying conditions

Drying method	Temperature (°C)	<i>a</i>	<i>b</i>	<i>c</i>	<i>R</i> ²	AME ^a
LPSSD	60	−0.8288	1.8170	0.0366	0.9864	0.0257
	70	−0.9026	1.9663	−0.0433	0.9916	0.0230
	80	−0.9492	1.9938	−0.0421	0.9971	0.0110
Vacuum drying	60	−0.7465	1.7048	0.0628	0.9850	0.0312
	70	−0.5871	1.5062	0.0882	0.9835	0.0233
	80	−0.4679	1.3828	0.0933	0.9877	0.0257

^a AME = absolute mean error.

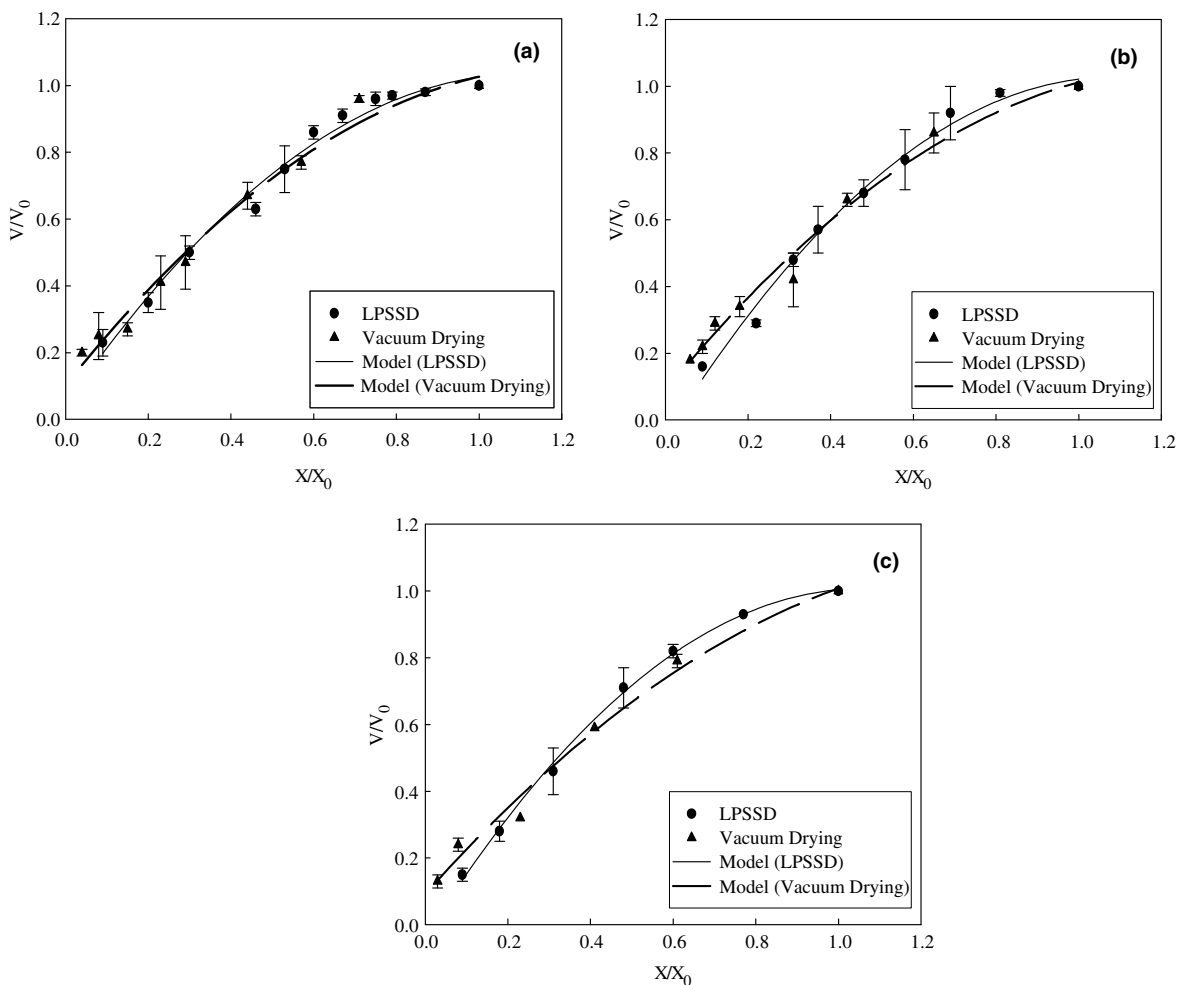


Fig. 6. Comparison of shrinkage of carrot cube undergoing LPSSD and vacuum drying at temperature: (a) 60 °C, (b) 70 °C and (c) 80 °C.

The comparison of the degree of shrinkage of carrot cube undergoing LPSSD at various drying temperatures is shown in Fig. 7a and b for vacuum drying. From these figures it is seen that the trends of shrinkage of carrot cube

at different temperatures were similar. However, small differences could be noticed from the results when using different drying temperatures. The degree of shrinkage at 60 °C was significantly different ($p < 0.05$) from those at

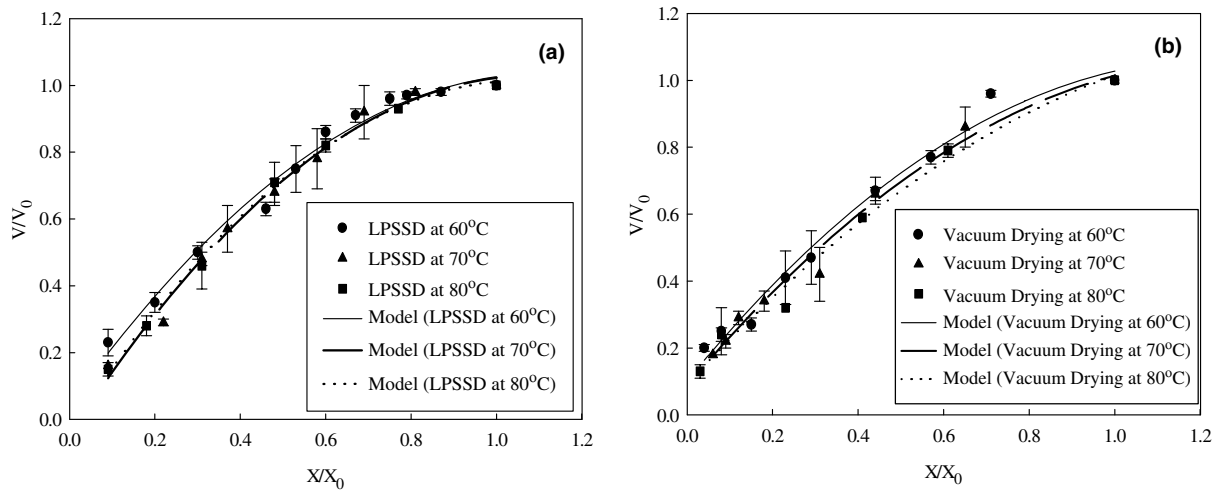


Fig. 7. Comparison of shrinkage of carrot cube at various temperatures undergoing: (a) LPSSD and (b) vacuum drying.

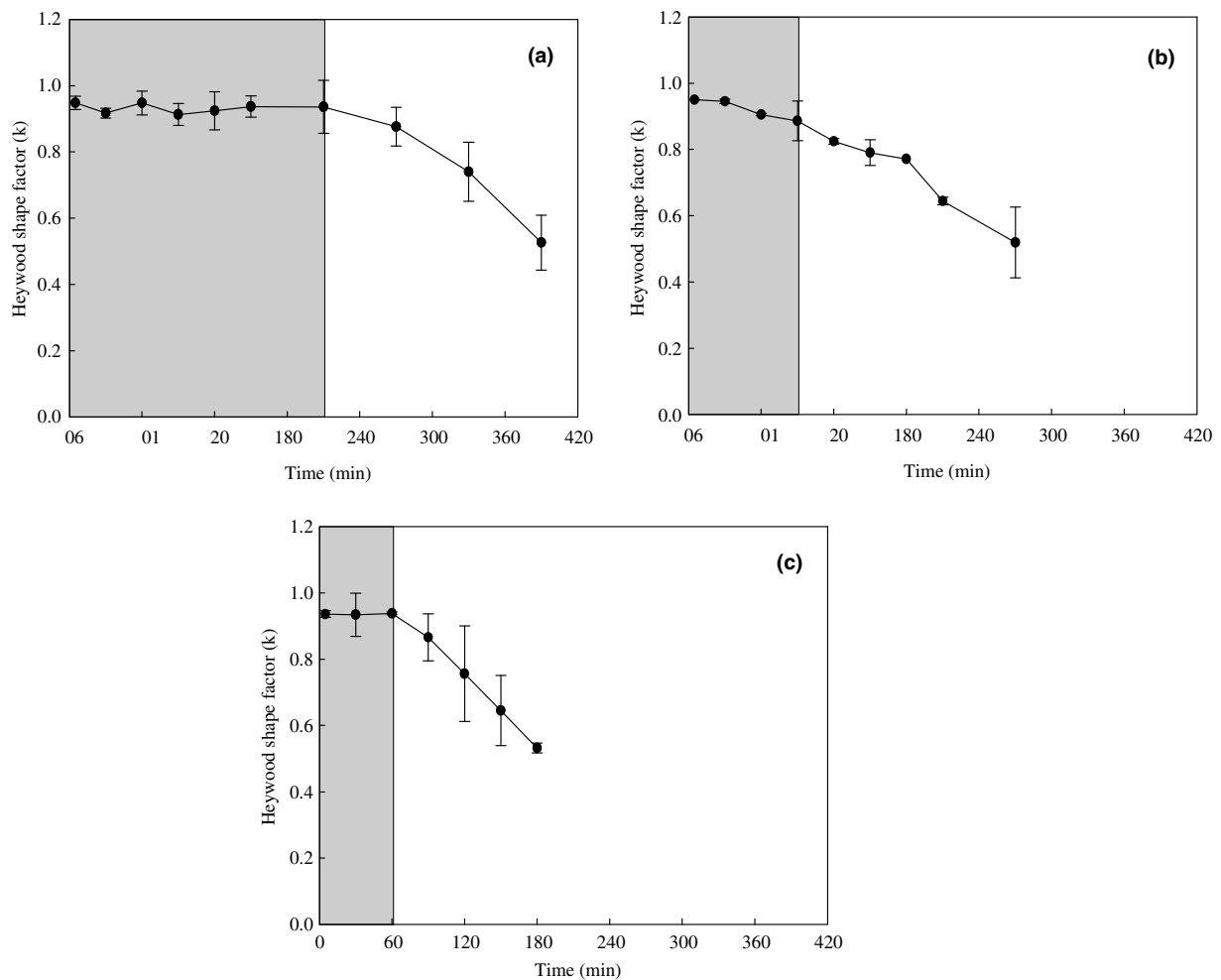


Fig. 8. Heywood shape factor of carrot cube during LPSSD at temperature: (a) 60 °C; (b) 70 °C and (c) 80 °C.

70 and 80 °C. This may be due to lower levels of temperature and moisture gradient induced stresses at lower drying temperatures. A result by Ochoa et al. (2002) was different, however. In their work it was observed that volume and area changes did not depend on drying conditions. The degree of shrinkage of carrot cube at the drying temperature of 70 °C was insignificantly different ($p > 0.05$) from that at 80 °C. This is probably due to the fact that the two drying temperatures might not be much different to cause any significant differences in the degree of shrinkage.

3.3. Pattern of shrinkage of carrot cube

Fig. 8 shows the evolution of Heywood shape factor of carrot cube during LPSSD at 60, 70 and 80 °C. It is seen that the results could be divided roughly into two portions. During an early stage of drying the Heywood shape factor remained almost constant, which implied that more or less uniform deformation occurred. During an early stage of drying the properties of the surface layers of the drying material might not differ much from those

of the center (Mujumdar, 1995). The duration of the uniform deformation periods was different at different drying temperatures, however. The duration of the uniform deformation period of LPSSD at 60, 70 and 80 °C was 210, 90 and 60 min, respectively. At the drying temperature of 60 °C the uniform deformation period was the longest because of the lowest temperature difference between the product and the heating medium leading to a lower water removal rate and hence smaller moisture and temperature gradient induced stresses. Towards the end of drying the Heywood shape factor decreased with drying time, which implied a non-uniform deformation during this later stage of drying. The deformation rates during this later stage were also different at different drying temperatures.

The shrinkage pattern of carrot cube undergoing vacuum drying (Fig. 9) was similar to that of LPSSD. The pattern could again be divided into two portions, uniform and non-uniform deformation periods. The uniform deformation period at 60 °C (150 min) was longer than that at 70 °C (60 min) for the same reason mentioned earlier for LPSSD. At 80 °C this period of uniform deformation did

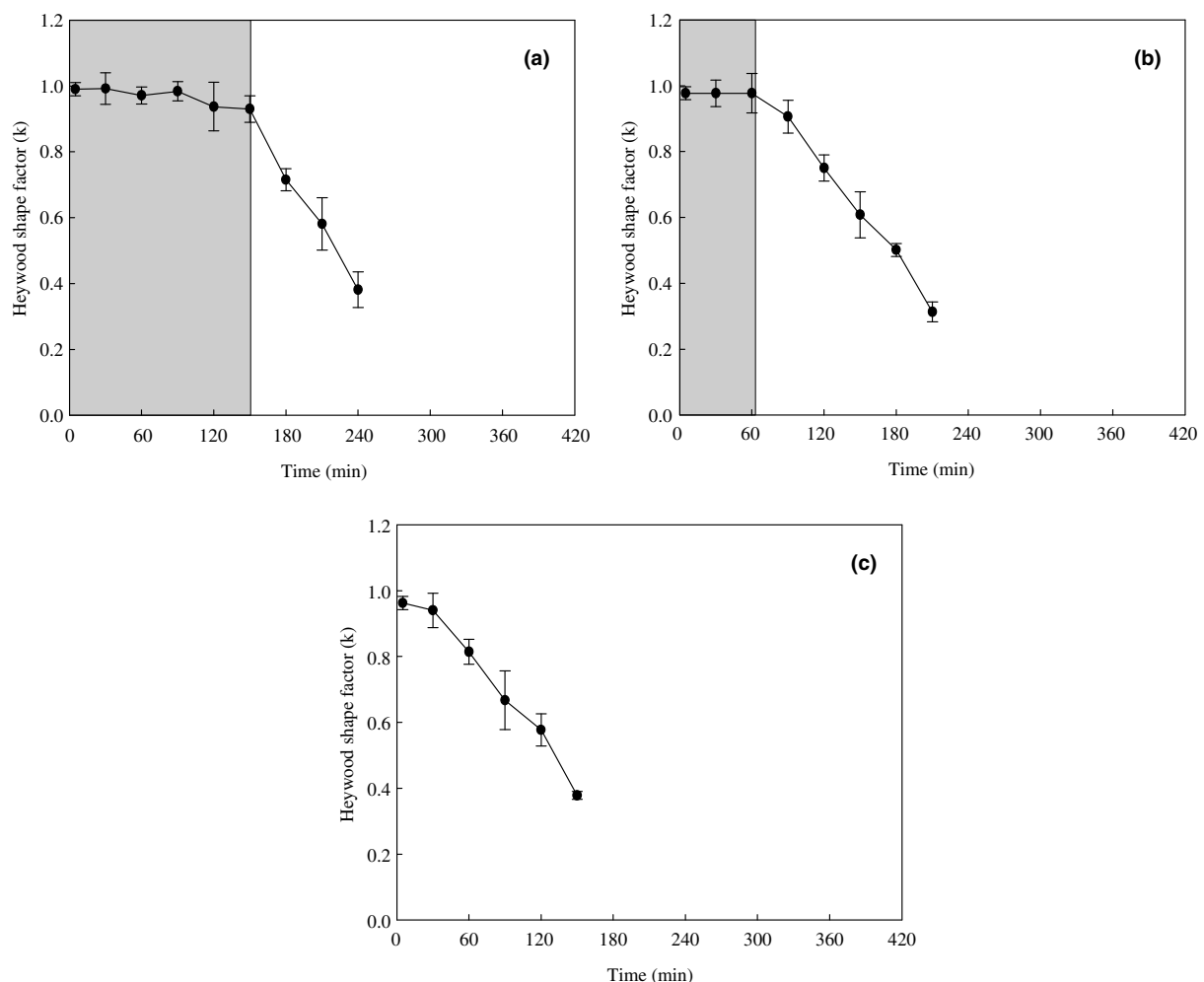


Fig. 9. Heywood shape factor of carrot cube during vacuum drying at temperature: (a) 60 °C, (b) 70 °C and (c) 80 °C.

not exist, however, since carrot cube deformed rapidly at this temperature. At higher temperature higher moisture gradients could be expected in the material and therefore higher internal stresses. In addition, the extent of damage

is a function of the drying temperature as well (Khraisheh et al., 1997).

The effect of drying temperature on the evolution of Heywood shape factor of carrot cube undergoing LPSSD

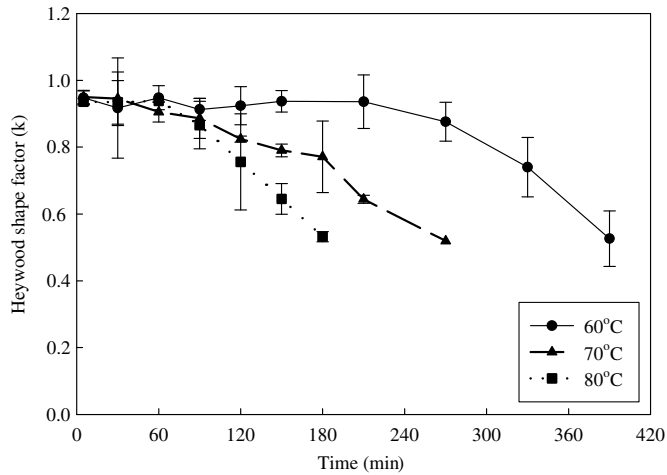


Fig. 10. Comparison of Heywood shape factor of carrot cube undergoing LPSSD at various temperatures.

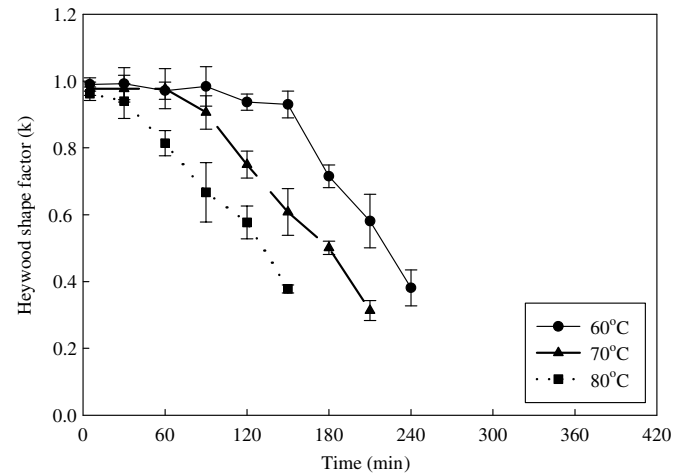


Fig. 11. Comparison of Heywood shape factor of carrot cube undergoing vacuum drying at various temperatures.

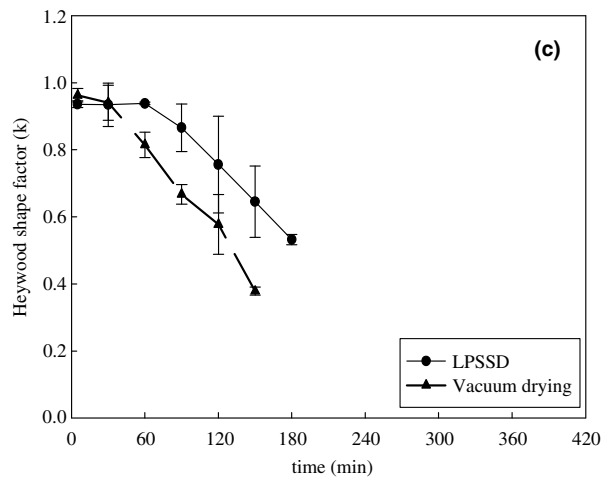
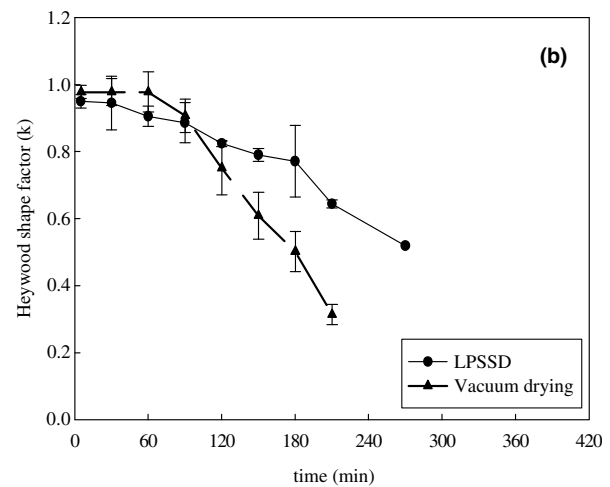
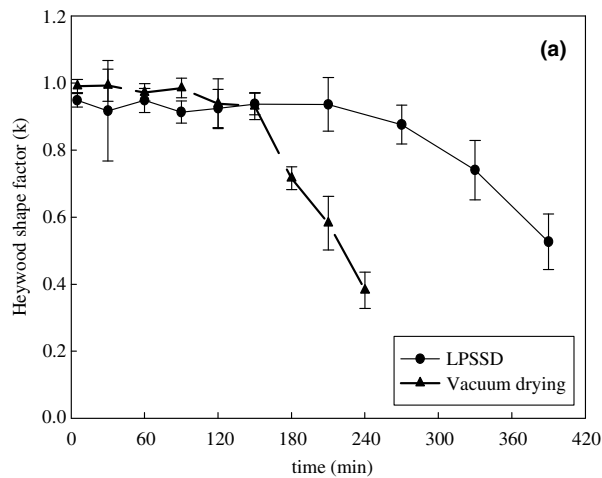


Fig. 12. Comparison of Heywood shape factor of carrot cube during LPSSD and vacuum drying at temperature: (a) 60 °C; (b) 70 °C and (c) 80 °C.

is shown in Fig. 10. As observed earlier, the pattern of shrinkage composed of two portions, uniform and non-uniform deformation periods. The uniform deformation periods varied with the drying temperature; this period was shorter at higher drying temperatures. So, it might be able to conclude that drying product at a lower temperature could maintain the shape of the product longer (or better) than drying at a higher temperature.

Consider then the non-uniform deformation period. The slope of the plot in this period could be used to represent the rate of deformation of the drying material. The slopes of the plots at 60, 70 and 80 °C were -0.0023 , -0.0027 and -0.0034 min^{-1} , respectively; the slope increased with the drying temperature. This again implies that drying the product at higher temperatures leads to a more rapid deformation of the product than doing so at lower temperatures.

Fig. 11 illustrates the shrinkage pattern of carrot cube undergoing vacuum drying. The period of uniform deformation was quite short compared with that of LPSSD. Considering the non-uniform deformation period the slopes of the plots at 60, 70 and 80 °C were -0.0044 ,

-0.0045 and -0.0045 min^{-1} , respectively. In this case, the slopes of all plots were almost the same indicating that the rates of non-uniform deformation were not much different at different drying conditions. This may be due to the fact that the properties of air are not as much dependent on the temperature as those of superheated steam, especially over a narrow range as that used in this work.

As mentioned earlier, the degrees of shrinkage of carrot cube undergoing two different drying methods were not significantly different. Fig. 12, on the other hand, shows the patterns of shrinkage of carrot cube during LPSSD

Table 2
Comparison of the deformation rates of carrot cube undergoing LPSSD and vacuum drying at various temperatures

Temperature (°C)	Rate of deformation (min^{-1})	
	LPSSD	Vacuum drying
60	-0.0023	-0.0044
70	-0.0027	-0.0045
80	-0.0034	-0.0045

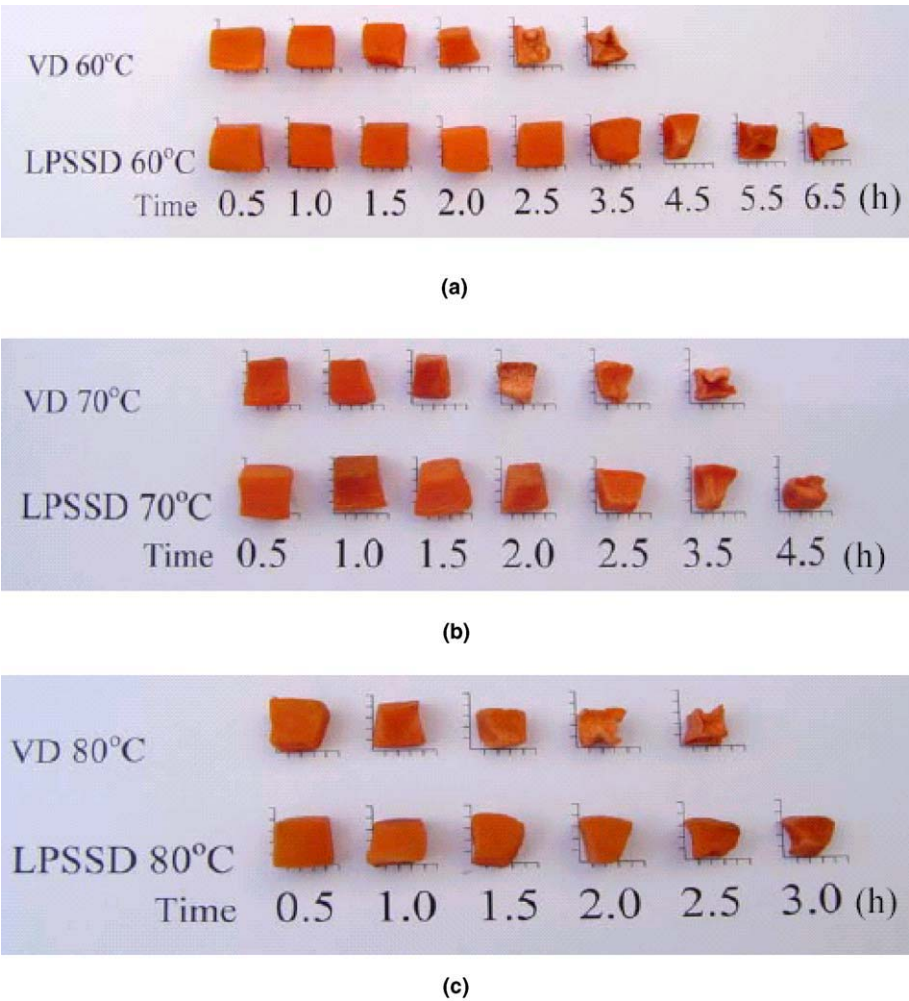


Fig. 13. Dried carrot undergoing vacuum drying and LPSSD at temperature: (a) 60 °C; (b) 70 °C and (c) 80 °C.

and vacuum drying at the same drying temperature. By comparing LPSSD and vacuum drying it is seen from this figure that the uniform deformation period of carrot cube undergoing LPSSD was longer than in the case of vacuum drying at every tested condition. This is because LPSSD yielded a slower drying rate than that in the case of vacuum drying at the same drying temperature. Slow drying product shrinks more uniformly into a solid core since the magnitude of internal stresses is lower (Mujumdar, 1995).

For the non-uniform deformation period the comparison of the deformation rates of LPSSD and vacuum drying, which were calculated from the slopes of the plots of the Heywood shape factor versus the drying time during the non-uniform deformation period, is shown in Table 2. It is seen that carrot undergoing vacuum drying deformed more rapidly and indeed less uniformly than that undergoing LPSSD at every drying condition tested. The final values of Heywood shape factor of carrot cube undergoing LPSSD stayed between 0.519 and 0.532 while they stayed between 0.313 and 0.381 in the case of vacuum drying. These results are consistent with the photographic results of Fig. 13, which shows the shapes of carrot cubes undergoing both LPSSD and vacuum drying at different conditions. Vacuum dried carrot deformed much more than LPSSD dried carrot although the two samples had similar degrees of shrinkage.

4. Conclusion

The drying kinetics as well as the degree and pattern of shrinkage of carrot cube undergoing LPSSD and vacuum drying at various temperatures were examined. In terms of drying kinetics the drying temperature affected in a normal fashion the moisture reduction rate of samples dried both by LPSSD and vacuum drying. The relationship between the degree of shrinkage and the moisture ratio was found to be almost second-order in nature at every tested condition. The degree of shrinkage of carrot cube undergoing LPSSD was not significantly different from that undergoing vacuum drying. However, the shrinkage pattern was found to depend both on the drying methods and drying conditions. Using only the degree of shrinkage to describe the shrinkage (and deformation) is therefore not enough. Further study should be done on refining the technique for evaluating the projected area of the drying sample; such technique as image analysis could be found useful as a more accurate result might be obtained. It should be noted also that there is obviously a limit to how well a single parameter can characterize the particle shape.

Acknowledgements

The authors express their sincere appreciation to the Commission on Higher Education, the Thailand Research Fund (TRF), as well as the International Foundation for Science (IFS), Sweden for supporting this study financially.

References

- Achanta, S., & Okos, M. (2000). Quality changes during drying of food polymers. In A. S. Mujumdar (Ed.), *Drying technology in agriculture and food sciences* (pp. 133–147). Enfield: Science Publishers.
- AOAC (1984). *Official methods of analysis* (14th ed.). Washington, DC: Association of Official Agricultural Chemists.
- Chemkhi, S., Zagrouba, F., & Bellagi, A. (2004). Mathematical modeling for drying of highly shrinkable media. *Drying Technology*, 22, 1023–1039.
- Corzo, O., & Bracho, N. (2004). Shrinkage of osmotically dehydrated sardine sheets at changing moisture contents. *Journal of Food Engineering*, 65, 333–339.
- Devahastin, S., Suvarnakuta, P., Soponronnarit, S., & Mujumdar, A. S. (2004). A comparative study of low-pressure superheated steam and vacuum drying of a heat sensitive material. *Drying Technology*, 22, 1845–1867.
- Khraisheh, M. A. M., Cooper, T. J. R., & Magee, T. R. A. (1997). Shrinkage characteristics of potatoes dehydrated under combined microwave and convective air conditions. *Drying Technology*, 15, 1003–1022.
- Madamba, P. S. (2003). Physical changes in bamboo (*Bambusa phyllostachys*) shoot during hot air drying: Shrinkage, density, and porosity. *Drying Technology*, 21, 555–568.
- Mihoubi, D., Zagrouba, F., Vaxelaire, J., Bellagi, A., & Roques, M. (2004). Transfer phenomena during the drying of a shrinkable product: Modeling and simulation. *Drying Technology*, 22, 91–109.
- Mujumdar, A. S. (1995). Superheated steam drying (2nd ed.). In A. S. Mujumdar (Ed.), *Handbook of industrial drying* (vol. 2, pp. 1071–1086). New York: Marcel Dekker.
- Ochoa, M. R., Kessler, A. G., Pirone, B. N., Marquez, C. A., & De Michelis, A. (2002). Volume and area shrinkage of whole sour cherry fruits (*Prunus cerasus*) during dehydration. *Drying Technology*, 20, 147–156.
- Raghavan, G. S. V., & Silveira, A. M. (2001). Shrinkage characteristics of strawberries osmotically dehydrated in combination with microwave drying. *Drying Technology*, 19, 405–414.
- Ratti, C. (1994). Shrinkage during drying of foodstuffs. *Journal of Food Engineering*, 23, 91–105.
- Reyes, A., Alvarez, P. I., & Marquardt, F. H. (2002). Drying of carrot in a fluidized bed. I. Effects of drying conditions and modelling. *Drying Technology*, 20, 1463–1483.
- Seville, J. P. K., Tüzün, U., & Clift, R. (1997). *Processing of particulate solids*. London: Blackie Academic & Professional.
- Suvarnakuta, P., Devahastin, S., Soponronnarit, S., & Mujumdar, A. S. (2005). Drying kinetics and inversion temperature in a low-pressure superheated steam-drying system. *Industrial & Engineering Chemistry Research*, 44, 1934–1941.
- Yang, H., Sakai, N., & Watanabe, M. (2001). Drying model with non-isotropic shrinkage deformation undergoing simultaneous heat and mass transfer. *Drying Technology*, 19, 1441–1460.
- Yang, W.-C. (2003). Particle characterization and dynamics. In W.-C. Yang (Ed.), *Handbook of fluidization and fluid-particle system* (pp. 1–24). New York: Marcel Dekker.

Neural network prediction of physical property changes of dried carrot as a function of fractal dimension and moisture content

Soraya Kerdpi boon ^a, William L. Kerr ^{b,*}, Sakamon Devahastin ^a

^a Department of Food Engineering, King Mongkut's University of Technology, Thonburi, 126 Pracha u-tid Road, Bangkok 10140, Thailand

^b Department of Food Science and Technology, University of Georgia, Athens, GA, USA

Received 22 May 2006; accepted 30 July 2006

Abstract

The relationship between microstructural and physical properties of dried foods is difficult to quantify. This study uses artificial neural network analysis (ANN) to predict shrinkage and rehydration of dried carrots, based on inputs of moisture content and normalized fractal dimension analysis ($\Delta D/D_0$) of the cell wall structure. Several drying techniques were used including conventional hot air (HAD), low pressure superheated steam (LPSSD), and freeze drying (FD). Dried carrot sections were examined by light microscopy and the fractal dimension (D) determined using a box counting technique. Optimized ANN models were developed for HAD, LPSSD, HAD + LPSSD, and HAD + LPSSD + FD, based on 1–10 hidden layers and neurons per hidden layer. ANN models were then tested against an independent dataset. Measured values of shrinkage and rehydration were predicted with an $R^2 > 0.95$ in all cases.

© 2006 Elsevier Ltd. All rights reserved.

Keywords: Artificial neural network; Carrot; Drying; Fractal analysis; Rehydration ratio; Shrinkage

1. Introduction

During food drying, moisture migrates from interior regions of the product to the surface and on into the surrounding air, resulting in changes in physical properties and structure of the product. Many studies have focused on changes of external properties of foods during drying, such as alterations in volume, area, and shape (Mayor & Sereno, 2004; Ochoa, Kessler, Pirone, Marquez, & De Michelis, 2002; Ratti, 1994). However, changes in these outward properties are primarily caused by internal changes, which are directly related to structural changes of the drying materials.

Structural changes in dried products can be viewed using light or electron microscopy. However, apparent differences in structural features caused by processing can be

difficult to quantify. Various techniques such as Fourier analysis, particle size distribution, or intensity measurements might be used depending on the structural feature of interest. Many foods, particularly those of a cellular nature, experience shrinkage, and convolution of the cell wall or membrane during drying. One approach then is to use fractal analysis to quantify structural changes in the microstructural features of dried products.

Fractals have been used to describe and quantify irregular fragments or complex shapes of materials such as shorelines, clouds, plants, brain cells, gold colloids, and sponge iron (Graf, 1991; Mandelbrot, 1982). Fractal analysis has also been used to study structural and mechanical attributes of some food products. From the particle contours seen in SEM images, Peleg and Normand (1985) characterized the ruggedness of instant coffee after agglomeration. Barletta and Barbosa-Canovas (1993) used machine-vision CCD technology to determine the contours of instant coffee and skim milk particles, and compared three methods for computing fractal values to describe ruggedness. Hsu, Lu, and Huang (2000) suggested that changes in the

* Corresponding author. Tel.: +1 706 542 1085; fax: +1 706 542 1050.
E-mail address: wkerr@uga.edu (W.L. Kerr).

Nomenclature

ANN artificial neural network
 D fractal dimension
 $\Delta D/D_0$ normalized fractal dimension
 FD freeze drying

HAD hot air drying
 LPSSD low pressure superheated steam drying

viscoelastic properties of rice starch and soy protein suspensions during gelatinization could be related to fractal dimension descriptions of the gel networks. Rubnov and Saguy (1997) determined fractal dimensions from SEM images of restructured potato products and found that fractal dimension correlated with oil uptake during frying. Chanona et al. (2003) applied fractal analysis to the changing surface temperature of drying agar gel slabs, showing that there were three stages of drying. Few studies have demonstrated the correlation between physical property changes and product structure during processing. Such correlations could aid in understanding and predicting the property changes of foods undergoing drying.

There are several methods for constructing a relationship between the physical properties and structure of dried foods, such as models based on theoretical constructs, regression analysis, or principal component analysis. The properties of dried foods vary substantially depending on the type of product, moisture content, drying type, and drying conditions. Thus, a promising approach is to use artificial neural network (ANN) analysis, which can be trained to consider and weight various inputs. The ANN is made up of a group of interconnected artificial neurons. Each neuron transforms an input and sends its output to other neurons to which it is connected. The receiving neuron determines a weighted sum of the inputs. Each artificial neuron transforms its input through a system of linear equations, which may include logarithmic or hyperbolic tangent functions. The network is trained with a subset of observations and optimized based on its ability to predict a set of known outcomes.

Neural networks are effective for modeling, optimization, and process control of complex problems (Goncalves, Minim, Coimbra, & Minim, 2005). ANN has been used to predict thermal conductivity of food as a function of moisture content, temperature, and apparent porosity (Sablani & Rahman, 2003); to predict thermal inactivation of bacteria (Lou & Nakai, 2001); and to design and optimize high-pressure processes in the food industry (Torrecilla, Otero, & Sanz, 2005).

The objective of this work was to develop models for predicting properties of dried carrot based on composition, drying technique, and microstructural features, in which these microstructural features were characterized in terms of normalized fractal dimension. The two key physical properties considered for dried carrot were %shrinkage and rehydration ratio.

2. Methodology

2.1. Drying techniques

Fresh carrots (*Daucus carota* var. *sativa*) were obtained from a local supermarket and kept at 4 °C. Prior to the start of each experiment, carrots were removed from refrigerated storage and allowed to reach room temperature (~24 °C). The carrots were then peeled and sliced. In this study, samples were prepared using only the cortex tissue to limit structural variations in samples. Samples were diced into 1 × 1 × 1 cm³ cubes. Carrots were dried using three different drying techniques, namely conventional hot air drying (HAD), low pressure superheated steam drying (LPSSD), and freeze drying (FD). Cubed samples were dried in a hot air tray dryer constructed from stainless steel, with air heated by a 6.6 kW heater, and the temperature controlled to within 0.1 °C with a PID controller (Kerdpi-boon & Devahastin, in press). Samples were dried at 60, 70 and 80 °C and air velocities of 0.5 and 1 m/s. LPSSD drying was accomplished in a unit with a 0.45 m × 0.45 m × 0.45 m drying chamber, as described by Devahastin, Suvar-nakuta, Soponronnarit, and Mujumdar (2004). Steam was produced in a boiler, passed through a steam reservoir and steam trap, then introduced into the chamber and maintained at 7 kPa, with a variable-speed electric fan used to distribute steam throughout the chamber. A vacuum pump (Model ET32030, Nash Engineering Co., Trumbull, CT) was used to help maintain vacuum in the drying chamber. The temperature of steam in the chamber was kept constant with a 1.5 kW electrical heater, controlled by a PID controller. As with HAD, LPSSD samples were dried at 60, 70 and 80 °C. A Labconco 77550 freeze dryer (Labconco, Kansas City, MS) was used for FD samples. Samples were frozen to −25 °C by a plate contact freezer, with a freezing rate on the order of 0.2 °C/min, and held at that temperature for 3 h. The freeze dryer was operated with a condenser temperature of −51 °C, and a temperature program rate of 0.2 °C/min. In separate runs, samples were removed for analysis at 0, 4, 8, 12 and 16 h.

2.2. Structure and property measurements

At regular intervals, samples were removed to determine moisture content, percent shrinkage, rehydration ratio and microstructural changes. Moisture content was determined by AOAC Method 7.003 (AOAC, 1984).

Shrinkage was determined from the change in volume of five pieces. Volumes were determined by displacement of a known volume of *n*-hexane in a graduated cylinder. Percent shrinkage was expressed as:

$$\% \text{Shrinkage} = \left(\frac{V_i - V}{V_i} \right) \times 100 \quad (1)$$

where V_i is the initial volume (prior to drying) and V is the volume after drying.

Rehydration properties were determined by immersing dried samples in boiling water (100 °C) for 10 min. The wetted sample was drained and the mass determined to the nearest 0.0001 g. The rehydration ratio was calculated as:

$$R = \frac{m}{m_0} \quad (2)$$

where m_0 is the mass of the dried and m is the mass of rehydrated sample.

Samples for microstructural analysis were prepared as described by Kerdpiroon and Devahastin (in press). Each sample was fixed in 10% formaldehyde, washed, and then dehydrated in a series of isopropyl alcohol solutions. Samples were then embedded with melted paraffin at 60 °C, cooled, and sectioned by Leica Jung RM2025 microtome (Leica Microsystems, Wetzlar, Germany) into 5 µm slices. Cell wall materials were dyed with haematoxylin and eosin, and then examined by light microscopy (Olympus Model LH30RF200, Tokyo, Japan). Images were collected with a CCD digital camera system using the PixelView Geo-Force 7300 multimedia card and capture software (Pro-Link Computer, City of Industry, CA).

2.3. Fractal analysis

Digital images of the carrot sections were attained from the microscope at a 520 × 520 pixel resolution, and viewed at approximately 500× total magnification. Images of a micrometer scale at the same conditions show that this corresponds to an image resolution of 0.71 µm/pixel. Images were grayscale, then thresholded to provide clear contrast between the cell wall and background.

Fractal dimension was calculated using a box counting method (Quevedo, Calos, Aguilera, & Cadoche, 2002). Square boxes with a specified size (r) were overlayed onto the image. The number of boxes ($N(r)$) which contained cell wall were counted. This was repeated for box sizes of 4, 5, 10, 13, 26, 65, 130, and 260 pixels. Fractal dimension is calculated as

$$D = \lim_{r \rightarrow 0} \frac{\log(N(r))}{\log(1/r)} \quad (3)$$

The fractal dimension was calculated using Matlab software (version 6.5) as detailed in Kerdpiroon and Devahastin (in press). Normalized fractal dimensions were reported as:

$$\Delta D/D_0 = \frac{D - D_0}{D_0} \quad (4)$$

where D_0 and D are the fractal dimensions of fresh and dried samples, respectively.

2.4. Artificial neural network training

Artificial neural networks were developed using Matlab 7 software, with the Neural Network Toolbox 4 (The Mathworks, Inc., Natick, MA, USA). The networks were simulated based on a multilayer feed forward neural network. This type of network is very powerful in function optimization modeling (Lou & Nakai, 2001). The input layer, hidden layers, and output layer structures are shown in Fig. 1. A back-propagation algorithm was used to implement supervised training of the network. During training, weighting functions for the inputs to each ANN were determined, such that the predicted output best matched the actual output from the data set. Weights were randomly assigned at the beginning of the training phase, according to the back-propagation algorithm. A hyperbolic tangent was used as the transfer function in each hidden layer, and a linear transfer function was used in the output layer. Minimization of error was accomplished using the Levenberg–Marquardt (LM) algorithm. Training was finished when the mean square error (MSE) converged and was less than 0.001. If the MSE did not go below 0.001, training was completed after 1,000,000 epochs, where an epoch represents one complete sweep through all the data in the training set.

The inputs included the normalized fractal dimension ($\Delta D/D_0$), moisture content (mc; kg water/kg), and drying method. The output layer consisted of %shrinkage and rehydration ratio. The number of hidden layers and number of neurons in each hidden layer were varied from 1 to 10 (1, 2, 4, 6, 8, or 10). Training was done for thirty trial configurations in each hidden layer/neuron combination, in order to find the combination of hidden layers and neurons that produced the minimum error.

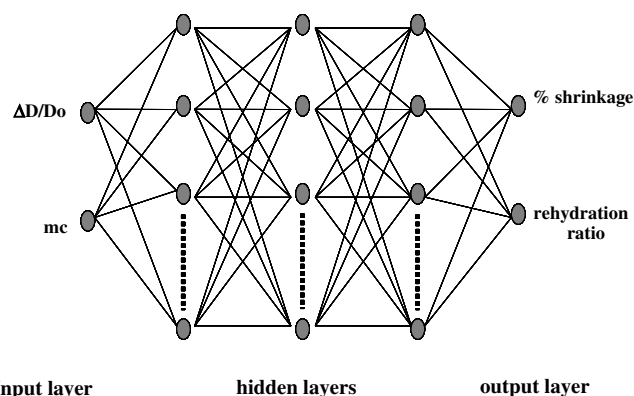


Fig. 1. Schematic diagram of multilayer neural network for prediction of physical properties used in this study.

2.5. Selection of optimal ANN configuration

The optimized configurations from training for each neuron were selected from thirty trial configurations based on neural network performance, which gave the minimum error from the training process. The average mean square error (MAE), standard deviation of MAE (STD_A), percentage of relative mean square error (%MRE), and standard deviation of %MRE (STD_R) were used to compare the performances of various ANN models, and were calculated as:

$$MAE = \frac{1}{N} \sum_{i=1}^N \Delta P_A \quad (5)$$

$$STD_A = \sqrt{\frac{\sum_{i=1}^N (\Delta P_A - \overline{\Delta P_A})^2}{N-1}} \quad (6)$$

$$\%MRE = \left(\frac{1}{N} \sum_{i=1}^N \Delta P_R \right) \times 100 \quad (7)$$

$$STD_R = \sqrt{\frac{\sum_{i=1}^N (\Delta P_R - \overline{\Delta P_R})^2}{N-1}} \quad (8)$$

where $\Delta P_A = |P_P - P_E|$, $\Delta P_R = |(P_P - P_E)/P_E|$, P_P is the predicted output (%shrinkage, rehydration ratio), and P_E the experimentally measured outputs.

3. Results and discussion

Typical light microscopy images are shown in Fig. 2 for HAD carrots. Visual inspection showed that longer drying times resulted in more extensive shrinkage and ruggedness of the carrot cell structure. Fig. 2 also shows the calculated

fractal dimension for each image shown. In general, fractal dimension increased with drying time corresponding to less orderly cell structures. A fractal dimension of 1 corresponds to a straight line, which exhibits self-similarity in 1 direction. A fractal dimension of 2 corresponds to a completely covered plane, which is self-similar in two independent directions. The two-dimensional images of the cell do not fall on a straight line, nor do they completely cover the image space, thus are expected to have a fractal dimension between 1 and 2. Due to the large number of data, the results are summarized in Table 1, which shows the range of normalized fractal dimension ($\Delta D/D_0$) for each of the drying methods. ($\Delta D/D_0$) varied from 0 to 0.094 for HAD, 0 to 0.092 for LPSSD, and 0 to 0.031 for FD. Table 1 also shows the range of moisture contents, the other major input for the ANN model.

The properties to be predicted included %shrinkage and rehydration ratio. The ranges of measured values are shown in Table 1. %Shrinkage varied from 0 to 88.7 for HAD, 0 to 91.4 for LPSSD, and 0 to 40.6 for FD. As expected, freeze drying resulted in the least changes in product volume. Rehydration ratio varied from 1 to 3.41 for HAD, 1 to 3.83 for LPSSD, and 1 to 4.34. It has been shown that LPSSD carrots are more readily rehydrated than HAD carrots, but not as well rehydrated as freeze dried carrots (Kerdpiboon & Devahastin, in press).

The normalized fractal dimension ($\Delta D/D_0$) could be used to monitor the physical property changes of carrot during drying (Kerdpiboon & Devahastin, in press). Both normalized fractal dimension and moisture content were used as inputs in the artificial neural network structure. The ANN optimization process was performed using a trial

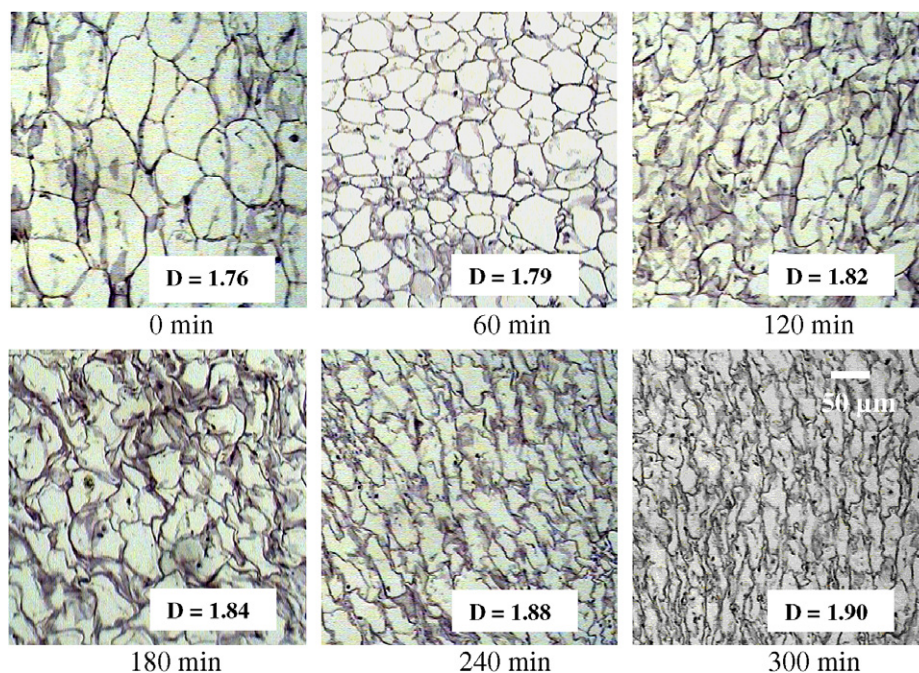


Fig. 2. LM micrographs for carrot undergoing hot-air drying at 60 °C. Inset shows the calculated fractal dimension for each image. Bar corresponds to 50 µm, with image resolution of 0.71 µm.

Table 1

Range of normalized fractal dimension and physical properties of carrot undergoing different drying techniques

Drying techniques	$\Delta D/D_0$	Moisture content (kg H ₂ O/100 kg)	%Shrinkage	Rehydration ratio (m/m_0)
HAD	0–0.094	12.3–0.15	0–88.7	1–3.41
LPSSD	0–0.092	12.2–0.21	0–91.4	1–3.83
Freeze dryer	0–0.031	12.0–0.09	0–40.6	1–4.34

and error technique. Data sets of inputs and outputs used to train the ANN consisted of HAD (66 cases), LPSSD (29 cases), HAD + LPSSD (95 cases), and HAD + LPSSD + freeze dryer (101 cases). Datasets for freeze drying were not considered separately as there were too few for successful training. Each dataset was divided into two groups, consisting of 75% for training/testing and 25% for validation.

During training, the datasets were used to determine the optimum number of hidden layers, and neurons per hidden layer, that gave the best predictive power. ANNs with between 1 and 10 hidden layers were tested (1, 2, 4, 6, 8, 10), and with 1–10 neurons per hidden layer. Each combination of hidden layers and neurons per hidden layer was trained for thirty trial configurations, with each trial start-

ing with a different set of randomized weights, and with the model error determined after each simulation. The results showed that the number of hidden layers, and neurons per hidden layer, that yielded minimum error was different for each drying technique (Table 2), and to a lesser extent the property being predicted. The minimum MRE for HAD was found with two hidden layers and four neurons per layer for shrinkage, and one hidden layer and 10 neurons for rehydration. For LPSSD (Table 3), the lowest MRE for both shrinkage and rehydration was found with two hidden layers and six neurons. A large number of hidden layers does not necessarily lower the error if there are enough numbers of neurons in each hidden layer (Torrecilla et al., 2005). The best prediction in most of the data sets contained two hidden layers.

Table 2

Errors in the prediction of physical properties with different number of hidden layers and neurons per layer for carrot undergoing HAD

No. of hidden	No. of neurons	%Shrinkage				Rehydration ratio (m/m_0)			
		MAE	STD _A	%MRE	STD _R	MAE	STD _A	%MRE	STD _R
1	1	5.70	4.58	8.76	8.92	0.23	0.15	12.7	10.6
	2	2.28	2.22	4.17	5.51	0.13	0.12	5.72	5.05
	4	1.95	2.18	3.86	5.54	0.12	0.11	5.42	4.65
	6	1.92	2.08	4.04	7.45	0.12	0.12	5.49	5.00
	8	1.94	2.15	4.13	5.87	0.13	0.12	5.69	4.90
	10	2.10	2.74	4.74	8.60	0.11	0.13	5.20	6.15
2	1	5.78	4.56	8.96	8.75	0.23	0.15	12.6	10.6
	2	2.15	2.19	4.21	5.68	0.12	0.12	5.54	5.20
	4	2.05	2.16	3.63	4.51	0.12	0.12	5.66	4.99
	6	2.12	2.12	4.33	5.97	0.12	1.35	5.38	5.01
	8	2.04	2.24	3.87	4.67	0.12	0.94	5.53	4.95
	10	2.25	2.40	4.75	7.52	0.12	0.12	5.70	5.76

Table 3

Errors in the prediction of physical properties with different number of hidden layers and neurons per layer for carrot undergoing LPSSD

No. of hidden	No. of neurons	%Shrinkage				Rehydration ratio (m/m_0)			
		MAE	STD _A	%MRE	STD _R	MAE	STD _A	%MRE	STD _R
1	1	6.78	4.90	9.68	7.30	0.15	0.12	9.93	6.69
	2	2.41	2.21	6.31	9.41	0.07	0.08	4.27	4.56
	4	1.59	3.31	3.57	4.44	0.06	0.08	3.75	4.29
	6	1.46	1.32	3.15	3.31	0.06	0.08	3.15	4.43
	8	1.47	1.33	3.52	3.82	0.07	0.08	4.18	4.54
	10	1.41	2.00	3.54	5.88	0.06	0.06	3.83	4.73
2	1	6.83	4.90	9.74	6.82	0.15	0.11	9.83	6.70
	2	2.23	1.67	4.47	3.25	0.06	0.06	4.17	3.34
	4	1.61	1.52	3.73	4.21	0.06	0.09	3.66	4.84
	6	1.30	1.79	2.82	3.57	0.04	0.06	2.66	3.67
	8	1.67	2.09	3.73	5.29	0.06	0.09	3.36	4.29
	10	2.51	3.50	5.59	9.50	0.08	0.09	4.77	5.63

Table 4

Errors in the prediction of physical properties with different number of hidden layers and neurons per layer for carrot undergoing HAD, LPSSD, HAD + LPSSD, and HAD + LPSSD + FD

Data from drying technique	%Shrinkage				Rehydration ratio (m/m_0)			
	MAE	STD _A	%MRE	STD _R	MAE	STD _A	%MRE	STD _R
HAD	2.05	2.16	3.63	4.51	0.12	0.12	5.66	4.99
LPSSD	1.30	1.79	2.82	3.57	0.04	0.06	2.66	3.67
HAD + LPSSD	2.56	2.56	5.28	7.62	0.14	0.14	6.67	6.23
HAD + LPSSD + FD	2.47	4.13	5.40	10.3	0.13	0.14	6.34	6.02

The ANN developed using combined HAD + LPSSD data had a minimum MRE with two hidden layers and eight neurons per hidden layer; that using combined HAD + LPSSD + FD data had minimum MRE with two hidden layers and six neurons per hidden layer. A comparison of errors associated with ANNs for each drying technique, as well as combinations of drying techniques, is shown in Table 4. LPSSD data had the least error during training (MRE = 2.82 and 2.66 for shrinkage and rehydration ratio, respectively), while that for HAD was somewhat higher (MRE = 3.63 and 5.20, respectively). ANNs developed for combined drying techniques had slightly higher errors than those developed for each drying technique individually. The MRE for HAD + LPSSD were 5.28 for shrinkage and 6.67 for rehydration, while those for HAD + LPSSD + FD were 5.40 and 6.34, respectively.

The system of equations representing the ANN for predicting %shrinkage and rehydration are shown in the Appendix. The equations show the inputs, transfer functions, and relative weight for each node. The equations

can be used in a computer program or spreadsheet to predict the physical properties of the dried carrots. These were implemented in a feed-forward algorithm to predict physical properties and compared with the independent validation sets of data. Plots of experimentally determined %shrinkage or rehydration ratio versus ANN predicted values are shown in Figs. 3–5. The correlation coefficients were greater than 0.95 in all cases. For HAD, $R^2 = 0.993$ for predicted shrinkage and 0.969 for rehydration. For LPSSD, $R^2 = 0.998$ and 0.993 for shrinkage and rehydration, respectively. When all drying methods were combined (HAD + LPSSD + FD), $R^2 = 0.987$ for predicted shrinkage and 0.956 for rehydration ratio.

The ability to predict shrinkage was slightly better than that for predicting rehydration ratio, as evidenced by the greater R^2 values for shrinkage. This is likely due to the fact that shrinkage is more highly interrelated with cellular changes throughout the volume of the dried carrot, and these are well-characterized by changes in the normalized fractal dimension. While rehydration is also dependent upon

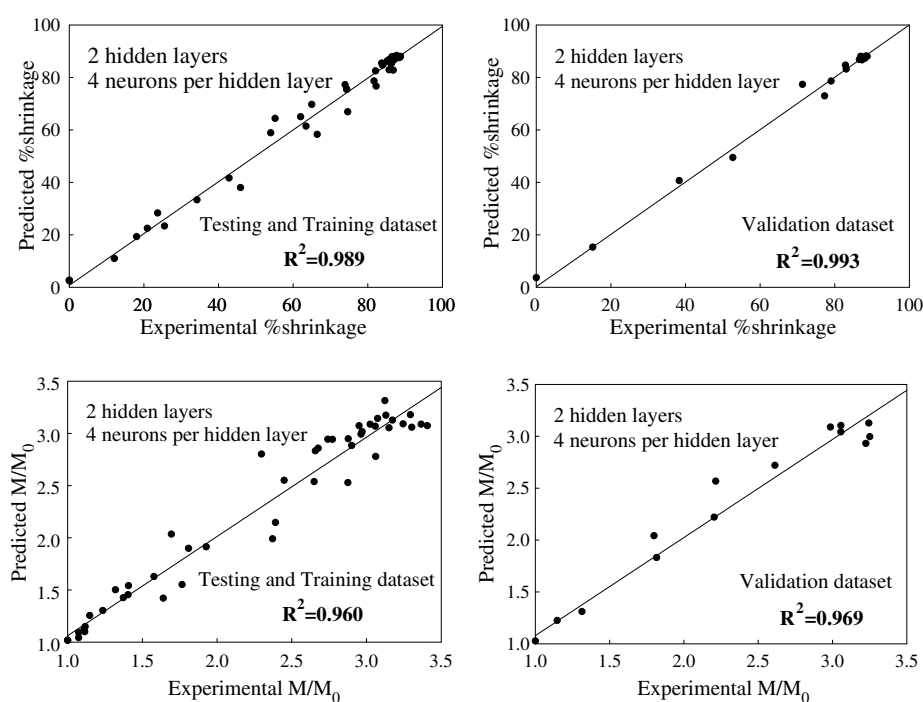


Fig. 3. Correlation of experimental and predicted physical properties with testing and training data sets, as well as validation data set for carrot undergoing HAD using the optimal ANN.

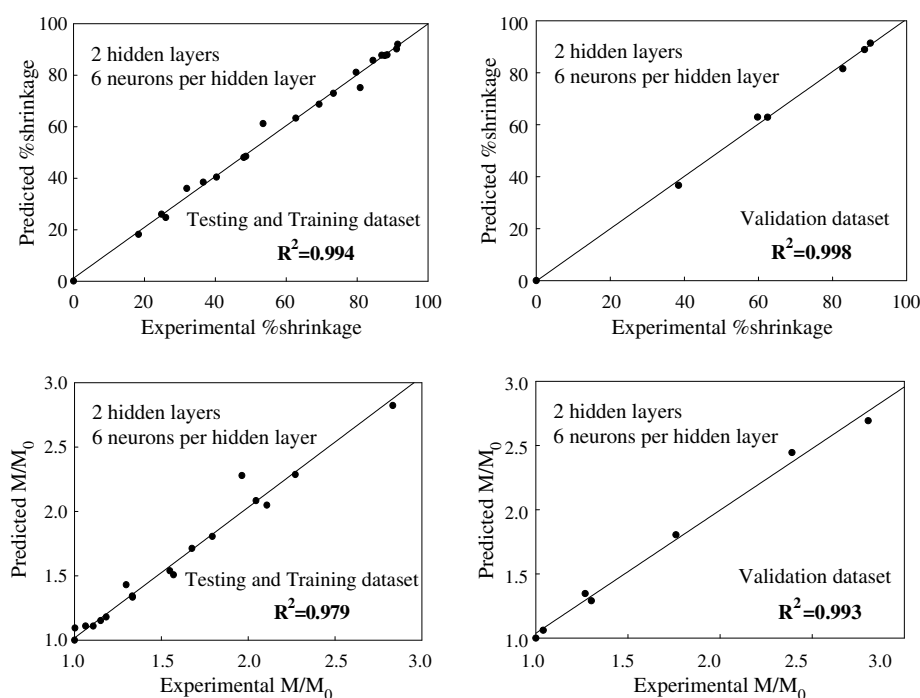


Fig. 4. Correlation of experimental and predicted physical properties with testing and training data sets, as well as validation data set for carrot undergoing LPSSD using the optimal ANN.

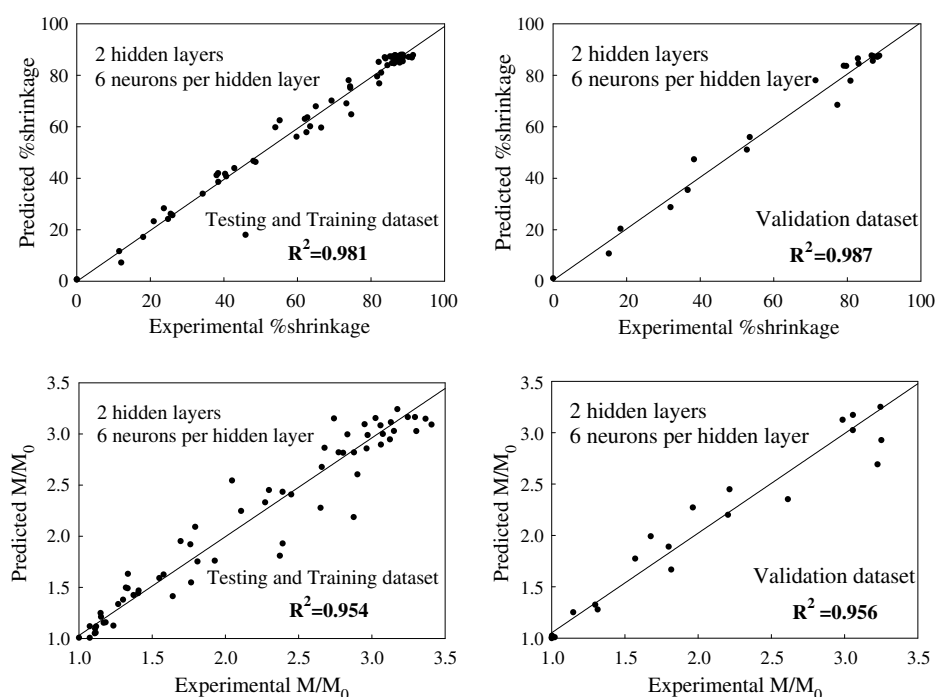


Fig. 5. Correlation of experimental and predicted physical properties with testing and training data sets, as well as validation data set for carrot using combined HAD + LPSSD + FD using the optimal ANN.

internal structural changes and the ability for water to diffuse within the carrot matrix, it may also depend upon limiting factors at the surface, such as case-hardening. These surface factors are more apparent with hot-air drying, and indeed we

found that rehydration for LPSSD was better predicted than for HAD ($R^2 = 0.993$ for LPSSD and 0.969 for HAD).

Artificial neural networks do have advantages and disadvantages. Network development can be computationally

expensive and time-consuming. Once developed, however, its use is straight-forward and can be easily implemented in programs, spreadsheets, calculators, or hardware devices. While predictive value can be very high, there are no particular mechanistic secrets to be learned from the system of equations representing the network. In our work, the ability to predict shrinkage and rehydration were very good. Studies using traditional regression techniques (Kerdpiboon & Devahastin, *in press*) showed R^2 values ranging from 0.844 to 0.984. While this is perhaps reasonable predictive power, the implementation of the ANN provided even better prediction capability.

4. Conclusion

Artificial neural networks can be used to predict the shrinkage and rehydration ratios of carrot undergoing different drying techniques in terms of normalized fractal dimension and moisture content. The optimal models from all the data sets had two hidden layers and 4–8 neurons in each hidden layer, depending on the complexity of each data set. Moreover, the optimal models can predict the %shrinkage and rehydration ratio with R^2 values greater than 0.969 in all cases, offering better predictive performance than with traditional regression techniques.

Fractal dimension was found to be a good measure of cell wall rugosity. Fractal dimensions have been used in many areas, including food science, to study morphological features. That does not mean that there are not other approaches, but this one is quite adequate. For example, for physical measurements of crispness/crunchiness of foods, there are several ways to analyze the jagged force/deformation curves. One might determine the total linear distance of the curve. Another approach is to determine the deviation about some model equation fit to the curve. Yet another approach is to use auto-correlation functions. And yet another approach is to use fractal dimensions to study the degree of jaggedness.

In this study, models based on fractal dimension and moisture content were found to have very good predictive value for the properties of dried carrots. As such, there is little incentive to find alternative parameters for quantifying morphological features.

Acknowledgments

We express appreciation to the Commission on Higher Education, the Thailand Research Fund and the International Foundation for Science in Sweden for financial support.

Appendix

HAD: two hidden layers/four neurons

x = moisture content

f = normalized fractal dimension

$$x1 = (x - (2.9173)) / (3.6868)$$

$$x2 = (f - (0.0544)) / (0.0298)$$

$$x3 = \tanh((-3.6532) * x1 + (0.3011) * x2 + (-1.5851))$$

$$x4 = \tanh((0.8610) * x1 + (0.0560) * x2 + (-0.6467))$$

$$x5 = \tanh((1.1348) * x1 + (-0.1271) * x2 + (1.1862))$$

$$x6 = \tanh((1.3475) * x1 + (0.2816) * x2 + (4.1462))$$

$$x7 = \tanh((-1.3689) * x3 + (1.6391) * x4 + (0.3131) * x5 + (-0.5434) * x6 + (1.4410))$$

$$x8 = \tanh((4.9423) * x3 + (1.2495) * x4 + (-2.2659) * x5 + (-1.3443) * x6 + (-2.2694))$$

$$x9 = \tanh((0.3076) * x3 + (-0.7299) * x4 + (0.6819) * x5 + (-0.1075) * x6 + (-0.7226))$$

$$x10 = \tanh((1.4197) * x3 + (-1.0404) * x4 + (1.6506) * x5 + (-1.1941) * x6 + (1.3532))$$

$$x11 = \text{purelin}((0.0469) * x7 + (0.4000) * x8 + (1.3336) * x9 + (1.0066) * x10 + (-0.2687))$$

$$x12 = \text{purelin}((-0.4735) * x7 + (1.5918) * x8 + (1.7325) * x9 + (-0.5560) * x10 + (1.8131))$$

$$\text{shrinkage} = ((29.9) * x11 + (65.6))$$

$$\text{rehydration} = ((0.87) * x12 + (2.21))$$

HAD + LPSSD + FD: two hidden layers/six neurons

x = moisture content

f = normalized fractal dimension

(continued on next page)

Appendix (continued)

$$x1 = (x - (3.4217)) / (3.8732)$$

$$x2 = (f - (0.0512)) / (0.0292)$$

$$x3 = \tanh((1.4735) * x1 + (-1.4626) * x2 + (-4.9553))$$

$$x4 = \tanh((1.7902) * x1 + (-2.5996) * x2 + (-3.1740))$$

$$x5 = \tanh((1.9172) * x1 + (0.4946) * x2 + (-0.8119))$$

$$x6 = \tanh((-3.0160) * x1 + (-0.2788) * x2 + (-2.2864))$$

$$x7 = \tanh((1.0300) * x1 + (-0.9892) * x2 + (-3.7330))$$

$$x8 = \tanh((-1.7226) * x1 + (1.0193) * x2 + (-1.8109))$$

$$x9 = \tanh((-1.5071) * x3 + (0.3235) * x4 + (-0.1621) * x5 + (-0.3690) * x6 + (-1.3489) * x7 + (-0.4828) * x8 + (2.3965))$$

$$x10 = \tanh((0.5054) * x3 + (-1.3033) * x4 + (-1.6142) * x5 + (1.9190) * x6 + (1.7592) * x7 + (-0.0554) * x8 + (-1.1052))$$

$$x11 = \tanh((-0.9494) * x3 + (-1.1667) * x4 + (0.2751) * x5 + (-1.8012) * x6 + (0.6882) * x7 + (1.2968) * x8 + (0.5427))$$

$$x12 = \tanh((-0.3766) * x3 + (-0.6707) * x4 + (0.3969) * x5 + (-1.1287) * x6 + (-0.4158) * x7 + (-1.0720) * x8 + (0.0877))$$

$$x13 = \tanh((0.2027) * x3 + (0.6496) * x4 + (1.0186) * x5 + (-0.7509) * x6 + (1.2507) * x7 + (-1.2624) * x8 + (1.0449))$$

$$x14 = \tanh((-0.3770) * x3 + (-1.0296) * x4 + (-1.0920) * x5 + (0.2778) * x6 + (0.2944) * x7 + (-1.2120) * x8 + (2.0312))$$

$$x15 = \text{purelin}((-1.2049) * x9 + (0.1499) * x10 + (1.3347) * x11 + (0.0638) * x12 + (-0.7283) * x13 + (-0.7560) * x14 + (0.8697))$$

$$x16 = \text{purelin}((0.9715) * x9 + (1.4665) * x10 + (-0.1211) * x11 + (-1.3050) * x12 + (-0.5546) * x13 + (0.6424) * x14 + (0.7259))$$

$$\text{shrinkage} = (30.6) * x15 + (60.8)$$

$$\text{rehydration} = (0.93) * x16 + (2.06)$$

References

- Association of Official Agricultural Chemists (AOAC) (1984). *Official method of analysis* (14th ed.). Washington DC: Association of Official Agricultural Chemists.
- Barletta, B. J., & Barbosa-Canovas, G. V. (1993). Fractal analysis to characterize ruggedness changes in tapped agglomerated food powders. *Journal of Food Science*, 58(5), 1030–1046.
- Chanona, P. J. J., Alamilla, B. L., Farrera, R. R. R., Quevedo, R., Aguilera, J. M., & Gutierrez, L. G. F. (2003). Description of the convective air-drying of a food model by means of the fractal theory. *Food Science and Technology International*, 9(3), 207–213.
- Devahastin, S., Suvarnakuta, P., Soponronnarit, S., & Mujumdar, A. S. (2004). A comparative study of low-pressure superheated steam and vacuum drying of a heat-sensitive material. *Drying Technology*, 22(8), 1845–1867.
- Goncalves, E. C., Minim, L. A., Coimbra, J. S. R., & Minim, V. P. R. (2005). Modeling sterilization process of canned foods using artificial neural networks. *Chemical Engineering and Processing*, 44(12), 1269–1276.
- Graf, J. C. (1991). The importance of resolution limits to the interpretation of fractal descriptions of fine particles. *Powder Technology*, 67(1), 83–85.
- Hsu, S., Lu, S., & Huang, C. (2000). Viscoelastic changes of rice starch suspensions during gelatinization. *Journal of Food Science*, 65(2), 215–220.
- Kerdpiiboon, S., & Devahastin, S. (in press). Fractal characterization of some physical properties of a food product under various drying conditions. *Drying Technology*.
- Lou, W., & Nakai, S. (2001). Application of artificial neural networks for predicting the thermal inactivation of bacteria: a combined effect of temperature, pH and water activity. *Food Research International*, 34(7), 573–579.
- Mandelbrot, B. B. (1982). *The fractal geometry of nature*. San Francisco: W. H. Freeman (pp. 1–65).
- Mayor, L., & Sereno, A. M. (2004). Modelling shrinkage during convective drying of food materials: a review. *Journal of Food Engineering*, 61(3), 373–386.
- Ochoa, M. R., Kesseler, A. G., Pirone, B. N., Marquez, C. A., & De Michelis, A. (2002). Volume and area shrinkage of whole sour cherry fruits (*Prunus cerasus*) during dehydration. *Drying Technology*, 20(1), 147–156.
- Peleg, M., & Normand, M. D. (1985). Characterization of the ruggedness of instant coffee particle shape by natural fractals. *Journal of Food Science*, 50, 829–831.
- Quevedo, R., Calos, L. G., Aguilera, J. M., & Cadoche, L. (2002). Description of food surfaces and microstructural changes using fractal image texture analysis. *Journal of Food Engineering*, 53(4), 361–371.
- Ratti, C. (1994). Shrinkage during drying of foodstuffs. *Journal of Food Engineering*, 23(1), 91–105.
- Rubnov, M., & Saguy, I. S. (1997). Fractal analysis and crust water diffusivity of a restructured potato product during deep-fat frying. *Journal of Food Science*, 62(1), 135–137, 154.
- Sablani, S. S., & Rahman, M. S. (2003). Using neural networks to predict thermal conductivity of food as a function of moisture content, temperature and apparent porosity. *Food Research International*, 36(6), 617–623.
- Torrecilla, J. S., Otero, L., & Sanz, P. D. (2005). Artificial neural networks: a promising tool to design and optimize high-pressure food processes. *Journal of Food Engineering*, 69(3), 299–306.



Volume 107, issue 4, 15 April 2008

ISSN: 0308-8146

FOOD CHEMISTRY

Managing Editor

G.G. Birch

Editors

P.M. Finglas

J.P. Roozen

F. Shahidi

Available online at

ScienceDirect
www.sciencedirect.com

This article was published in an Elsevier journal. The attached copy is furnished to the author for non-commercial research and education use, including for instruction at the author's institution, sharing with colleagues and providing to institution administration.

Other uses, including reproduction and distribution, or selling or licensing copies, or posting to personal, institutional or third party websites are prohibited.

In most cases authors are permitted to post their version of the article (e.g. in Word or Tex form) to their personal website or institutional repository. Authors requiring further information regarding Elsevier's archiving and manuscript policies are encouraged to visit:

<http://www.elsevier.com/copyright>



Isomerisation kinetics and antioxidant activities of β -carotene in carrots undergoing different drying techniques and conditions

Bhudsawan Hiranvarachat^a, Peamsuk Suvarnakuta^b, Sakamon Devahastin^{a,*}

^a Department of Food Engineering, King Mongkut's University of Technology Thonburi, 126 Pracha u-tid Road, Bangkok 10140, Thailand

^b Department of Food Science and Technology, Thammasat University, Paholyothin Road, Pathum Thani 12121, Thailand

Received 18 June 2007; received in revised form 23 July 2007; accepted 4 October 2007

Abstract

Carrots are known as a natural source of β -carotene. In order to preserve the latter, carrots must generally be processed, and drying is one of the most common methods for processing carrots. During drying β -carotene in carrots suffers degradation. β -Carotene degradation is generally due to thermal degradation and isomerisation. In this work, the drying kinetics as well as the isomerisation kinetics and antioxidant activities of β -carotene in carrots undergoing hot air drying, vacuum drying and low-pressure superheated steam drying (LPSSD) were determined within the temperature range of 60–80 °C and, in the case of vacuum drying and LPSSD, at a pressure of 7 kPa. A high performance liquid chromatography (HPLC) method was used to determine the β -carotene contents and its isomerisation kinetics, while the antioxidant activities of various combinations of all-*trans*- and *cis*-forms of β -carotene in carrots were evaluated using the Trolox equivalent antioxidant capacity (TEAC) assay.

© 2007 Elsevier Ltd. All rights reserved.

Keywords: Antioxidant activity; Degradation; Hot air drying; Low-pressure superheated steam drying; *cis/trans*-Isomerisation; Vacuum drying

1. Introduction

β -Carotene is one of the common carotenoid hydrocarbons that contain specific end groups or two-beta rings. It acts as provitamin A, which is converted by humans to vitamin A (Retinol) (Sergio & Russell, 1999; Patrick, 2000). Moreover, β -carotene has high antioxidant activity, by scavenging peroxyl radicals, which occur as a result of oxidation reactions, especially at low oxygen tension (Larson, 1988). Since carotene stereoisomers display different chemical properties and antioxidant activities, the knowledge of various factors affecting formation of all-*trans*- and *cis*-isomers of β -carotene in foods is of interest (Marx, Stuparic, Schieber, & Carle, 2003).

Carrots (*Daucus carota* var. *sativa*) are one of the most important root crops. The consumption of carrots and

their related products has increased steadily, partly due to the antioxidant activity of β -carotene in carrots (Rubatzky, Quiros, & Simon, 1999). However, in the food industry, carrots must generally be processed prior to their use and drying is one of the most frequently used processes. Many techniques have been developed to dry carrots, with the goal of maintaining their nutritional value, especially β -carotene, as much as possible.

Different drying techniques and conditions are known to affect the quality of a food product, either in terms of its physical properties, chemical properties or biochemical properties. In the food industry, hot air drying is widely used, although it often leads to much quality degradation, especially in terms of the nutritional properties. Several other drying techniques have therefore been proposed and studied (Devahastin, Suvarnakuta, Soponronnarit, & Mujumdar, 2004). Although there are some works that report the study of β -carotene degradation in carrots undergoing different drying techniques and conditions

* Corresponding author. Tel.: +66 2 470 9246; fax: +66 2 470 9240.
E-mail address: sakamon.dev@kmutt.ac.th (S. Devahastin).

(Suvarnakuta, Devahastin, & Mujumdar, 2005), no information is so far available on the effect of drying on the *cis/trans*-isomerisation of β -carotene in carrots.

Naturally, β -carotene exists in the all-*trans* form. After processing, however, some all-*trans* form is converted into its different *cis*-isomers (Aman, Schieber, & Carle, 2005). Heat, light and the presence of sensitizers promote isomerisation of *trans*-carotenoids to their *cis*-form (Dutta, Chaudhuri, & Chakraborty, 2005).

Lessin, Catigani, and Schwartz (1997) studied the quantification of *cis/trans*-isomers of carotenoids in canned carrots and other vegetables. They found that all-*trans*- β -carotene was lower in all processed samples, as compared to the fresh samples. Only all-*trans*- β -carotene was found in fresh carrots while 9-*cis*- β -carotene and 13-*cis*- β -carotene occurred after canning. Canning caused a 33% increase in total *cis*-isomers. This change in isomeric compositions was due to *cis/trans*-isomerisation, which occurred as a direct result of the thermal processing.

Chen, Peng, and Chen (1995) studied the thermal degradation of canned carrot juices. They found that canning of carrot juices at 121 °C led to the formation of 13-*cis*-isomer, which was the predominant isomer in that study. This result was consistent with that of Marx et al. (2003), who studied the effects of pasteurisation and sterilisation on *cis/trans*-isomerisation of β -carotene in carrot juices. They found that in the case of pasteurisation, only 13-*cis*- β -carotene occurred. On the other hand, in the case of sterilisation, 9-*cis*- β -carotene and 13-*cis*- β -carotene occurred. 9-*cis*- β -carotene was found at temperatures higher than 90 °C for processing times longer than 60 min.

As mentioned earlier, β -carotene has high antioxidant activity. Many investigators have thus studied the antioxidant activities of various isomers of β -carotene in different products undergoing processing. Bohm, Puspitasari-Nienaber, Ferruzzi, and Schwartz (2002), for example, studied the antioxidant activities of different geometrical isomers

of β -carotene and other carotenoids using TEAC assay. They reported that all-*trans*- β -carotene had higher antioxidant activity than 13-*cis*- β -carotene.

The objectives of this study were to investigate the effects of selected drying techniques, i.e., hot air drying, vacuum drying and low-pressure superheated steam drying (LPSSD), on the isomerisation kinetics and antioxidant activities of β -carotene in carrots at different conditions. The relationship between the amount of different isomers of β -carotene, as well as their antioxidant activities, and carrot moisture content were also investigated.

2. Materials and methods

2.1. Materials

Fresh carrots (*D. carota* var. *sativa*) were purchased from a local market and stored at 4 °C. Before starting each drying experiment, carrots were peeled and diced (only the cortex part was used) into 1 cm³ cubes. The moisture content of fresh carrots was determined by drying the samples at 105 °C for 24 h in a hot air oven (Memmert, model 800, Schwabach, Germany).

2.2. Experimental set-up

2.2.1. Low-pressure superheated steam dryer

A schematic diagram of the low-pressure superheated steam dryer and its accessories is shown in Fig. 1. The dryer consists of a stainless steel drying chamber with inner dimensions of 45 × 45 × 45 cm³; a steam reservoir, which received steam from a boiler and maintained its pressure at around 200 kPa; and a liquid ring vacuum pump (Nash, model ET32030, Trumbull, CT), which was used to maintain the vacuum in the drying chamber (fixed at 7 kPa in this study). An electric heater, rated at 1.5 kW, which was controlled by a PID controller (Omron, model

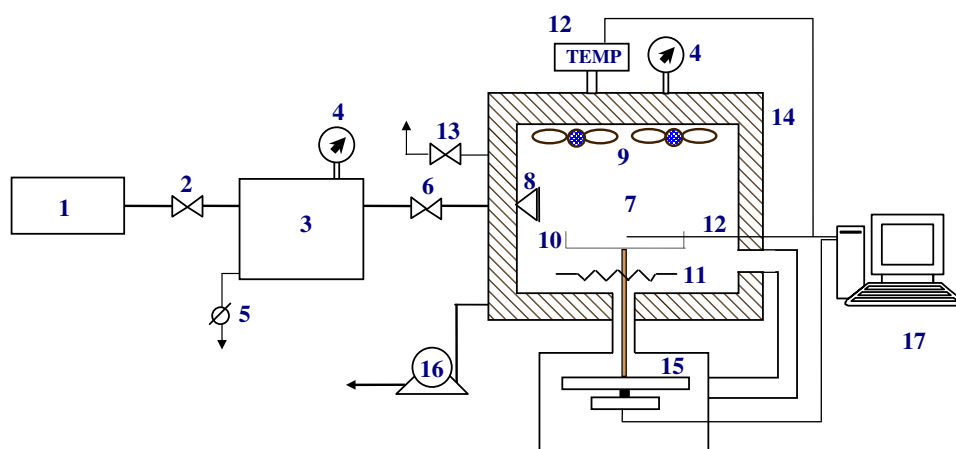


Fig. 1. A schematic diagram of the low-pressure superheated steam dryer and associated units. 1, boiler; 2, steam valve; 3, steam reservoir; 4, pressure gauge; 5, steam trap; 6, steam regulator; 7, drying chamber; 8, steam inlet and distributor; 9, electric fans; 10, sample holder; 11, electric heater; 12, on-line temperature sensor and logger; 13, vacuum purge valve; 14, insulator; 15, on-line weight indicator and logger; 16, vacuum pump; 17, PC with installed data acquisition card.

E5CN, Tokyo, Japan) was installed in the drying chamber to control the steam temperature and to minimise the condensation of steam in the drying chamber during the start-up period. Two variable-speed electric fans were used to disperse steam throughout the drying chamber. The sample holder was made of a stainless steel screen with dimensions of $16.5 \times 16.5 \text{ cm}^2$. The change of the mass of the sample was detected continuously (at 60 s intervals) using a load cell (Minebea, model UCG-3 kg, Nagano, Japan). The temperatures of the steam and of the drying sample were also measured continuously using type-K thermocouples, which were connected to an expansion board (Omega Engineering, model no. EXP-32, Stamford, CT). Thermocouple signals were multiplexed to a data acquisition card (Omega Engineering, model no. CIO-DAS16Jr.) installed in a PC. Labtech Notebook software (version 12.1, Laboratory Technologies Corp., Andover, MA) was then used to read and record the temperature data.

2.2.2. Vacuum dryer

For vacuum drying experiments the same experimental set-up was used as for the LPSSD experiments without the application of steam to the drying chamber.

2.2.3. Hot air dryer

A schematic diagram of the hot air dryer used is illustrated in Fig. 2. It consists of a stainless steel drying chamber ($45 \times 45 \text{ cm}^2$), in which the sample was placed. The inlet air that was used to dry the sample was heated up to the desired temperature by an electric heater rated at 9 kW. The sample was placed on a tray made of a stainless steel screen. The air velocity over the drying tray was fixed at 0.8 m/s.

2.3. β -Carotene analysis

Analysis of the total amount of β -carotene was performed using the methods described by [Suvarnakuta et al. \(2005\)](#). A sample of 5–8 g of dried carrots was ground for 2 min using a stainless steel pulveriser (Waring, model SS110, Torrington, CT). The ground sample was then placed in a flask filled with 40 ml of ethanol. 2 N potassium hydroxide (40 ml) was added, to saponify the solution, at 70°C for 30 min. The extract was then cooled down immediately to 0°C . β -Carotene was then extracted three times

with 5 ml of diisopropyl ether and the aqueous layer was discarded. The extracted solution was filtered through a 0.45 μm filter before being injected into a liquid chromatograph column.

A symmetry[®] C₃₀ 5 μm (4.6 mm \times 250 mm) HPLC column (YMC, Kyoto, Japan) was used for the analysis of different isomers of β -carotene. The HPLC system consisted of a pump and a controller (Waters, model 600, Milford, MA), a tunable absorbance detector (Waters, model 486). A sample of 75% methanol and 25% methyl tert-butyl ether (MTBE) was used as the mobile phase and its flow rate was set at 2 ml/min. A UV detector, at 450 nm, was used for detecting β -carotene. The mobile phase was degassed using an ultrasonic generator.

From the preliminary experiments, it was found that only 13-*cis*- β -carotene formed as a result of isomerisation; only this *cis*-isomer was then tested for in the subsequent study. A standard of all-*trans*- β -carotene was purchased from Fluka (Buchs, Switzerland). 13-*cis*- β -Carotene was obtained by iodine-catalysed photoisomerisation of all-*trans*- β -carotene as previously described by [Aman et al. \(2005\)](#). Briefly, all-*trans*- β -carotene was dissolved in diisopropyl ether containing two drops of 1% iodine. The solution was then exposed to ambient light for 30 min.

A typical chromatogram of β -carotene isomers of interest is shown in Fig. 3. The concentration of all-*trans*- β -carotene was calculated from the peak area of its chromatogram while the *cis*-isomer proportion was calculated from the relative peak area of the *cis*- β -carotene divided by the peak area of the *trans*- β -carotene in each sample.

Quantification of β -carotene was carried out based on a β -carotene standard curve. The standard curve was prepared daily by injecting solutions of HPLC β -carotene standard in diisopropyl ether at six concentrations (0, 2, 4, 6, 8 and 10 g/ml). All standard curves showed good linearity ($r^2 > 0.99$).

The measured all-*trans*- β -carotene content is expressed in terms of the β -carotene retention ratio, while the *cis*-proportion is reported in terms of the *cis/trans* ratio:

$$\beta\text{-Carotene retention ratio} = \frac{\beta_t}{\beta_i} \quad (1)$$

$$\text{cis-Proportion} = \frac{\beta_{cis}}{\beta_{trans}} \quad (2)$$

where β_i and β_t are the β -carotene contents of fresh and dried carrots (mg/100 g solids), respectively. β_{cis} and β_{trans} refer to the peak area of *cis*- β -carotene and the peak area of *trans*- β -carotene, respectively. All *trans*- and *cis*- β -carotene measurements were performed in duplicate and the data presented are an average of the two measurements.

2.4. Antioxidant activities measurement

Antioxidant activities of various combinations (or proportions) of isomers of β -carotene in carrots were determined following the TEAC procedure similar to that of

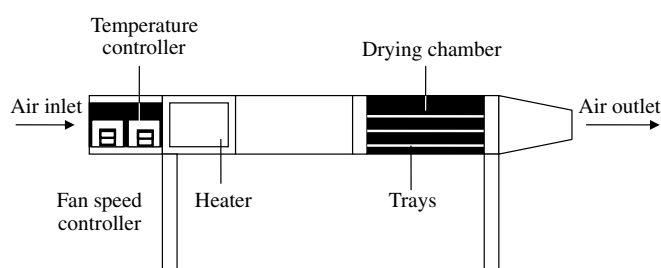


Fig. 2. A schematic diagram of hot air dryer and associated units.

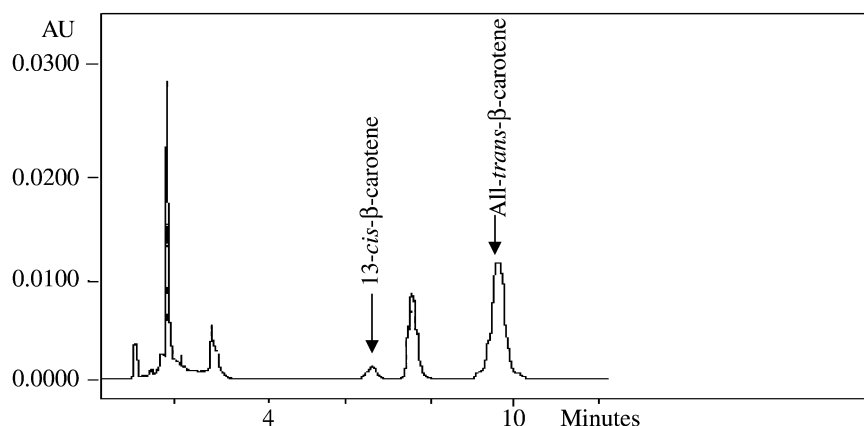


Fig. 3. Typical chromatogram of β -carotene in carrots at a wavelength of 450 nm.

Miller, Sampson, Candxias, Bramly, and Rice-Evans (1996) with some modifications. $\text{ABTS}^{\cdot+}$ radical cation was prepared by passing a 5 mM aqueous stock solution of ABTS (2,2'-azino-bis(3-ethylbenzothiazoline-6-sulphonic acid)) through manganese dioxide on a Whatman No. 5 filter paper. Excess manganese dioxide was removed twice from the filtrate by passing it through a 0.45 μm syringe filter. This solution was then diluted with ethanol to an absorbance of 0.70 (0.02) at 734 nm and pre-incubated at ambient temperature for 1 h prior to its use. Trolox (6-hydroxy-2,5,7,8-tetramethylchroman-2-carboxylic acid) was used as an antioxidant standard. 2.5 mM Trolox was prepared in phosphate buffer saline (PBS) at pH 7.4 for use as a stock solution. $\text{ABTS}^{\cdot+}$ solution (1 ml) and 200 μl of Trolox solution were well mixed using a vortex mixer (Scientific Industries Inc., model G-560E, Bohemia, NY) for 30 s.

UV–Vis scanning spectrophotometer (Shimadzu, model UV-2101PC, Nagoya, Japan) was used for the determination of antioxidant activity. The absorbance was taken at 734 nm exactly at 1 min after initiation of vortex mixing. A standard curve of Trolox was prepared by measuring solutions of Trolox standard in PBS at five concentrations (0, 25, 50, 75 and 100 μM). The standard curves showed good linearity ($r^2 > 0.99$).

To determine the antioxidant activities of various combinations of isomers of β -carotene, β -carotene was diluted in diisopropyl ether (1:9). $\text{ABTS}^{\cdot+}$ solution (1 ml) and 200 μl of the isomers solution were mixed for 30 s using the vortex mixer. The absorbance was then measured at the above wavelength.

The measured antioxidant activities of various combinations of all-*trans*-form and *cis*-form of β -carotene are expressed in terms of % relative inhibition:

$$\% \text{ Relative inhibition} = \frac{\% \text{ inhibition of dried carrots}}{\% \text{ inhibition of fresh carrots}} \quad (3)$$

where % inhibition of dried carrots and fresh carrots refer to the % inhibition of $\text{ABTS}^{\cdot+}$ by the combinations of various isomers of β -carotene in dried and fresh carrots,

respectively. To calculate % inhibition the following equation was used:

$$\% \text{ inhibition} = \frac{(A_{\text{solvent}} - A_{\beta\text{-carotene}}) \times 100}{A_{\text{solvent}}} \quad (4)$$

where A_{solvent} and $A_{\beta\text{-carotene}}$ are the absorbance of diisopropyl ether and the combinations of various isomers of all-*trans*-form and *cis*-form of β -carotene in carrots, respectively. All measurements were performed in duplicate and the data presented are an average of the two measurements.

2.5. Statistical analysis

The experiments were completely randomised. All data were analysed using the analysis of variance (ANOVA). Differences between mean values were established using Duncan multiple range test at a confidence level of 95% ($p = 0.05$). SPSS (version 13; SPSS Inc., Chicago, IL) was used to perform all statistical calculations.

3. Results and discussion

3.1. Drying kinetics of carrots

Since the results of the isomerisation of β -carotene in carrots undergoing different drying techniques and conditions were compared at the same moisture content, the drying curves of carrots undergoing different drying treatments and conditions were first constructed. Carrots that had an initial moisture content in the range of 9–11 kg/kg dry weight basis, (d.b.) were dried to a final moisture content of around 0.1 kg/kg (d.b.).

The drying curves and temperature profiles of carrots undergoing hot air drying, vacuum drying and LPSSD are shown in Figs. 4 and 5, respectively. Three different drying temperatures (60, 70 and 80 $^{\circ}\text{C}$) were employed in each set of experiments.

As can be seen in Fig. 4, although vacuum drying was a faster drying process than LPSSD and hot air drying, the differences between the drying times of LPSSD and vacuum drying were smaller at higher drying temperatures.

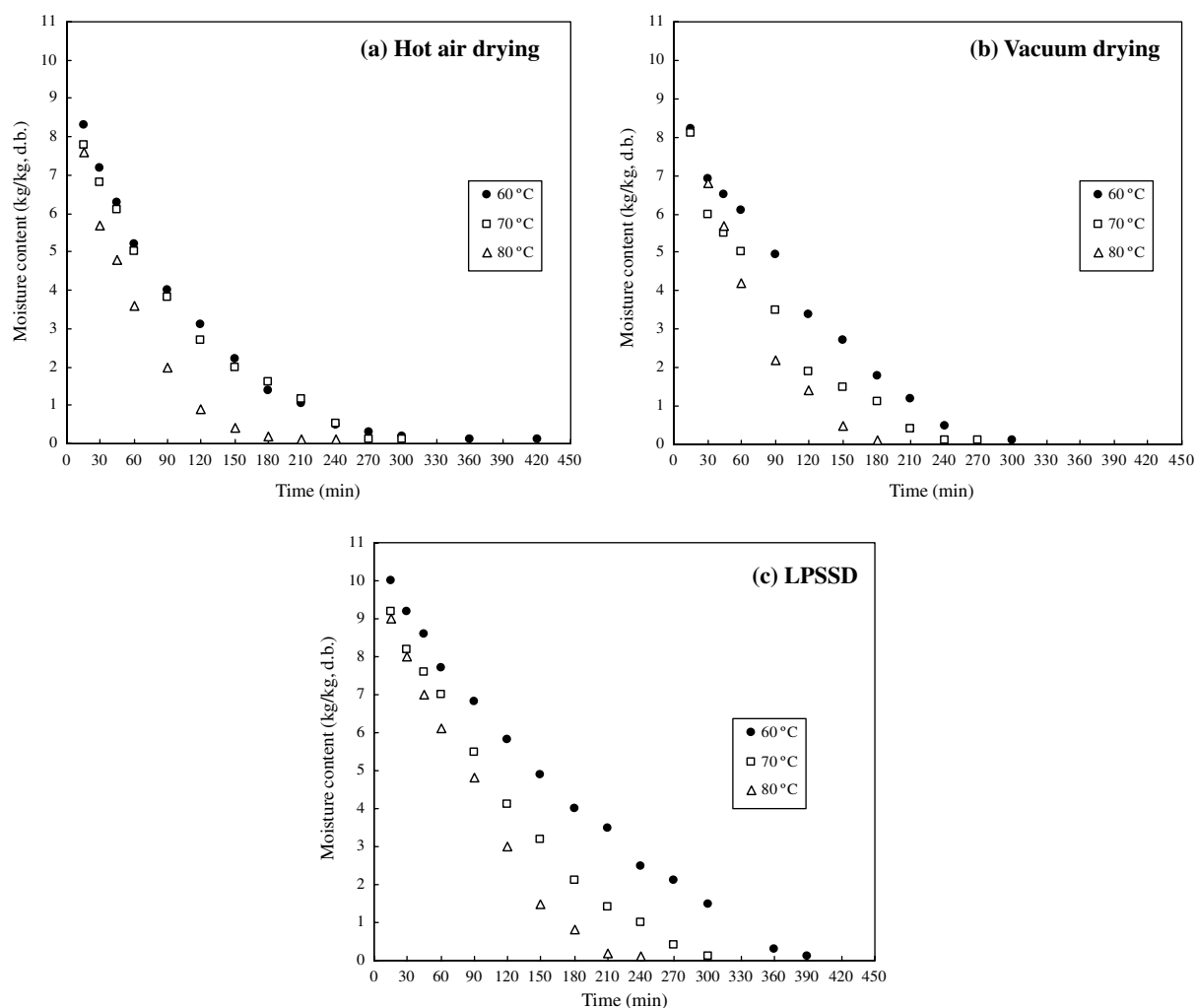


Fig. 4. Drying curves of carrots subjected to various drying treatments.

In the case of hot air drying, it took as much time to dry carrots to the final desired moisture content as did LPSSD. This is because the falling rate period of hot air drying was longer than that of LPSSD. The drying behaviour was characterised as follows: the drying rates increased with an increase in the drying temperature, due to an increased driving force for heat transfer, which is obviously related to mass transfer. Moisture diffusivities are also higher at higher temperatures.

3.2. Overall degradation kinetics of β -carotene

The β -carotene contents of fresh carrots varied slightly in the range of 68–76 mg/100 g (d.b.). The ratio of the β -carotene content of dried carrots to the fresh (β -carotene retention ratio) is therefore used to report the results in this study.

The β -carotene retention in carrots during hot air drying, vacuum drying and LPSSD is shown in Figs. 6–8, respectively. The β -carotene retention, in the case of hot air drying (Fig. 6), decreased continuously. It was observed, however, that the β -carotene retention at differ-

ent temperatures was only slightly different. The falling rate of β -carotene started at the moisture content around 5.5 kg/kg (d.b.), which corresponded to a carrot temperature of 45–60 °C (see also Figs. 4a and 5a). This is due to the fact that lipoxygenase, which is an aerobic catalyst of oxidation reactions, is activated at around 60 °C (Cui, Xu & Sun, 2004).

β -Carotene retention in the cases of vacuum drying and LPSSD (Figs. 7 and 8) was not significantly higher than that in the case of hot air drying. In the case of LPSSD, only slight changes, over the moisture content range of 3–8 kg/kg (d.b.), of β -carotene occurred due to the fact that the activities of lipoxygenase and peroxidase, which are responsible for the oxidative degradation of β -carotene, were reduced due to many effects, including the absence of oxygen in the drying chamber and the lower product temperature (Fig. 5a, b, c). At moisture contents below 3 kg/kg (d.b.), β -carotene content started to decrease continuously. This is because the temperature of the carrots started to rise again (Fig. 5c); thermal degradation thus started to be significant.

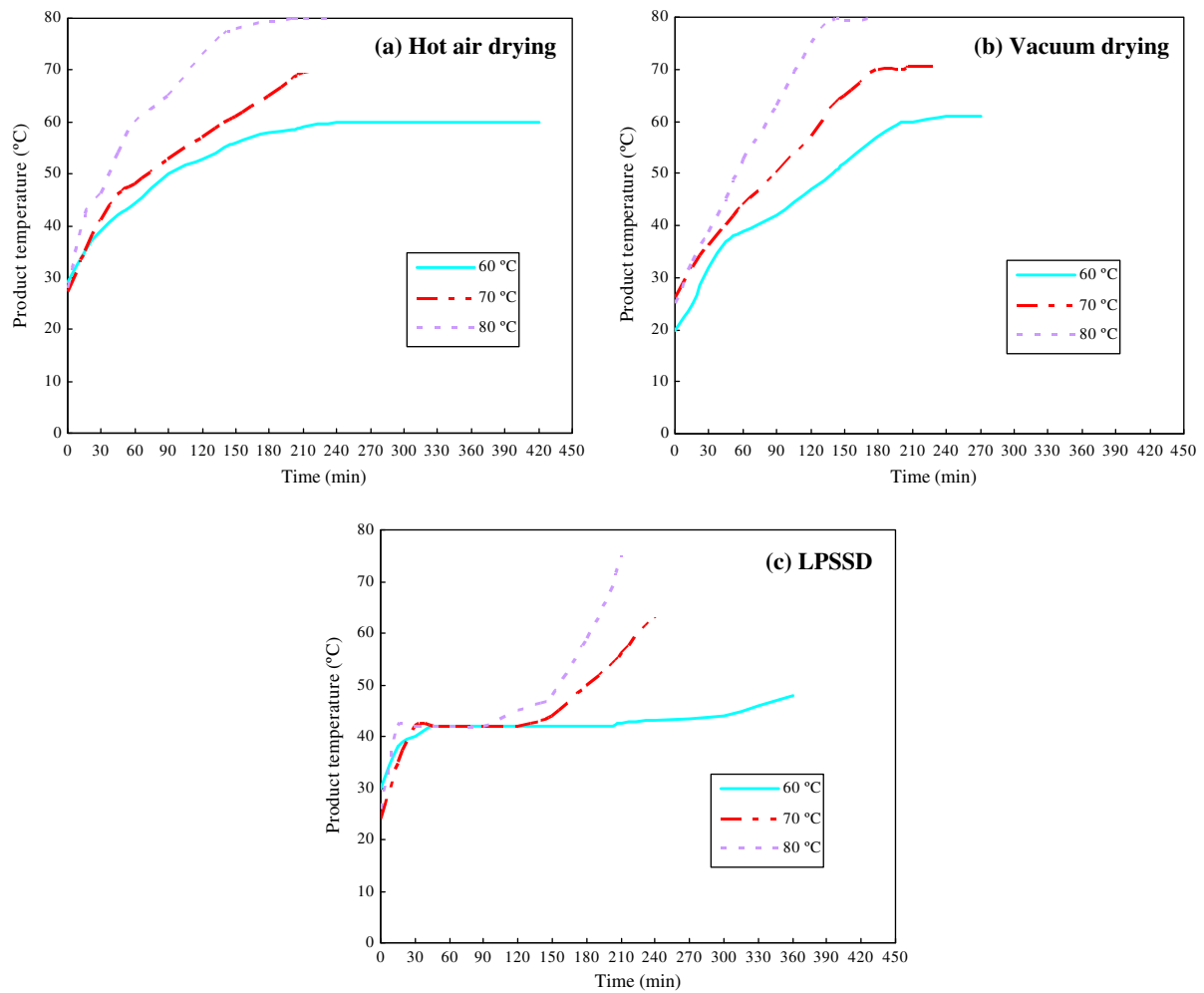


Fig. 5. Temperature profiles of carrots subjected to various drying treatments.

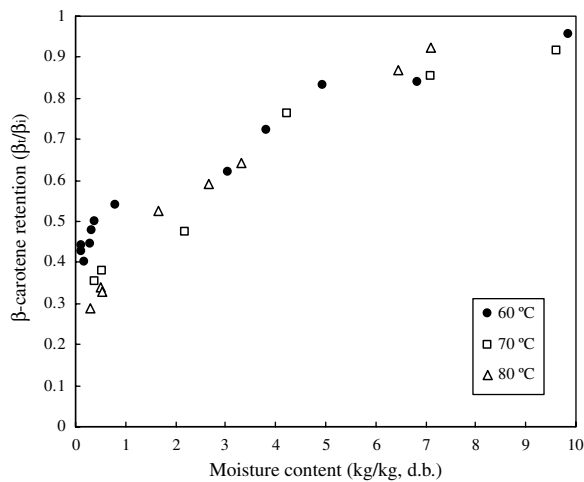


Fig. 6. Relationship between β -carotene retention and moisture content of carrots undergoing hot air drying.

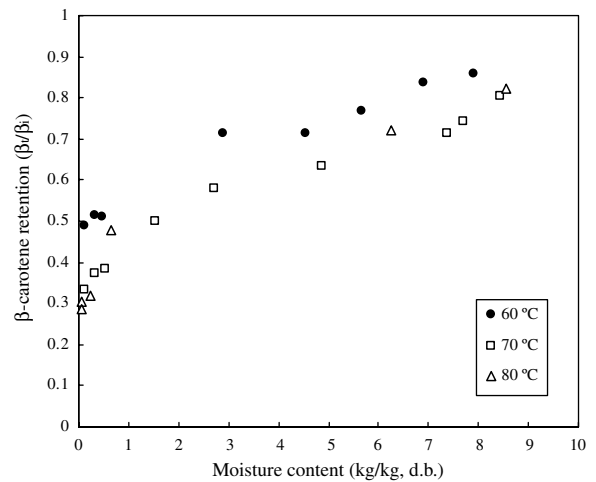


Fig. 7. Relationship between β -carotene retention and moisture content of carrots undergoing vacuum drying.

In the case of vacuum drying, the trend of β -carotene degradation was similar to that of LPSSD. However, because the level of vacuum pressure used in this study was not too low (7 kPa absolute), there still existed

some oxygen that could participate in oxidation reactions. Higher temperatures, in comparison with the case of LPSSD (Figs. 5b and c) also led to more degradation.

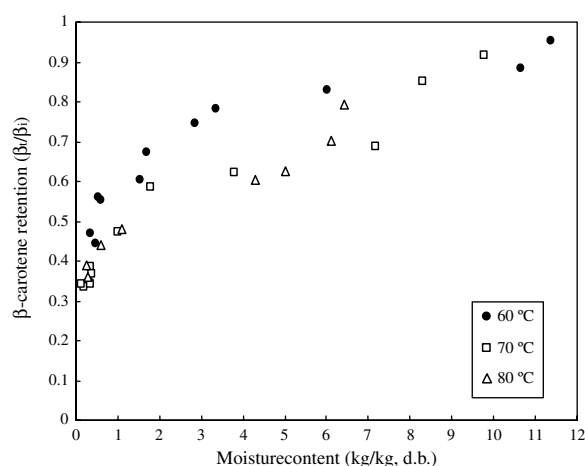


Fig. 8. Relationship between β -carotene retention and moisture content of carrots undergoing LPSSD.

3.3. Isomerisation kinetics of β -carotene

β -Carotene can be degraded either by thermal degradation or isomerisation degradation and it is known that thermal treatment promotes the formation of *cis*-isomers from all-*trans*- β -carotene in carrots (Sergio & Russell, 1999; Aman et al., 2005). In all dried (and drying) samples of this study, 13-*cis*- β -carotene was the only isomer detected by HPLC, as previously mentioned.

In the case of hot air drying (Table 1), 13-*cis*- β -carotene occurred when the product temperature, as seen in Fig. 5a, approached the drying air temperature, which was equal to or higher than 60 °C. Increased rates of isomerisation in this range of temperature are ascribed mainly to the elevated temperature, as also noted by Cui, Xu, and Sun (2004). However, the moisture contents of carrots when the formation of *cis*-isomer started were not much differ-

ent, i.e., 0.5, 0.4 and 0.5 kg/kg (d.b.) at 60, 70 and 80 °C, respectively. The *cis*-proportions were also not significantly different, in the range of 0.01–0.06.

For vacuum drying (Table 1), 13-*cis*- β -carotene occurred when the product temperature (Fig. 5b) was more than 50 °C. As can be seen from Table 1, the *cis*-isomer occurred at moisture contents lower than 1.8, 2.2 and 2.2 kg/kg (d.b.) at 60, 70 and 80 °C, respectively.

For LPSSD, the starting points of the formation of 13-*cis*-isomer are reported instead in terms of the elapsed drying time. As can be seen in Table 1 the formation of 13-*cis*-isomer started after 150, 120 and 60 min when drying was performed at 60, 70 and 80 °C, respectively. The formation of *cis*-isomer, in the case of LPSSD, started much earlier than in the case of hot air drying and vacuum drying. This is probably due to the fact that carrots were held at a constant temperature corresponding to the boiling point of water at 7 kPa (around 40 °C) for an extended period of time, compared with hot air drying and vacuum drying (Fig. 5c and Table 1). Normally, if the processing temperature is maintained for a long time (like in the case of pasteurisation or sterilisation), the formation of 13-*cis*- β -carotene increases (Marx et al., 2003).

The formation of 13-*cis*- β -carotene in the case of LPSSD started much earlier than in the cases of hot air drying and vacuum drying. However, as can be seen in Table 1, the proportions of 13-*cis*- β -carotene at various conditions were not significantly different, in the range of 0.01–0.1.

3.4. Antioxidant activities of β -carotene

The percent relative inhibition of β -carotene in carrots undergoing hot air drying, vacuum drying and LPSSD is shown in Table 2. Percent relative inhibition, in the case

Table 1
Formation of 13-*cis*- β -carotene during different drying conditions

Drying time (min)	<i>cis</i> -Proportion (<i>cis/trans</i>) ^a								
	Hot air drying			Vacuum drying			LPSSD		
	60 °C	70 °C	80 °C	60 °C	70 °C	80 °C	60 °C	70 °C	80 °C
60	n.d. ^b	n.d.	n.d.	n.d.	n.d.	n.d.	n.d.	n.d.	0.006 ± 0.003
90	n.d.	n.d.	n.d.	n.d.	n.d.	0.019	n.d.	n.d.	0.013 ± 0.001
120	n.d.	n.d.	n.d.	n.d.	0.017 ± 0.012	0.030 ± 0.028	n.d.	0.005	0.026 ± 0.003
150	n.d.	n.d.	0.03	0.016 ± 0.009	0.018 ± 0.005	0.017 ± 0.002	0.004	0.014	0.023 ± 0.004
180	n.d.	0.017 ± 0.004	0.067 ± 0.031	0.019 ± 0.002	0.035 ± 0.012	0.055 ± 0.015	0.006	0.007 ± 0.001	0.052 ± 0.037
210	n.d.	0.038 ± 0.029		0.014 ± 0.008	0.029 ± 0.003		0.009 ± 0.007	0.027	0.072 ± 0.036
240	n.d.	0.036 ± 0.024		0.015	0.031 ± 0.008		0.008 ± 0.002	0.016 ± 0.007	
270	n.d.	0.034 ± 0.004		0.019 ± 0.004	0.030		0.006 ± 0.002	0.024 ± 0.005	
300	0.049	0.049		0.021 ± 0.002			0.016 ± 0.002	0.032 ± 0.016	
330	0.047						0.01 ± 0.002	0.028 ± 0.005	
360	0.036						0.021 ± 0.001		
390	0.024 ± 0.021						0.023 ± 0.012		
420	0.026 ± 0.018						0.011 ± 0.001		
450	0.009								
480	0.016								

^a Mean ± SD of two replicates.

^b n.d. = not detectable; *cis*-isomers calculated as percentage of all-*trans*- β -carotene.

Table 2

Antioxidant activities of various combinations (or proportions) of isomers of β -carotene in carrots (during different drying conditions) in terms of % relative inhibition

Drying time (min)	% Relative inhibition ^a								
	Hot air drying			Vacuum drying			LPSSD		
	60 °C	70 °C	80 °C	60 °C	70 °C	80 °C	60 °C	70 °C	80 °C
15	0.896 ± 0.039	0.813 ± 0.139	0.806 ± 0.014	0.806 ± 0.101	0.715 ± 0.085	0.784 ± 0.098	0.938 ± 0.008	0.787 ± 0.074	0.798 ± 0.038
30	0.849 ± 0.018	0.842 ± 0.052	0.787 ± 0.054	0.718 ± 0.085	0.560 ± 0.045	0.639 ± 0.056	0.857 ± 0.158	0.908 ± 0.011	0.742 ± 0.153
45	0.853 ± 0.058	0.795 ± 0.027	0.547 ± 0.245	0.814 ± 0.105	0.643 ± 0.008	0.613 ± 0.070	0.869 ± 0.075	0.814 ± 0.079	0.719 ± 0.096
60	0.864 ± 0.011	0.852 ± 0.179	0.693 ± 0.062	0.739 ± 0.060	0.680 ± 0.183	0.606 ± 0.038	0.824 ± 0.175	0.930 ± 0.029	0.712 ± 0.167
90	0.775 ± 0.042	0.682 ± 0.266	0.489 ± 0.235	0.631 ± 0.008	0.450 ± 0.057	0.534 ± 0.152	0.789 ± 0.267	0.832 ± 0.084	0.678 ± 0.169
120	0.776 ± 0.032	0.685 ± 0.239	0.473 ± 0.039	0.698 ± 0.011	0.566 ± 0.195	0.589 ± 0.145	0.777 ± 0.109	0.757 ± 0.017	0.578 ± 0.253
150	0.723 ± 0.154	0.706 ± 0.277	0.735 ± 0.268	0.527 ± 0.080	0.501 ± 0.108	0.507 ± 0.162	0.766 ± 0.174	0.762 ± 0.045	0.597 ± 0.109
180	0.633 ± 0.142	0.643 ± 0.040	0.585 ± 0.100	0.544 ± 0.006	0.570 ± 0.100		0.779 ± 0.122	0.770 ± 0.070	0.539 ± 0.225
210	0.709 ± 0.214	0.580 ± 0.269	0.433 ± 0.146	0.561 ± 0.099	0.587 ± 0.197		0.683 ± 0.152	0.692 ± 0.191	0.562 ± 0.027
240	0.788 ± 0.113	0.494 ± 0.459		0.589 ± 0.109	0.509 ± 0.145		0.647 ± 0.203	0.642 ± 0.072	
270	0.725 ± 0.085	0.492 ± 0.116		0.556 ± 0.035			0.634 ± 0.138	0.647 ± 0.024	
300	0.630 ± 0.062	0.482 ± 0.398					0.654 ± 0.148	0.595 ± 0.154	
330	0.638 ± 0.157						0.684 ± 0.066	0.676 ± 0.036	
360	0.656 ± 0.097						0.621 ± 0.149		
390	0.685 ± 0.087						0.647 ± 0.131		
420	0.591 ± 0.011						0.621 ± 0.038		
450	0.587 ± 0.169								
480	0.323 ± 0.025								

^a Mean ± SD of two replicates.

of hot air drying, decreased continuously with decreasing moisture content. A significant drop in the % relative inhibition started at a moisture content around 1 kg/kg (d.b.), which corresponded to a β -carotene retention (Fig. 6) of about 55%. This early drop in antioxidant activities (as compared with the cases of vacuum drying and LPSSD, as will be discussed shortly) is due to the fact that the antioxidant activity of β -carotene depends on the oxygen tension presented in the system and hot air drying is the most obvious aerobic process in the present study (Burton & Ingold, 1984; Stahl & Sies, 2003).

For vacuum drying and LPSSD (Table 2), % relative inhibition remained almost constant over the moisture ranges of 1–10 and 2–12 kg/kg (d.b.), respectively. However, in the case of vacuum drying, a drop in the activities could be observed at moisture contents lower than 1 kg/kg (d.b.). As can be seen also from Fig. 7 over the moisture content range of 0.1–1 kg/kg (d.b.), a dropping period of % relative inhibition started when the β -carotene retention was around 30%. In the case of LPSSD (Table 2), a dropping period started when the moisture content was around 2 kg/kg (d.b.), which corresponded to a β -carotene retention of around 35% (Fig. 8).

In the case of vacuum drying and LPSSD (Table 2), the % relative inhibition at low moisture content was higher than in the case of hot air drying. At the final moisture content of 0.1 kg/kg (d.b.), the losses in the % relative inhibition were about 50% and 45% in the case of vacuum drying and LPSSD, respectively, while in the case of hot air drying the loss was about 70%. This is due to the low oxygen contents in the cases of vacuum drying and LPSSD.

Percent relative inhibition in the case of hot air drying implied lower antioxidant activities at the final moisture

content of 0.1 kg/kg (d.b.) than in the cases of vacuum drying and LPSSD. This result corresponded to the previously mentioned results of the isomerisation kinetics of β -carotene, in which LPSSD and vacuum drying could better preserve β -carotene than hot air drying by partially converting all-*trans*- β -carotene into 13-*cis*- β -carotene. In the present study, however, the formation of 13-*cis*- β -carotene in all cases did not much affect the antioxidant activities of various combinations of isomers of β -carotene. It can be seen from Table 1 that the relative amounts of 13-*cis*- β -carotene at various conditions were not significantly different, in the range of 0.01–0.1.

4. Conclusions

The isomerisation kinetics of β -carotene in carrots undergoing hot air drying, vacuum drying and LPSSD were investigated in this study. It was found that vacuum drying and LPSSD led to more conversion of all-*trans*- β -carotene to 13-*cis*- β -carotene, while total degradation, vacuum drying and LPSSD led to less total degradation of β -carotene than hot air drying.

Antioxidant activities of various combinations (or proportions) of isomers of β -carotene in carrots undergoing different drying techniques were determined using the TEAC assay. It was found that carrots undergoing LPSSD had higher antioxidant activity than those subjected to the other drying treatments. It could thus be concluded that, at the final moisture content of 0.1 kg/kg (d.b.), LPSSD at 60 °C was the best treatment to preserve β -carotene and antioxidant activities of carrots.

Since the drop in the total β -carotene retention at various drying conditions tended to occur more significantly

than the formation of 13-*cis*- β -carotene, the thermal degradation was noted to be more important than isomerisation degradation.

Acknowledgements

The authors express their sincere appreciation to the Commission on Higher Education, the Thailand Research Fund (TRF), and the International Foundation for Science (IFS) in Sweden for supporting this study financially.

References

- Aman, R., Schieber, A., & Carle, R. (2005). Effects of heating and illumination on *trans-cis* isomerization and degradation of β -carotene and lutein in isolated spinach chloroplasts. *Journal of Agricultural and Food Chemistry*, 53, 9512–9518.
- Bohm, V., Puspitasari-Nienaber, N., Ferruzzi, M. G., & Schwartz, S. J. (2002). Trolox equivalent antioxidant capacity of different geometrical isomers of α -carotene, β -carotene, lycopene and zeaxanthin. *Journal of Agricultural and Food Chemistry*, 50, 221–226.
- Burton, G. W., & Ingold, K. U. (1984). β -Carotene: An unusual type of lipid antioxidant. *Science*, 224, 569–573.
- Chen, B. H., Peng, H. Y., & Chen, H. E. (1995). Changes of carotenoids, color and vitamin A contents during processing of carrot juices. *Journal of Agricultural and Food Chemistry*, 43, 1912–1918.
- Cui, Z. W., Xu, S. Y., & Sun, D. W. (2004). Effect of microwave-vacuum drying on the carotenoids retention of carrot slices and chlorophyll retention of Chinese chive leaves. *Drying Technology*, 22, 563–575.
- Devahastin, S., Suvarnakuta, P., Soponronnarit, S., & Mujumdar, A. S. (2004). A comparative study of low-pressure superheated steam and vacuum drying of a heat-sensitive material. *Drying Technology*, 22, 1845–1867.
- Dutta, D., Chaudhuri, U. R., & Chakraborty, R. (2005). Structure, health benefits, antioxidant property and processing and storage of carotenoids. *African Journal of Biotechnology*, 4, 1510–1520.
- Larson, R. A. (1988). The antioxidants of higher plants. *Phytochemistry*, 4, 969–978.
- Lessin, W. J., Catigani, G. L., & Schwartz, S. J. (1997). Quantification of *cis-trans* isomers of provitamin A carotenoids in fresh and processed fruits and vegetables. *Journal of Agricultural and Food Chemistry*, 45, 3728–3732.
- Marx, M., Stuparic, M., Schieber, A., & Carle, R. (2003). Effects of thermal processing on *trans-cis*-isomerization of β -carotene in carrot juices and carotene-containing preparations. *Food Chemistry*, 83, 609–617.
- Miller, N. J., Sampson, J., Candxias, L. P., Bramly, P. M., & Rice-Evans, C. A. (1996). Antioxidant activities of carotenes and xanthophylls. *FEBS Letters*, 384, 240–242.
- Patrick, L. (2000). β -Carotene: The controversy continues. *Alternative Medicine Review*, 5, 530–545.
- Rubatzky, V. E., Quiros, C. F., & Simon, P. W. (1999). *Carrots and related vegetable umbelliferae*. CABI: Oxon.
- Sergio, A. R. P., & Russell, M. R. (1999). β -carotene and other carotenoids as antioxidant. *Journal of the American College of Nutrition*, 18, 426–433.
- Stahl, W., & Sies, H. (2003). Antioxidant activity of carotenoids. *Molecular Aspects of Medicine*, 24, 345–351.
- Suvarnakuta, P., Devahastin, S., & Mujumdar, A. S. (2005). Drying kinetics and β -carotene degradation in carrot undergoing different drying processes. *Journal of Food Science*, 70, S520–S526.

Effects of drying methods and conditions on drying kinetics and quality of Indian gooseberry flake

Siporn Methakhup, Naphaporn Chiewchan*, Sakamon Devahastin

Department of Food Engineering, King Mongkut's University of Technology Thonburi, 91 Pracha u-tid Road, Bangkok 10140, Thailand

Received 10 June 2004; received in revised form 10 August 2004; accepted 11 August 2004

Abstract

Vacuum drying and low-pressure superheated steam drying (LPSSD) of Indian gooseberry flake (used to prepare Indian gooseberry tea) were carried out at various drying conditions to monitor the drying kinetics and quality degradation of the product during drying. In terms of drying kinetics, the vacuum drying took shorter time to dry the product than LPSSD at every drying condition. In terms of quality, it was found that only the product subjected to vacuum drying at 75 °C and absolute pressure of 7 kPa had similar level of ascorbic acid retention compared to those samples of LPSSD at every condition. The total color difference of this sample was, however, slightly higher than that of product dried by LPSSD. Nevertheless, since the color changes were not of much concern to the consumers of Indian gooseberry tea, vacuum drying at 75 °C and 7 kPa was proposed as the most favorable condition for drying of Indian gooseberry flake in terms of energy consumption.

© 2004 Swiss Society of Food Science and Technology. Published by Elsevier Ltd. All rights reserved.

Keywords: Ascorbic acid; Color; Low-pressure superheated steam drying; Page's equation; Vacuum drying

1. Introduction

Indian gooseberry (*Phyllanthus emblica* Linn.) or “Ma-khaam Pom” in Thai (Chatchavalchokchai, 1987) is indigenous in tropical Southeast Asia, including Thailand, and is known as a rich source of vitamin C. The fruit is commonly consumed as a health food in both fresh and various preserved forms such as pickles, dried fruits, and beverage products (Montri, 1998).

Indian gooseberry tea is an alternative product to instant beverage powder and pasteurized juice. It is usually consumed for thirst quenching. In Indian gooseberry tea processing, drying is the main thermal treatment, which affects the quality of the product such as its ascorbic acid content and color. This quality loss has an influence on the consumer satisfaction. Therefore, a suitable drying process, which involves an

identification of a suitable drying method and conditions, is important to minimize the quality loss of the product.

Vacuum drying has been applied widely to dry various heat-sensitive products in which qualities such as color, texture and various vitamins are deteriorated at elevated temperatures. Drouzas and Schubert (1996) studied drying of banana using microwave-vacuum drying at pressures of 15–300 mbar (1.5–30 kPa) and at magnetron levels of 150–850 W. The results showed no significant variations as far as the drying rates under different pressures were concerned. Moreover, better product quality (as examined by taste, aroma, smell and rehydration tests) was also obtained when using higher levels of vacuum. Markowski and Bialobrzewski (1997) studied the drying kinetics of celery slice (10 mm thick, 57 mm diameter) using vacuum drying. Experiments were carried out at temperatures in the range of 25–50 °C and the pressure inside the drying chamber was maintained at 10 ± 0.2 kPa. The results showed no

*Corresponding author. Tel.: +662-470-9243; fax: +662-470-9240.
E-mail address: naphaporn.rat@kmutt.ac.th (N. Chiewchan).

constant drying rate period in all cases. The samples dried at lower temperature level re-adsorbed more water than those dried at higher temperatures. The results also proved that vacuum drying could be used for preservation of high quality celery slices in terms of color and flavor. More recently, [Jaya and Das \(2003\)](#) studied the vacuum drying of mango pulp of various thicknesses (2, 3, and 4 mm) and temperatures (65, 70, and 75 °C) under 30–50 mm of mercury absolute pressure. A mathematical model based on the moisture diffusivity of the drying product was found to give close prediction of moisture content of the pulp at different times of drying. Color change of reconstituted pulp was found to depend more on the pulp thickness than the drying temperature.

Recently, a novel concept of low-pressure superheated steam drying (LPSSD) has been proposed as an alternative to drying heat-sensitive products since it can combine the advantages of drying at reduced temperature to those of conventional superheated steam drying ([Mujumdar & Devahastin, 2000](#)). [Elustondo, Elustondo, and Urbicain \(2001\)](#) studied sub-atmospheric pressure superheated steam drying of foodstuffs at pressures of 10,000–20,000 Pa, temperatures of 60–90 °C and steam circulating velocities of 2–6 m/s. A semi-empirical mathematical model was also developed and a simplified expression, which had two experimentally determined parameters, was derived and used to predict the drying rates of tested samples. A model proposed was found to predict the drying kinetics reasonably well. No mention about the dried product quality was given, however. [Devahastin, Suvarnakuta, Soponronnarit, and Mujumdar \(2004\)](#) studied the drying kinetics and various quality parameters of the dried carrot cubes undergoing both LPSSD and vacuum drying. Effects of pressure (absolute of 7–10 kPa) and temperature (60–80 °C) on the drying characteristics as well as quality attributes, i.e. volume, shrinkage, apparent density, color and rehydration behavior, of the dried product subjected to the two drying processes were also evaluated and compared. Although LPSSD required longer dwell time to achieve the same final moisture content than vacuum drying, some of the quality attributes were superior to those obtained in vacuum drying.

However, no data are available, either in terms of the drying kinetics and quality of Indian gooseberry undergoing either of these drying techniques. Therefore, the aim of this work was to study the drying kinetics as well as the quality degradation (in terms of ascorbic acid and color degradation) of Indian gooseberry flake undergoing both vacuum and LPSSD. The information obtained could be used to design an appropriate drying process to minimize the quality degradation of Indian gooseberry flake, which is used as the main ingredient of Indian gooseberry tea.

2. Material and methods

2.1. Experimental setup

A schematic diagram of the low-pressure superheated steam dryer and its accessories is shown in [Fig. 1](#). The dryer consists of a stainless steel drying chamber, insulated with rock wool; a steam reservoir, which received the steam from the boiler; and a liquid ring vacuum pump (Nash, ET32030, Germany), which was used to maintain the vacuum in the drying chamber. Steam trap was installed to reduce the excess steam condensation in the reservoir. An electric heater was controlled by a PID controller (Omron, E5CN, Japan). A variable-speed electric fan was used to disperse steam throughout the drying chamber. The steam inlet was made into a cone shape and was covered with a screen to help distributing the steam in the chamber. The change of the mass of the sample was detected continuously using a load cell (Minebea, Ucg-3 kg, Japan). The temperatures of the steam and of the drying sample were also measured continuously using type K thermocouples. Thermocouple signals were multiplexed to a data acquisition card (Omega Engineering, CIO-DAS16Jr., USA) installed in a PC. LABTECH NOTEBOOK software (version 12.1, Laboratory Technologies Corp., USA) was then used to read and record the temperature data. More detailed experimental setup could be referred in [Devahastin et al. \(2004\)](#). The same experimental setup was also used for vacuum drying experiments but without the application of steam to the drying chamber.

2.2. Experimental procedure

Fresh Indian gooseberry fruit was purchased from a local market and stored in a refrigerator at 5 °C. After rinsing the fruit, its seeds were removed using a stainless-steel knife. The flesh was cut into small pieces and blended for 1 min using a blender (Moulinex, AS184, France). Forty grams of the prepared sample was spread on a sample holder, which was made of an aluminum foil. The sample was then dried either by a vacuum or a low-pressure superheated steam dryer at temperatures of 65 and 75 °C and absolute pressures of 7, 10 and 13 kPa. During drying mass of samples was recorded at every 10 min interval. The dryer was operated until the mass of the sample reached its equilibrium value. The sample was then dried in a hot air oven (Mettler, ULM 600 II, Germany) at 105 °C until its mass, which was measured by a digital balance (Sartorius, RC 250S, Germany), was constant in order to obtain its bone-dry mass. Page's equation was used to fit the experimental data to calculate the drying time required for reducing the moisture content of Indian gooseberry flake to 7.5% (d.b.). This final moisture content was selected since it is

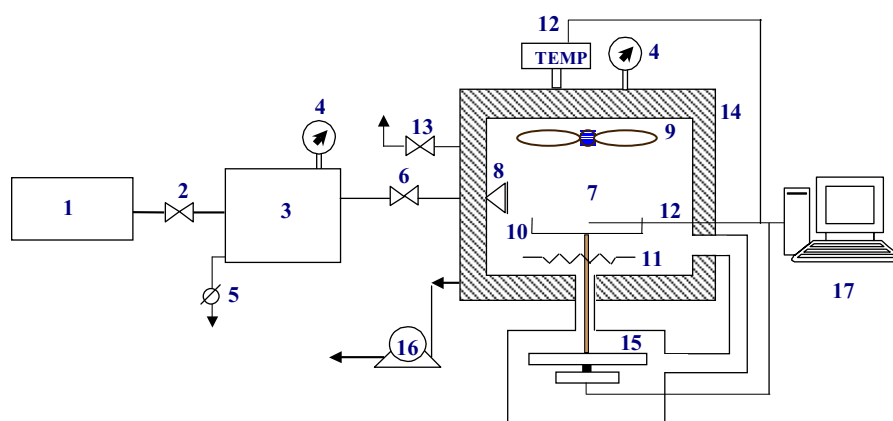


Fig. 1. Schematic diagram of low-pressure superheated steam dryer and associated units. 1, boiler; 2, steam valve; 3, steam reservoir; 4, pressure gauge; 5, steam trap; 6, steam regulator; 7, drying chamber; 8, steam inlet and distributor; 9, electric fan; 10, sample holder; 11, electric heater; 12, on-line temperature sensor and logger; 13, vacuum break-up valve; 14, insulator; 15, on-line mass indicator and logger; 16, vacuum pump; 17, PC with installed data acquisition card.

the maximum allowable final moisture content of a similar product, i.e., black tea (Thai Industrial Standard Institute (TISI), 1983). The new set of prepared sample, which had a pH value (measured by a pH meter, Tüv Rheinland, CG 841, Germany) in the range of 2.2–2.7, was dried again at the same conditions until its moisture content reached 7.5% (d.b.) using the time estimated from Page's equation. Moisture content (Association of Official Analytical Chemists, (AOAC), 1990), ascorbic acid and color of fresh and dried Indian gooseberry flake were measured. All experiments were performed in duplicate.

2.3. Total ascorbic acid (TAA) determination

TAA was measured by Roe and Kuther's method (Damrongnukool, 2000). The assay estimates the intensity of osazone formed by the coupling of 2,4-dinitrophenylhydrazine (DNPH) with the oxidative forms of ascorbic acid, which are dehydroascorbic acid (DHAA) and diketogulonic acid (DKGA), using a spectrophotometer (Shimadzu, UV-2101 PC, Japan).

2.4. Color measurement

The colors of fresh and dried Indian gooseberry flake were measured by a colorimeter (JUKI, JP7100, Japan) with 2° North skylight as the light source. The colorimeter was calibrated against a standard white plate for powder ($L = 91.78$, $a = -0.28$, $b = 0.07$) before each measurement. A glass cylinder containing fresh/dried Indian gooseberry flake was placed above the light source and covered with a lid. Three Hunter parameters, namely L (lightness), a (redness/greenness), and b (yellowness/blueness) were measured and the total color difference (ΔE) was calculated from ΔL , Δa and Δb values.

2.5. Statistical analysis

The data were analysed and presented as mean values with standard deviations. Differences between mean values were established using Duncan's-multiple range tests. Values were considered at 95% level of significance ($\alpha < 0.05$) and a statistical program SPSS was used to perform the calculation.

3. Results and discussion

3.1. Drying kinetics of Indian gooseberry flake

The drying curves of Indian gooseberry flake (initial moisture content of 380–470% d.b.) undergoing different drying techniques at various conditions are shown in Figs. 2–4. Moisture ratio (MR) of sample were fitted to Page's equation as follows:

$$MR = \frac{M_t - M_{eq}}{M_i - M_{eq}} = \exp(-Kt^N), \quad (1)$$

where MR is the moisture ratio; M_t is the moisture content at time t (kg/kg); M_{eq} is the equilibrium moisture content (kg/kg); M_i is the initial moisture content (kg/kg); K is the drying constant; N is the degree of nonlinearity of the drying curve.

Fig. 2 shows the drying curves of Indian gooseberry dried by vacuum drying. The dehydration times for reaching the equilibrium moisture contents (4.2–5.7% d.b.) were approximately 200, 210 and 230 min when using the drying temperature of 65 °C and absolute pressures of 7, 10 and 13 kPa, respectively. For drying at 75 °C at the same levels of absolute pressure, the drying times to reach the equilibrium moisture contents (2.4–3.8% d.b.) were reduced by roughly 20%, namely, 160, 170 and 190 min, respectively. This is due to the fact

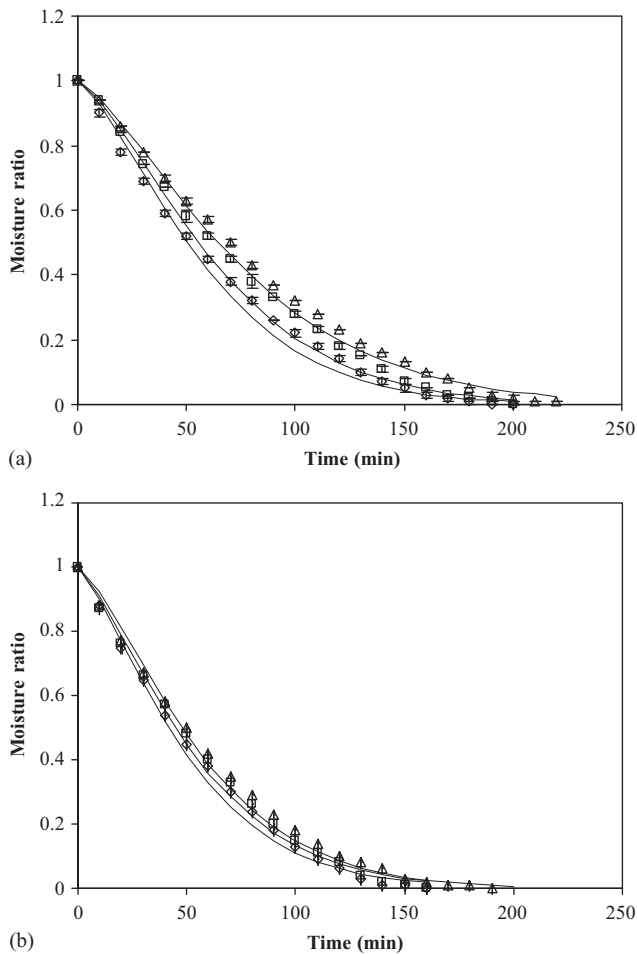


Fig. 2. Drying curves of Indian gooseberry flake undergoing vacuum drying at temperatures (a) 65 °C and (b) 75 °C; absolute pressures of 7 kPa (\diamond), 10 kPa (\square) and 13 kPa (\triangle). Solid line (—) represents curve fitting using Page's equation.

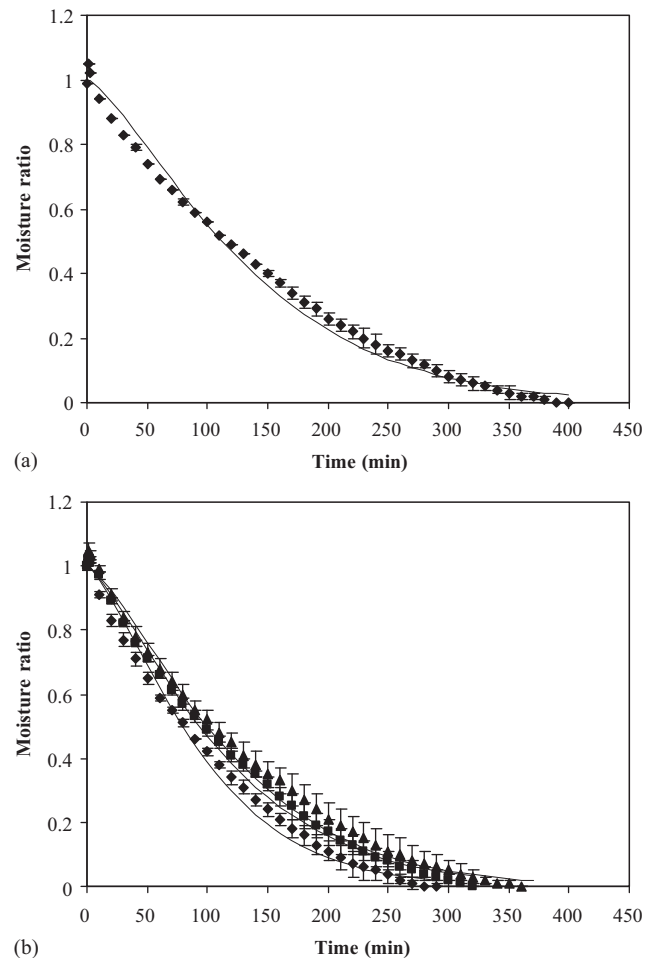


Fig. 3. Drying curves of Indian gooseberry flake undergoing LPSSD at temperatures (a) 65 °C and (b) 75 °C; absolute pressures of 7 kPa (\diamond), 10 kPa (\blacksquare) and 13 kPa (\blacktriangle). Solid line (—) represents curve fitting using Page's equation.

that drying at higher temperature implied a larger driving force for heat transfer, which was, in this case, the temperature difference between the drying medium and the temperature close to the wet-bulb temperature since the chamber was not at low-enough pressure and the effect of convection (due to the fan) was still significantly present. A higher drying temperature also led to a higher value of moisture diffusivity. In addition, it has also been reported by [Prabhanjan, Ramaswamy, and Raghavan \(1995\)](#) that the higher drying temperature provided a larger water vapor pressure deficit or the difference between the saturated water vapor pressure and partial pressure of water vapor in air at a given temperature, which is one of the driving forces for drying. Similar behavior was observed by [Jaya and Das \(2003\)](#).

It can also be seen in [Figs. 2\(a\) and \(b\)](#) that higher rates of drying were obtained when the absolute pressure of the dryer was decreased. This is because

decreasing of an absolute pressure resulted in a lower boiling point of water. The decrease of a boiling point of water resulted in an increase of the driving force for the outward moisture diffusion process. Hence, escaping of water molecules from the drying product became easier and faster.

[Fig. 3](#) shows the drying behavior of Indian gooseberry flake undergoing LPSSD at similar conditions to the vacuum drying reported earlier. It can be seen that during the first few minutes of superheated steam drying, there was an increase in moisture content of the sample due to the steam condensation on its surface. Such results are similar to the works reported by several investigators, e.g. [Tang and Cenkowski \(2000\)](#) and [Devahastin et al. \(2004\)](#).

Similar to drying in the vacuum system, the times needed to reach the equilibrium moisture content of Indian gooseberry flake dried at 65 °C were longer than those at 75 °C and lowering the absolute pressure could

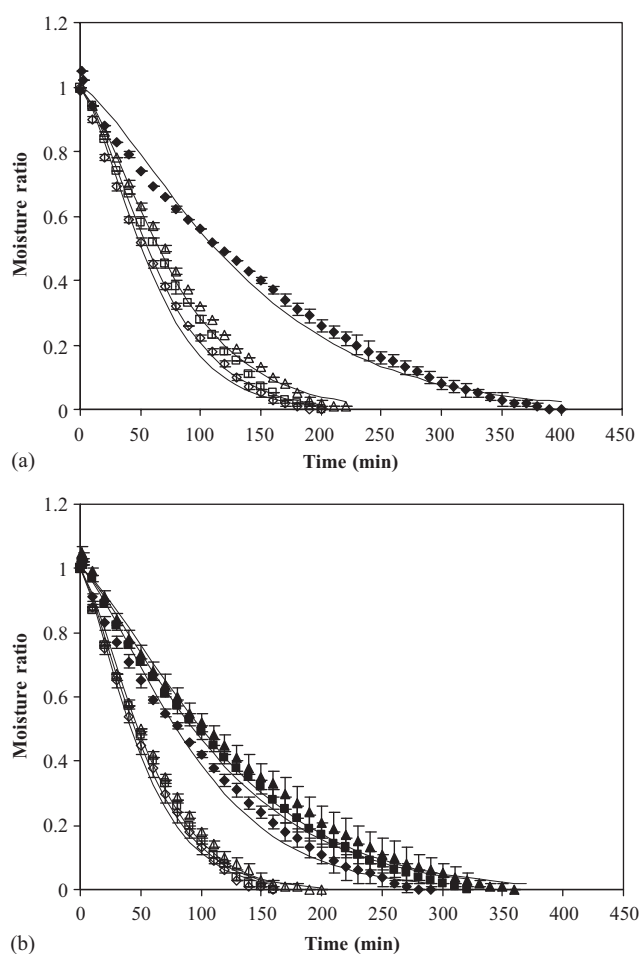


Fig. 4. Comparison of drying curves of Indian gooseberry flake at temperatures. (a) 65 °C and (b) 75 °C. Vacuum drying at 7 kPa (◇), 10 kPa (□) and 13 kPa (△). LPSSD at 7 kPa (◆), 10 kPa (■) and 13 kPa (▲). Solid line (—) represents curve fitting using Page's equation.

reduce the moisture faster than doing so at higher absolute pressures. An increase of the absolute pressure caused the saturation temperature to increase and hence reduced the driving force for heat transfer and hence the reduced drying rates (Urbaniec & Malaczewski, 1997). From the experimental data, the time taken for the sample to reach its moisture content of 6.4% (d.b.) was approximately 400 min at 65 °C and at an absolute pressure of 7 kPa. For drying at 75 °C and absolute pressures of 7, 10 and 13 kPa, it took approximately 290, 330 and 370 min, respectively, to obtain the equilibrium moisture contents in the range of 4.4–6.1% (d.b.). Increasing the temperature from 65 to 75 °C at an absolute pressure of 7 kPa decreased the dehydration time by approximately 27.5%.

Fig. 4 compares the drying characteristics of Indian gooseberry flake undergoing vacuum drying and LPSSD at various conditions. It was found that after the condensation stage, the shape of the drying curves of LPSSD were very similar to those of vacuum drying.

However, the longer drying times were observed for the samples undergoing LPSSD. This is due to the existence of the condensation period and the lower evaporation rate of LPSSD than that of vacuum drying at these conditions.

As seen in Fig. 4(b), it was found that the impact of the operating pressure on the rate of moisture reduction was more pronounced in the case of LPSSD than in the case of vacuum drying.

3.2. Empirical modeling of the drying process

To describe the drying behavior of Indian gooseberry flake undergoing both types of drying processes a well-known Page's equation (Ramesh & Rao, 1996; Cronin & Kearney, 1998; Karathanos & Belessiotis, 1999) was used to fit the experimental data.

Table 1 lists the drying constants obtained by application of Page's equation to the experimental data. A good agreement was found between the experimental and fitted values with the R^2 -values of 0.9334–0.9862. It can be seen that K -values for vacuum drying were higher than LPSSD. This is because the moisture reduction rate of superheated steam drying was lower than that of vacuum drying at the conditions tested in this work.

Considering the two drying processes at the same temperature, parameter K of both LPSSD and vacuum drying decreased as the absolute pressure increased. This is due to the fact that a lower absolute pressure led to a lower boiling point of water. Thus, the evaporation of water from the sample was enhanced. At the same pressure, parameter K increased as temperature increased because an increase of the drying temperature increased the driving force of heat and mass transfer (through an increase of the value of moisture diffusivity). For parameter N , it did not possess a clear trend. The results for parameters K and N were similar as those found by Karathanos and Belessiotis (1999), Park, Vohnikova, and Brod (2002), and El-Aouar, Azoubel, and Murr (2003).

3.3. Quality degradation of Indian gooseberry flake

Table 2 shows the TAA content in fresh and dried Indian gooseberry flake samples. The average initial ascorbic acid content was about 1.04 g/100 g sample. The change of ascorbic acid was expressed as percentage of retention. The percentage of retention of TAA is calculated according to the following equation (Ramesh, Wolf, Tevini, & Jung, 2001):

% Retention

$$= \frac{(\text{mass of dried sample}) \times (\text{conc. of TAA in dried sample})}{(\text{mass of fresh sample}) \times (\text{conc. of TAA in fresh sample})} \quad (2)$$

Table 1
Parameters of Page's equation and calculated drying times for various drying methods and conditions

Drying method	Condition		Page's parameter		R^2	Drying time to reach 7.5% (d.b.) (min)
	T (°C)	P_{abs} (kPa)	K ($\times 10^{-3} \text{ min}^{-1}$)	N		
VD ^a	65	7	2.86	1.4	0.9862	170
		10	2.4	1.41	0.9593	190
		13	2.29	1.37	0.9806	200
	75	7	5.02	1.32	0.9804	145
		10	4.24	1.36	0.9334	150
		13	3.33	1.38	0.9868	160
LPSSD ^b	65	7	1.3	1.33	0.9507	400
		10	—	—	—	—
		13	—	—	—	—
	75	7	1.89	1.35	0.9618	280
		10	1.59	1.35	0.9799	320
		13	1.45	1.34	0.9687	370

^aVD stands for vacuum drying.

^bLPSSD stands for low-pressure superheated steam drying.

All dried Indian gooseberry flake tended to lose some ascorbic acid as compared to the fresh one. The percentage of retention of ascorbic acid was in the range of 64–94% for vacuum drying and 93–96% for LPSSD. For vacuum drying, it was found that the ascorbic acid retention of the sample increased as the drying temperature increased. This may be due to the shorter drying time required to dry the samples to the desired moisture content (Jayaraman & Gupta, 1995; Maharaj & Sankat, 1996). However, the pressure had only a little effect on the ascorbic acid retention. This may be explained by the fact that the drying times were not much affected by the operating pressure and that the level of oxygen content (which caused the aerobic degradation of vitamin C) was not much different at different pressures.

For LPSSD, the ascorbic acid retention was not significantly different at different drying conditions even though the drying times were different. The results implied that no oxygen was available in the drying system and thus presented no effect on the ascorbic acid degradation during drying.

Generally, an increasing level of ascorbic acid degradation is resulted from slower drying methods (Nindo, Sun, Wang, Tang, & Powers, 2003). From the drying kinetics, it was found that drying by LPSSD took longer than vacuum drying at the same drying conditions. However, Table 2 shows that LPSSD could preserve ascorbic acid better than vacuum drying. This is because the level of ascorbic acid oxidation in the vacuum drying system was higher than in LPSSD. The ability to maintain vitamin C of the superheated steam drying system has, in fact, been reported earlier by other investigators (e.g. Moreira, 2001).

The effects of drying methods and conditions on the color of the sample were also determined. Table 3 shows the values of Hunter parameters (L, a, b) and the total color difference (ΔE) of Indian gooseberry flake. It was found that LPSSD and vacuum drying at every condition resulted in a decrease of an L-value and an increase of an a-value of dried sample compared with the fresh one. However, b-value of the dried sample was similar to that of fresh sample. These results implied that the browning reaction and pigment destruction occurred in the dried sample (Iyota, Nishimura, Nomura, Konishi, & Yoshida, 2002; Maskan, 2001; Maskan, Kaya, & Maskan, 2002). However, the overview of color changes of sample could be observed from the ΔE value, which is calculated using Eq. (3).

$$\Delta E = [(\Delta L)^2 + (\Delta a)^2 + (\Delta b)^2]^{1/2}. \quad (3)$$

In the vacuum drying system, drying at 65 °C and an absolute pressure of 7 kPa could preserve the color of the sample better than at other conditions. This is due to the fact that the main cause of color change in vacuum drying was chlorophyll degradation and nonenzymatic browning reaction, which is Maillard reaction and ascorbic acid oxidation since oxygen and light, which are the causes of these reactions existed at the lowest level in the system. Because Maillard reaction depends on temperature and duration of heat treatment (Chua, Hawlader, Chou, & Ho, 2002), drying at lower temperatures gave better color retention than drying at higher temperatures. However, there were no significant differences between drying at 65 °C, absolute pressures of 10 and 13 kPa and drying at 75 °C.

For LPSSD, it was found that there were no significant differences in terms of color between different drying conditions. In this case, the main cause of color change was the Maillard reaction. Other causes of color changes were the ascorbic acid and chlorophyll degradation. However, these degradations had negligible effect on the color of the sample when compared to Maillard reaction since the system had no oxygen.

When considering the color retention of the sample dried using two different methods, it was found that LPSSD could retain the color better than the vacuum

Table 2
Total ascorbic acid content of fresh and dried samples^a

Drying method	Conditions		Ascorbic acid (g/100 g)		% Retention
	<i>T</i> (°C)	<i>P</i> _{abs} (kPa)	Fresh	Dried	
VD ^b	65	7	1.08 _± 0.07	3.67 _± 0.13	71.52 ^{ab} _± 1.97
		10	1.06 _± 0.09	3.50 _± 0.25	66.89 ^a _± 2.51
		13	0.94 _± 0.05	3.07 _± 0.30	64.84 ^a _± 6.01
	75	7	0.96 _± 0.02	3.84 _± 0.18	94.46 ^{cd} _± 2.57
		10	0.99 _± 0.02	3.72 _± 0.11	89.46 ^c _± 2.78
		13	0.98 _± 0.11	3.34 _± 0.03	78.13 ^b _± 2.83
LPSSD ^c	65	7	1.05 _± 0.06	3.99 _± 0.22	93.46 ^{cd} _± 1.58
		10	—	—	—
		13	—	—	—
	75	7	1.06 _± 0.04	4.04 _± 0.08	95.35 ^d _± 3.49
		10	1.09 _± 0.08	4.03 _± 0.11	95.67 ^d _± 2.10
		13	1.04 _± 0.08	3.99 _± 0.11	94.96 ^{cd} _± 2.14

^aMean \pm SD (*n* = 2). Means in the same column having the same letter are not significantly different (α < 0.05).

^bVD stands for vacuum drying.

^cLPSSD stands for low-pressure superheated steam drying.

drying system. This is because the degree of ascorbic acid and chlorophyll degradation of LPSSD was much lower than that of the vacuum drying system.

The color results presented here are somewhat different from those studied in potato drying by [Iyota et al. \(2002\)](#) who reported that potato dried in superheated steam at temperatures ranging from 170 to 240 °C were glossier and reddish than that dried in hot air drying. This is due to the effect of high temperature used and also the effect of the amount of soluble polysaccharides available in potato.

Since for Indian gooseberry tea production, dried Indian gooseberry flake was filled in a tea bag before it was soaked into water by a consumer, the color of the dried product was not of much concern in this study. Therefore, it could be concluded that drying in the vacuum system at temperature of 75 °C and absolute pressure of 7 kPa was most suitable for Indian gooseberry flake. This is because these conditions gave the highest ascorbic acid retention while the color did not change much from the natural sample. Further, vacuum drying at 75 °C and absolute pressure 7 kPa also had the shortest drying time.

4. Conclusion

The effects of drying methods and conditions on the drying kinetics and quality degradation of Indian gooseberry flake were examined in this study. The drying temperature was found to have an effect on the moisture reduction rates of samples dried both by vacuum drying and LPSSD. However, pressure seemed to have an obvious effect only for LPSSD. Further, it was found that vacuum drying took shorter time to dry the product than that required by LPSSD at all drying conditions. The drying curves could be well fitted by Page's equation. For both LPSSD and vacuum drying, the drying constant *K* increased with an increase of temperature and a decrease of absolute pressure while the product constant *N* was not affected by these factors. Parameter *K* of vacuum drying was higher than that of LPSSD.

The quality studies showed that, except for vacuum drying at 75 °C and absolute pressures of 7 and 10 kPa, LPSSD could retain ascorbic acid better than the vacuum drying. In addition, LPSSD could preserve the color of the sample better than the vacuum drying at all

Table 3
Hunter parameters and total color difference (ΔE) of dried samples^a

Drying method	Conditions		$\Delta L/L_0$	$\Delta a/a_0$	$\Delta b/b_0$	ΔE
	T (°C)	P_{abs} (kPa)				
VD ^b	65	7	0.06 \pm 0.00	−0.91 \pm 0.01	0.01 \pm 0.01	3.83 ^b \pm 0.09
		10	0.08 \pm 0.00	−1.39 \pm 0.07	0.02 \pm 0.02	5.40 ^{cd} \pm 0.10
		13	0.07 \pm 0.01	−0.98 \pm 0.22	0.00 \pm 0.04	4.99 ^c \pm 1.04
	75	7	0.08 \pm 0.00	−0.71 \pm 0.01	−0.02 \pm 0.01	5.61 ^{cd} \pm 0.28
		10	0.09 \pm 0.00	−1.11 \pm 0.01	−0.02 \pm 0.00	6.42 ^d \pm 0.26
		13	0.07 \pm 0.01	−1.56 \pm 0.58	0.03 \pm 0.02	5.38 ^{cd} \pm 0.66
LPSSD ^c	65	7	0.04 \pm 0.00	−0.88 \pm 0.97	0.04 \pm 0.01	3.09 ^{ab} \pm 0.19
		10	—	—	—	—
		13	—	—	—	—
	75	7	0.03 \pm 0.01	−0.64 \pm 0.04	0.04 \pm 0.02	2.48 ^a \pm 0.44
		10	0.04 \pm 0.00	−0.49 \pm 0.18	0.04 \pm 0.01	2.88 ^{ab} \pm 0.18
		13	0.04 \pm 0.04	−0.64 \pm 0.23	0.02 \pm 0.04	2.93 ^{ab} \pm 0.39

^aMean \pm SD ($n=2$). Means in the same column having a same letter are not significantly different ($\alpha < 0.05$).

^bVD stands for vacuum drying.

^cLPSSD stands for low-pressure superheated steam drying.

drying conditions tested. For vacuum drying, temperature had a significant effect on ascorbic acid content and color of the product while absolute pressure did not significantly affect the quality. For LPSSD, on the other hand, the drying conditions did not affect the ascorbic acid and color of dried product.

It could be concluded that drying in a vacuum system at a temperature of 75 °C, absolute pressure of 7 kPa was the most suitable condition for drying Indian gooseberry flake since this condition gave highest ascorbic acid retention while the color did not change much from the natural sample and had shortest drying time. However, in the case where the importance of color could not be neglected, the conclusion would be different from that obtained in this study.

Acknowledgements

The authors would like to express their appreciation to the Thailand Research Fund (TRF), National Research Council of Thailand and the International

Foundation for Science (Sweden) for supporting this study financially.

References

- Association of Official Analytical Chemists (AOAC). 1990. *Official method of analysis* (15th ed.). Virginia: Association of Official Analytical Chemists.
- Chatchavalchokchai, N. (1987). *Effect of some ruminants on seed quality of Phyllanthus emblica Linn., Elaeocarpus madopetalous Pierre, Spondias pinnata Kurz and Terminalia chebula Retz*. M.Sc. Thesis. Botany Program. Faculty of Science. Kasetsart University, Thailand.
- Chua, K. J., Hawlader, M. N. A., Chou, S. K., & Ho, J. C. (2002). On the study of time-varying temperature drying—effect on drying kinetics and product quality. *Drying Technology*, 20, 1559–1577.
- Cronin, K., & Kearney, S. (1998). Monte Carlo modelling of a vegetable tray dryer. *Journal of Food Engineering*, 35, 233–250.
- Damrongnukool, J. (2000). *Determination of vitamin C contents in commercial fruit juice*. M.Sc. Thesis. Home Economics Program. Faculty of Home Economics. Kasetsart University, Thailand.
- Devahastin, S., Suvarnakuta, P., Soponronnarit, S., & Mujumdar, A. S. (2004). A comparative study of low-pressure superheated steam and vacuum drying of a heat-sensitive material. *Drying Technology*, in press.

- Drouzas, A. E., & Schubert, H. (1996). Microwave application in vacuum drying of fruits. *Journal of Food Engineering*, 28, 203–209.
- El-Aouar, A. A., Azoubel, P. M., & Murr, F. E. X. (2003). Drying kinetics of fresh and osmotically pre-treated papaya (*Carica papaya* L.). *Journal of Food Engineering*, 59, 85–91.
- Elustondo, D., Elustondo, M. P., & Urbicain, M. J. (2001). Mathematical modeling of moisture evaporation from foodstuffs exposed to subatmospheric pressure superheated steam. *Journal of Food Engineering*, 49, 15–24.
- Iyota, H., Nishimura, N., Nomura, T., Konishi, Y., & Yoshida, K. (2002). Effect of initial steam condensation on color changes of potatoes during drying in superheated steam. *Proceedings of the 13th international drying symposium, Part B*, pp. 1352–1359.
- Jaya, S., & Das, H. (2003). A vacuum drying model for mango pulp. *Drying Technology*, 21, 1215–1234.
- Jayaraman, K. S., & Gupta, D. K. (1995). Drying of fruits and vegetables. In A.S. Mujumdar (Ed.), *Handbook of industrial drying* 2nd ed (pp. 643–687). New York: Marcel Dekker.
- Karathanos, V. T., & Belessiotis, V. G. (1999). Application of a thin-layer equation to drying data of fresh and semi-dried fruits. *Journal of Agricultural Engineering Research*, 74, 355–361.
- Maharaj, V., & Sankat, C. K. (1996). Quality changes in dehydrated dasheen leaves: Effects of blanching pre-treatments and drying conditions. *Food Research International*, 29, 563–568.
- Markowski, M., & Bialobrzewski, I. (1997). Celery slice vacuum drying kinetics. In R. Jowitt (Ed.), *Engineering & food at ICEF 7 Part 2* (pp. 93–96). Boston: Sheffield Academic Press.
- Maskan, M. (2001). Kinetics of colour change of kiwifruits during hot air and microwave drying. *Journal of Food Engineering*, 48, 169–175.
- Maskan, A., Kaya, S., & Maskan, M. (2002). Effect of concentration and drying process on color change of grape juice and leather (pestil). *Journal of Food Engineering*, 54, 75–80.
- Montri, N. (1998). *In vitro propagation of Phyllanthus emblica* L. M.Sc. Thesis. Horticulture Program. Faculty of Science. Kasetsart University, Thailand.
- Moreira, R. G. (2001). Impingement drying of foods using hot air and superheated steam. *Journal of Food Engineering*, 49, 291–295.
- Mujumdar, A. S., & Devahastin, S. (2000). Fundamental principles of drying. In S. Devahastin (Ed.), *Mujumdar's practical guide to industrial drying* (pp. 1–22). Brossard: Exergex Corp.
- Nindo, C. I., Sun, T., Wang, S. W., Tang, J., & Powers, J. R. (2003). Evaluation of drying technologies for retention of physical quality and antioxidants in asparagus (*Asparagus officinalis* L.). *Lebensmittel-Wissenschaft und-Technologie*, 36, 507–516.
- Park, K. J., Vohnikova, Z., & Brod, F. P. R. (2002). Evaluation of drying parameters and desorption isotherms of garden mint leaves (*Mentha crispa* L.). *Journal of Food Engineering*, 51, 193–199.
- Prabhanjan, D. G., Ramaswamy, H. S., & Raghavan, G. S. V. (1995). Microwave-assisted convective air drying of thin layer carrots. *Journal of Food Engineering*, 25, 283–293.
- Ramesh, M. N., & Rao, P. N. S. (1996). Drying studies of cooked rice in a vibrofluidised bed drier. *Journal of Food Engineering*, 27, 389–396.
- Ramesh, M. N., Wolf, W., Tevini, D., & Jung, G. (2001). Influence of processing parameters on the drying of spice paprika. *Journal of Food Engineering*, 49, 63–72.
- Tang, Z., & Cenkowski, S. (2000). Dehydration dynamics of potatoes in superheated steam and hot air. *Canadian Agricultural Engineering*, 42(1), 43–49.
- Thai Industrial Standard Institute. (1983). *Black tea* (14p).
- Urbaniec, K., & Malaczewski, J. (1997). Experimental investigations of beet pulp drying in superheated steam under pressure. *Drying Technology*, 15, 2005–2013.

Drying and heat transfer behavior of banana undergoing combined low-pressure superheated steam and far-infrared radiation drying

Chatchai Nimmol^{a,*}, Sakamon Devahastin^b, Thanit Swasdisevi^a, Somchart Soponronnarit^a

^a School of Energy, Environment and Materials, King Mongkut's University of Technology Thonburi, 126 Pracha u-tid Road, Bangkok 10140, Thailand

^b Department of Food Engineering, King Mongkut's University of Technology Thonburi, 126 Pracha u-tid Road, Bangkok 10140, Thailand

Received 15 January 2007; accepted 20 February 2007

Available online 4 March 2007

Abstract

The present study aimed at investigating the use of a drying system combining the concept of already proven low-pressure superheated steam drying and far-infrared radiation (LPSSD–FIR) for banana. The effects of various operating parameters, i.e., drying medium temperature and pressure, on the drying kinetics and heat transfer behavior of banana as well as the energy consumption of the process were investigated and discussed. Comparison was also made with similar sets of data obtained from the system with combined far-infrared radiation and vacuum drying (VACUUM–FIR) and the system using only low-pressure superheated steam drying (LPSSD). The results showed that LPSSD–FIR and VACUUM–FIR took shorter drying time compared to LPSSD at all drying conditions. In terms of the specific energy consumption, it was observed that the specific energy consumption of the vacuum pump was much higher than that of the far-infrared radiator or electric heater. It was also found that the specific energy consumption of LPSSD–FIR and VACUUM–FIR were lower than that of LPSSD at all drying conditions. Based on the drying rates and the specific energy consumption of all tested processes, LPSSD–FIR at 90 °C and 7 kPa was suggested.

© 2007 Elsevier Ltd. All rights reserved.

Keywords: Banana; Drying kinetics; Drying rates; Specific energy consumption; Vacuum drying

1. Introduction

Fresh banana perishes rapidly after harvesting and appropriate technology is generally applied to prolong its shelf life. Drying is one of the possible means that can be used to preserve banana from being deteriorated and also to reduce the cost of transportation and storage as well as to produce products that would not be able to obtain otherwise. There are many drying techniques available to dry banana. Most common techniques for drying banana are hot air drying [1–3]. However, hot air drying is a very energy-intensive operation and leads to much degradation of product quality. Microwave drying is an alternative means that can be used to dry banana [4]. Although the

drying process is accelerated with the use of microwave, some product quality is poor if microwave is not properly applied [5–7].

Recently, low-pressure (or subatmospheric-pressure) superheated steam drying (LPSSD) has been proposed and applied to many food products [8–10]. Since superheated steam in the case of LPSSD can be produced at the temperature lower than 100 °C due to reduced pressure environment, quality degradation of the products due to elevated temperature is alleviated. Generally, it has been shown that products dried by LPSSD have superior quality than those dried by conventional hot air and even vacuum drying. However, LPSSD is a rather slow drying process resulting in higher energy requirement. In order to reduce the energy requirement of the process, it is necessary to add an extra source of energy to the system. Far-infrared radiation (FIR), which has received much attention recently, is one possible means for the above purpose

* Corresponding author. Tel.: +66 2 470 8695; fax: +66 2 470 8663.
E-mail address: ccnimmol@gmail.com (C. Nimmol).

[11–13]. During FIR drying, the energy in the form of electromagnetic wave is absorbed directly by the product without loss to the environment leading to considerable energy savings [14–16].

To attain the advantages of the above-mentioned drying techniques, the combination of low-pressure superheated steam and far-infrared radiation drying is proposed as a novel drying technology for food and other biomaterials. In this study, the effects of various operating parameters, i.e., drying medium temperature and pressure, on the drying kinetics and heat transfer behavior of banana used as a model material as well as the energy consumption of the process were investigated and discussed. Comparison was also made with similar sets of data obtained from the system with combined far-infrared radiation and vacuum drying and from the system using LPSSD alone.

2. Experimental set-up, materials and methods

2.1. Experimental set-up

A schematic diagram of the combined low-pressure superheated steam and far-infrared radiation drying system is shown in Fig. 1. The dryer consists of a stainless steel drying chamber, insulated with rock wool, with inner dimensions of $45 \times 45 \times 45 \text{ cm}^3$; a steam reservoir, which received the steam from a boiler and maintained the steam pressure at around 200 kPa; a liquid ring vacuum pump (Nash, ET32030, Trumbull, CT), which was used to maintain the vacuum in the drying chamber; a far-infrared radiator (Infrapara, A-2T-500, Malaysia) rated at 500 W with a surface area of $60 \times 120 \text{ mm}^2$, which was used to supply thermal radiation to the drying sample and the drying medium; and electric heater rated at 1500 W, which was used to maintain the superheated steam temperature in the case of low-pressure superheated steam drying experiments. The distance between the far-infrared radiator and the sample holder, made of a stainless steel screen with dimensions of $15 \times 15 \text{ cm}^2$, was set at 165 mm.

The operation of the far-infrared radiator was controlled through the temperature of the drying medium

(air or superheated steam) measured at 30 mm above the sample surface, via the use of a proportional-integral-derivative (PID) controller (Shinko, JCS-33A-R/M, Japan) with an accuracy of $\pm 0.1^\circ\text{C}$. Similar to the far-infrared radiator, the operation of the electric heater was also controlled by a PID controller (Omron, model E5CN, Japan) with an accuracy of $\pm 0.1^\circ\text{C}$. The change of the mass of the sample during drying was detected continuously (at 1 min interval) using a load cell (Minebea, Ucg-3 kg, Nagano, Japan) with an accuracy of $\pm 0.2 \text{ g}$. The temperatures of the drying medium and of the drying sample were measured continuously using type K thermocouples. The thermocouple used to measure the drying medium temperature was located at the same position as the thermocouple that was used for sending the signal to the PID controller to control the far-infrared radiator. The thermocouples were partly covered with an aluminum foil acting as a radiation shield. The average surface temperature of the far-infrared radiator was also measured using a type K thermocouple. Thermocouple signals were multiplexed to a data acquisition card (Omega Engineering, CIO-DAS16Jr., Stamford, CT) installed in a PC. LABTECH NOTEBOOK software (version 12.1, Laboratory Technologies Corp., MA) was then used to read and record the temperature data.

2.2. Materials

Gros Michel banana (*Musa Sapientum* L.) was used as the tested material in this study. Fresh banana with an initial moisture content [17] in the range of 2.65–3.10 kg/kg (d.b.) and selected ripeness level of green tip (color index no. 5) was obtained from a local supermarket and stored at 4°C . Prior to the start of each experiment banana was peeled and sliced by a slicing machine to 3 mm thick. The sliced samples were then cut into 30 mm diameter using a die.

2.3. Methods

To perform a drying experiment approximately 16 pieces of prepared banana slices were placed on the sample

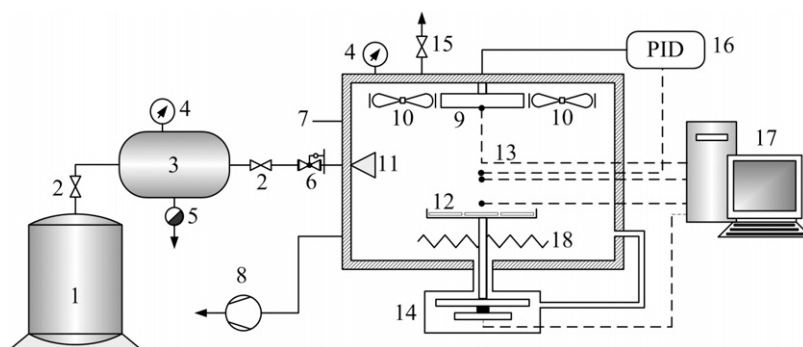


Fig. 1. A schematic diagram of the combined low-pressure superheated steam and far-infrared radiation drying system: (1) boiler, (2) steam valve, (3) steam reservoir, (4) pressure gauge, (5) steam trap, (6) steam regulator, (7) drying chamber, (8) vacuum pump, (9) far-infrared radiator, (10) electric fans, (11) steam inlet and distributor, (12) sample holder, (13) thermocouples, (14) load cell, (15) vacuum break-up valve, (16) PID controller, (17) PC with data acquisition card and (18) electric heater.

holder. To reduce the amount of steam condensation in the drying chamber during the start-up of a combined low-pressure superheated steam and far-infrared radiation drying (LPSSD–FIR) experiment, the far-infrared radiator was turned on to heat up the sample and to maintain the drying chamber temperature to the desired value without the application of steam to the drying chamber during the first 5 min of the drying process. The flow rate of steam into the drying chamber was maintained at about 26 kg/h and the speed of the electric fans was fixed at around 2100 rpm.

For a drying experiment using far-infrared radiation under vacuum (VACUUM–FIR) the same experimental set-up was used. Since the forced convection in the drying chamber led to lower temperatures of the far-infrared radiator and of the samples leading to lower drying rates, the electric fans were not used in this case.

For an experiment using LPSSD alone the same experimental set-up as that of LPSSD–FIR system was used. However, the electric heater located beneath the sample holder was used instead of the far-infrared radiator. Similar to LPSSD–FIR, preheating of the drying chamber was performed to reduce the initial condensation of steam.

The experiments were carried out at the drying medium (air or superheated steam) temperatures of 70, 80 and 90 °C and chamber absolute pressures of 7 and 10 kPa. Banana slices were dried until reaching their equilibrium moisture content at each operating condition. All experiments were performed in duplicate. It should be noted that the required final moisture content of banana slices should be lower than 0.035 kg/kg (d.b.).

2.4. Calculation of moisture ratio and drying rate

Because of the variation in initial moisture content of fresh banana, moisture ratio was used to describe the drying behavior of banana in this study. To calculate the drying rate, an appropriate empirical equation was fitted to the experimental moisture removal data (drying curve) and was then differentiated with respect to time. The moisture ratio and drying rate are defined as

$$MR = \frac{X - X_e}{X_i - X_e} \quad (1)$$

$$R = -\frac{dX}{dt} \quad (2)$$

where MR is the moisture ratio, R is the drying rate (kg kg^{-1} (d.b.) min^{-1}), X is the moisture content at any time (kg/kg (d.b.)), X_i is the initial moisture content (kg/kg (d.b.)), X_e is the equilibrium moisture content of sample (kg/kg (d.b.)) and t is time (min).

2.5. Evaluation of specific energy consumption and total steam consumption

In this study, the energy consumption of the drying processes, measured directly using a kilowatt-hour meter,

composed of the electric energy required to maintain the vacuum in the drying chamber and electric energy required to generate thermal energy. The former was the electric energy consumed by the vacuum pump and the latter was the energy consumed by the far-infrared radiator (for LPSSD–FIR and VACUUM–FIR) or the electric heater (for LPSSD), depending on the drying method employed. Since the electric fans consumed very small amount of electric energy, the energy consumption of the electric fans was neglected.

The efficiency of energy utilization during drying was evaluated through the specific energy consumption, which is the measure of the energy required during the process to remove 1 kg of water in the product being dried. The specific energy consumption of the vacuum pump and of the far-infrared radiator or electric heater was calculated by

$$SEC_{\text{vacuum}} = \frac{E_{\text{vacuum}}}{m_{\text{water}}} \quad (3)$$

$$SEC_{\text{radiator/heater}} = \frac{E_{\text{radiator/heater}}}{m_{\text{water}}} \quad (4)$$

where SEC_{vacuum} is the specific energy consumption of the vacuum pump (kWh/kg water), $SEC_{\text{radiator/heater}}$ is the specific energy consumption of the far-infrared radiator or electric heater (kWh/kg water), E_{vacuum} is the measured electric energy consumption of the vacuum pump (kWh), $E_{\text{radiator/heater}}$ is the measured electric energy consumption of the far-infrared radiator or electric heater (kWh) and m_{water} is the amount of water removed (kg), which could be estimated as the difference between the initial and final masses of the product.

Since the flow rate of steam into the drying chamber was maintained at about 26 kg/h, the total steam consumption during LPSSD–FIR and LPSSD experiments was estimated by multiplying the value of steam flow rate by the time required to attain the desired final product moisture content at each drying condition.

3. Results and discussion

Fig. 2 shows the drying curves of banana slices undergoing different drying methods at various conditions. In the case of LPSSD–FIR it is seen from Fig. 2a that the drying time decreased with an increase in the drying temperature, as expected. This is because the temperature difference between the sample and superheated steam at a higher drying temperature was greater than that at a lower temperature, hence a larger driving force for heat transfer, which is also related to the rate of mass transfer. The moisture diffusivity is also higher at a higher temperature. In addition, the drying time also decreased with a decrease in the drying pressure. This is due to the fact that water evaporated at lower temperature when drying was performed at a lower pressure. It can also be seen that the rates of moisture reduction were more affected by the drying temperature than by the drying pressure when drying was performed

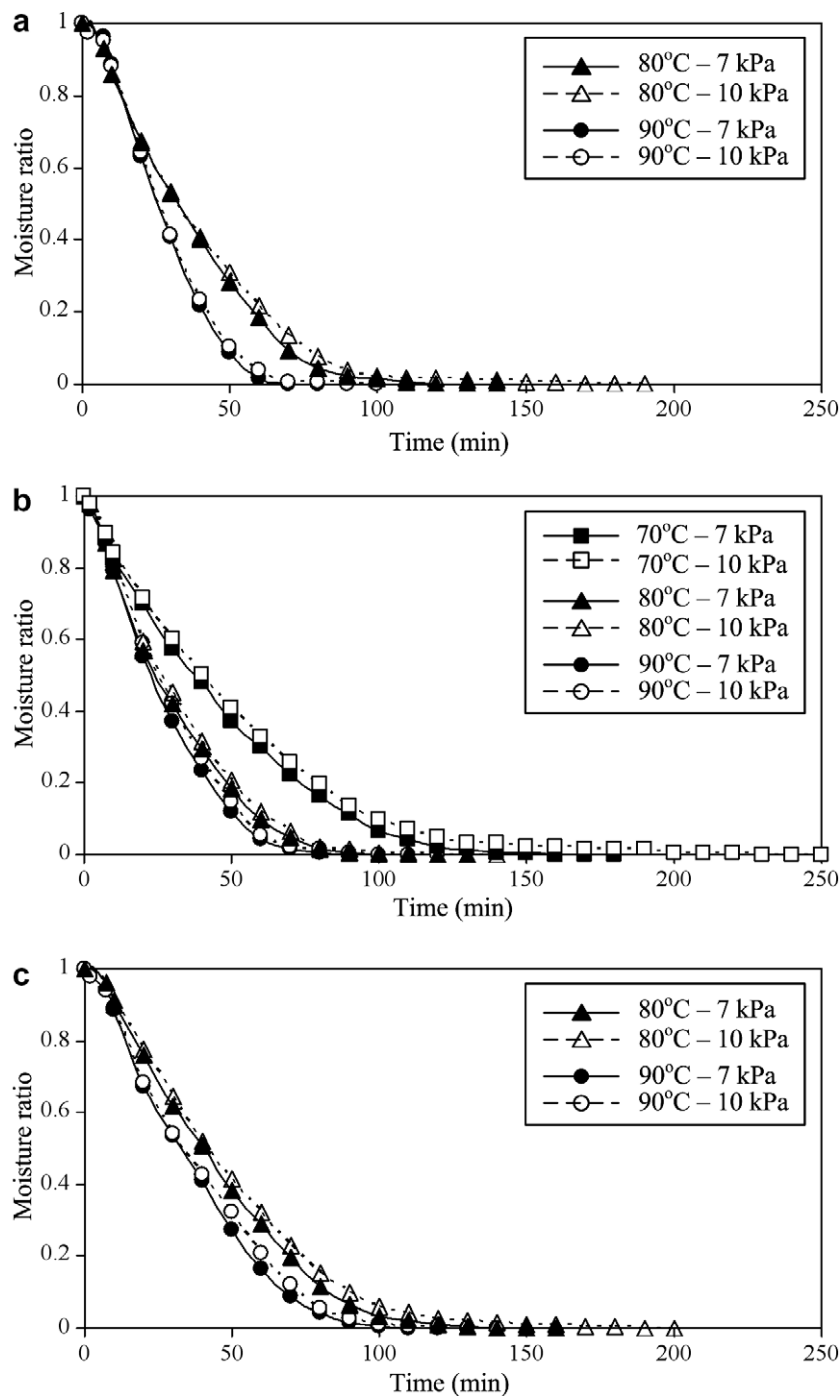


Fig. 2. Drying curves of banana slices undergoing (a) LPSSD-FIR, (b) VACUUM-FIR and (c) LPSSD.

at 80 and 90 °C. This may be due to the fact that temperature is the dominant factor influencing the superheated steam thermal properties, especially at higher drying temperatures.

It should be noted that, although the drying chamber was preheated via the use of the far-infrared radiator during the first 5 min of the process as mentioned earlier, small amount of steam condensation still occurred and could be observed over a short period; the results were not shown in Fig. 2a, however. Moreover, when drying was performed at

70 °C the sample could not reach the required final moisture content during the first 250 min of drying even at the lowest drying pressure tested (7 kPa). This is because of an excessive amount of steam condensation in the drying chamber. This phenomenon was also observed in the case of drying at 10 kPa (drying curves at 70 °C are not shown in Fig. 2a).

In the case of VACUUM-FIR (see Fig. 2b) the phenomenon was similar to that of LPSSD-FIR; drying at higher temperatures and lower pressures required shorter

drying time. Unlike LPSSD–FIR, however, the sample dried at the lowest drying temperature (70 °C) could reach the required final moisture content. This is because no steam condensation existed. It was also found that the effect of chamber pressure was not obvious at all drying temperatures. This may again be due to the fact that temperature is the main factor influencing the air thermal properties within the operating ranges tested.

In the case of LPSSD it was found from Fig. 2c that the drying time was shorter when drying was carried out at higher temperatures and lower pressures. Similar to LPSSD–FIR, the steam condensation still occurred during the initial stage of the process at all drying conditions and the sample could not reach the required final moisture content when drying was performed at 70 °C. The effect of the chamber pressure on the rate of moisture reduction was again not significant.

It is seen from Fig. 2a and c that the differences in the rates of moisture reduction of the samples dried at 80 and 90 °C during LPSSD–FIR were more clearly observed compared with those of the samples dried by LPSSD at 80 and 90 °C. This may be due to the fact that volumetric heating generated by the use of far-infrared radiation during LPSSD–FIR at 90 °C caused much larger temperature gradients within the sample than those within the sample dried by LPSSD at the same drying temperature resulting in a faster rate of moisture removal.

It was again found from Fig. 2 (see also Table 1) that the samples dried by LPSSD–FIR and VACUUM–FIR required less drying time than that of the samples dried by LPSSD at all drying conditions. This is because of the influences of volumetric heating caused by the use of far-infrared

radiation. In addition, it was observed that the samples dried by VACUUM–FIR required less drying time than that dried by LPSSD–FIR at lower drying temperatures (70 and 80 °C). However, LPSSD–FIR required shorter drying time (higher drying rates) when drying was conducted at 90 °C for all drying pressures tested. This is due to the sharp increase in the differences between the superheated steam temperature and the sample temperature in the case of LPSSD–FIR (see Figs. 4 and 5). On the other hand, the differences between the air temperature and the sample temperature in the case of VACUUM–FIR increased only slightly as the drying temperature increased. This suggested that the effective inversion temperature [18] calculated from the overall drying rates (the rates in both constant rate and falling rate periods) was somewhere between 80 and 90 °C. The details of the sample temperature evolution will be discussed again in subsequent sections.

Comparing with hot air drying [1–3], it was found that LPSSD–FIR and VACUUM–FIR required much less drying time (faster drying processes). This indicated that moisture transfer within the sample was rapid during the process applying far-infrared radiation.

Fig. 3 shows the plots of drying rates versus moisture content of banana slices undergoing different drying methods at various conditions. It can be seen from this figure that drying rates increased with an increase in the drying temperature and a decrease in the drying pressure in all cases.

In the case of LPSSD–FIR and VACUUM–FIR (see Fig. 3a and b) it was found that drying rates increased rapidly during an initial stage of drying (warming-up period). Since the radiation absorptivity of food products increased

Table 1
Specific energy consumption and total steam consumption of different drying methods

Drying method	Temp (°C)	Pressure (kPa)	Drying time (min)	Energy consumption (kWh)		Specific energy consumption (kWh/kg water)		Total steam consumption ^b (kg)
				E_{vacuum}	$E_{\text{radiator/heater}}$	$\text{SEC}_{\text{vacuum}}$	$\text{SEC}_{\text{radiator/heater}}$	
LPSSD–FIR	70	7	N/A ^a	N/A	N/A	N/A	N/A	N/A
		10	N/A	N/A	N/A	N/A	N/A	N/A
	80	7	140	3.50	0.49	128.57	18.00	60.67
		10	190	4.75	0.53	174.49	19.47	82.33
	90	7	90	2.25	0.41	82.65	15.06	39.00
		10	100	2.50	0.42	91.84	15.43	43.33
VACUUM–FIR	70	7	185	4.63	0.20	169.90	7.35	–
		10	255	6.38	0.23	234.19	8.45	–
	80	7	130	3.25	0.25	119.39	9.18	–
		10	145	3.63	0.27	133.16	9.92	–
	90	7	110	2.75	0.33	101.02	12.12	–
		10	120	3.00	0.34	110.21	12.49	–
LPSSD	70	7	N/A	N/A	N/A	N/A	N/A	N/A
		10	N/A	N/A	N/A	N/A	N/A	N/A
	80	7	160	4.00	0.54	146.90	19.84	69.33
		10	200	5.00	0.71	183.68	26.08	86.67
	90	7	115	2.88	0.61	105.61	22.41	49.83
		10	135	3.38	0.68	123.98	24.98	58.50

^a N/A implies that the final moisture content of 0.035 kg/kg (d.b.) was not obtainable at this condition.

^b The flow rate of steam into the drying chamber was maintained at about 26 kg/h.

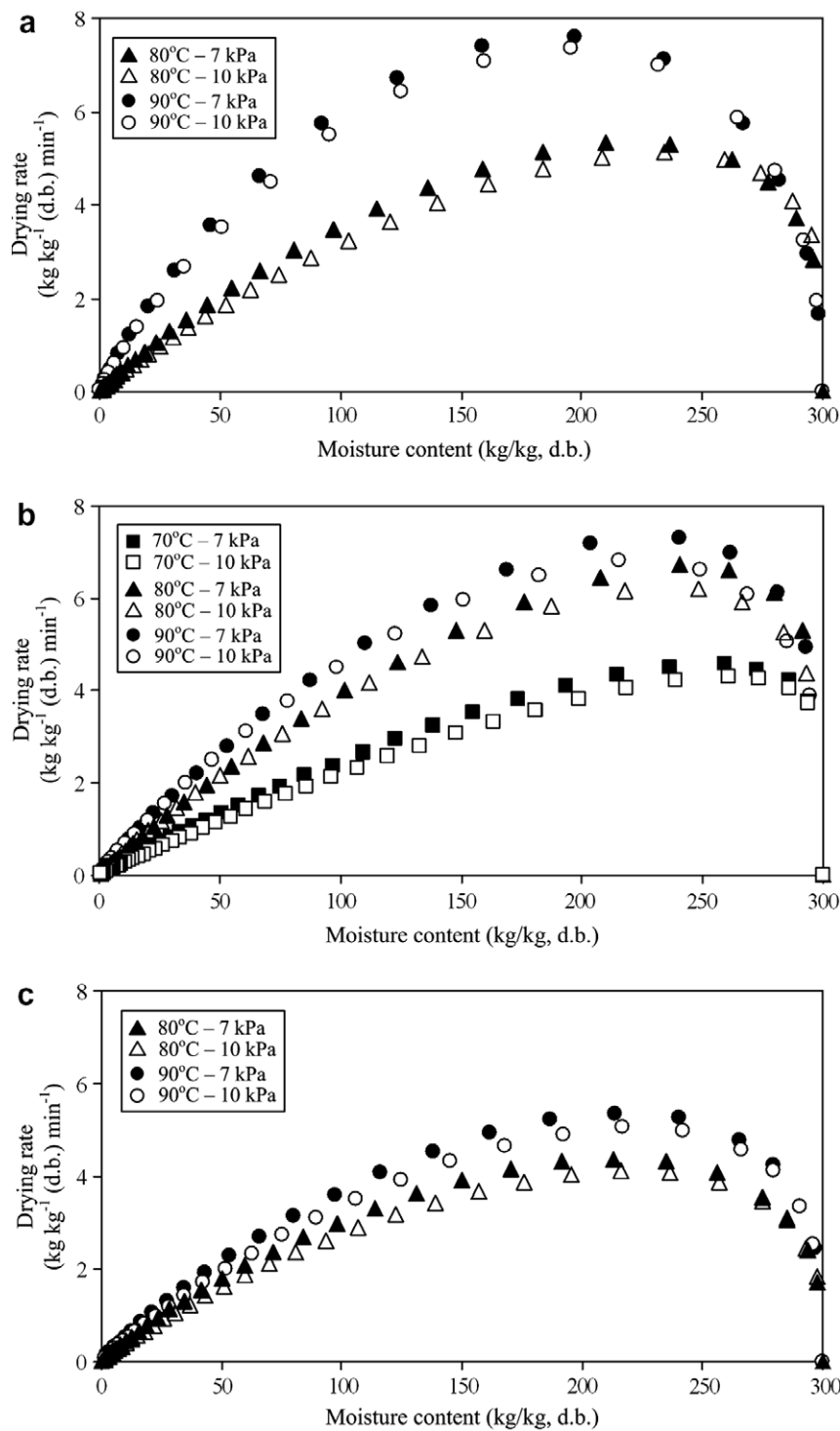


Fig. 3. Drying rates of banana slices undergoing (a) LPSSD-FIR, (b) VACUUM-FIR and (c) LPSSD.

with an increase in moisture content [15], thermal energy obtained from far-infrared radiation was more absorbed by banana slices during the initial stage of the process during which the sample moisture content was still high. This phenomenon is in agreement with that reported by Mongpraneet et al. [12,13] and Wang [19] who investigated the effect of far-infrared radiation on the drying characteristics of onion. However, Pathare and Sharma [20], who investi-

gated the use of infrared-convective drying for drying of onion, showed that the warming-up period was not observed. This is probably due to the fact that forced convection in the drying chamber accelerated the cooling effects, which reduced the temperature of the infrared heater and of the sample.

After the warming-up period the constant drying rate periods were observed; the duration of this period varied

with the drying techniques and conditions, however. In the case of LPSSD–FIR, it is seen that the period of constant drying rate was very short when drying was performed at the highest temperature (90 °C). For VACUUM–FIR the period of constant drying rate was almost not observed at all drying conditions even at the lowest drying temperature (70 °C). Drying process after this period took place in the falling rate period as indicated by a steady decrease in the drying rates. These results were contrary to those reported by many researchers such as Nguyen and Price [3] and Maskan [4] who found that drying of banana slices using hot air was in the falling rate period without the period of constant drying rate. Maskan [4] also reported that no period of constant drying rate was observed when microwave was applied. Although many researchers reported that the entire drying process took place in the falling rate period during hot air drying of some food products as mentioned above, the period of constant drying rate was clearly observed by Demirel and Turhan [1] during drying of banana slices using hot air at low drying temperature (40 °C). This implied that drying conditions employed are an important factor influencing the drying rate.

In the case of LPSSD (Fig. 3c) the characteristics of this drying process were also similar to those of LPSSD–FIR. However, the periods of constant drying rate were more obviously observed. The period of constant drying rate was longer, especially at lower drying temperature (80 °C in this case). It should be noted that at the same drying conditions drying rates of LPSSD–FIR and VACUUM–FIR were higher than that of LPSSD, especially when com-

paring with that of LPSSD–FIR at 90 °C. This is again because of the influence of volumetric heating caused by the application of far-infrared radiation.

The changes in moisture ratio and temperature of banana slices undergoing different drying methods at different conditions are shown in Figs. 4–6. As revealed by these figures the temperature evolution patterns were affected by both the drying methods and drying conditions. In the case of LPSSD–FIR, it can be seen from Fig. 4 that the temperature of the samples fell suddenly within the first 3 min of the process. This is due to the rapid reduction of the chamber pressure, which led to some flash evaporation of surface moisture [21]. After this period the temperature of the samples rose rapidly to the level close to the boiling point of water corresponding to the chamber pressure (not at the boiling point since far-infrared radiation was also present) and then remained unchanged at this level until the surface of the samples started to dry. In addition, it was observed that the period of constant sample temperature was longer when drying was conducted at lower temperatures and high pressures. This observation was in consistence with the period of constant drying rates (see Fig. 3a). Since heat transfer in the case of LPSSD–FIR simultaneously took place by radiation from the far-infrared radiator and by convection from superheated steam, the temperature of the samples rose steadily to the level higher than the pre-determined medium temperature. This is due to the fact that thermal radiation from the far-infrared radiator contributed additional energy to the drying medium and the samples. After this period the temperature of the samples remained almost unchanged. This is because

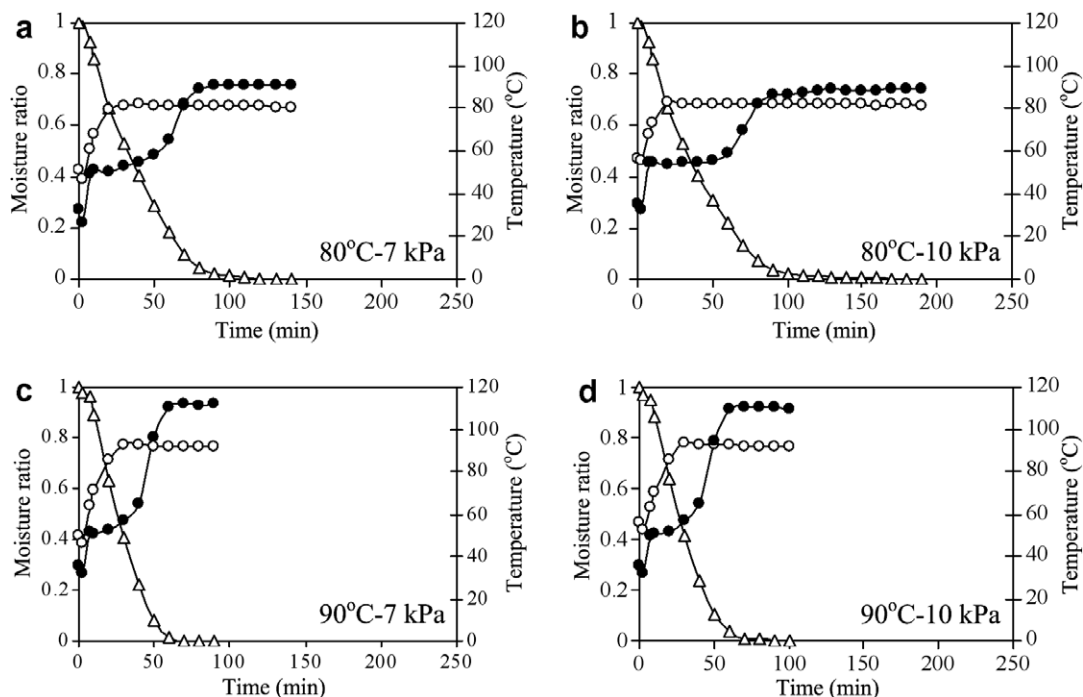


Fig. 4. Changes in moisture content and temperature of banana slices undergoing LPSSD–FIR at different drying conditions (–△– moisture ratio, –○– drying medium temperature, –●– sample temperature).